NASA, CR-54190
ADL 65958-02-01

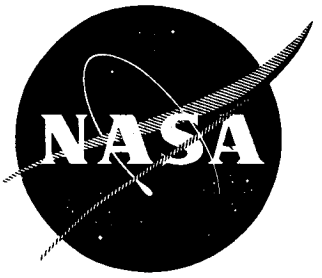

DESIGN AND OPTIMIZATION OF SPACE THERMAL PROTECTION FOR CRYOGENS – ANALYTICAL TECHNIQUES AND RESULTS

by

Jacques M. Bonneville

prepared for

NATIONAL AERONAUTICS AND SPACE ADMINISTRATION

CONTRACT NAS 3-4181

ARTHUR D. LITTLE, INC.

Requests for copies of this report should be referred to

National Aeronautics and Space Administration
Office of Scientific and Technical Information
Attention: AFSS-A
Washington, D.C. 20546

DESIGN AND OPTIMIZATION OF SPACE THERMAL PROTECTION FOR CRYOGENS--ANALYTICAL TECHNIQUES AND RESULTS

TOPICAL REPORT

DECEMBER 18, 1964

Report No. 65958-02-01

Arthur D. Little, Inc.
Acorn Park
Cambridge 40, Massachusetts

Prepared for
Technical Management
National Aeronautics and Space Administration
Lewis Research Center
Cleveland, Ohio
Advance Rocket Technology Branch
James J. Kramer
James Barber

Contract No. NAS3-4181

Table of Contents

	Page
List of Figures	iv
ABSTRACT	vii
SUMMARY	viii
NOMENCLATURE	x
I. INTRODUCTION	I-1
A. Role Played by Various Thermal Protection Schemes	I-1
B. Steps Involved in Solving the Thermal Problem	I-2
C. Organization of this Report	I-3
D. Acknowledgments	I-4
II. THE SPACE THERMAL ENVIRONMENT	II-1
A. Total Incident Power	II-1
B. Incident Power Distribution	II-2
C. Accounting for Vehicle Movements	II-3
III. THE ENVIRONMENT EXTERNAL TO A TANK	III-1
A. The Radiative Environment	III-1
B. The Conductive Environment, Inter-Component Heat Flow	III-5
C. A Special Problem: Internal Pipe Radiation	III-13
IV-A. MULTILAYER INSULATION--GENERAL DISCUSSION	IV-1
1. Disturbing Influences	IV-1
a. Gas Conduction	IV-1
b. Radiation Transfer Within Multilayer Insulations	IV-7
c. Gas Leakage from Cryogenic Fuel Tanks	IV-11
d. Venting During Ascent	IV-20
e. Solid Conduction	IV-20
2. Conclusions from Experimental Evidence	IV-21
3. Concepts Based on Truly Radiative Shielding	IV-23
a. Adiabatic Wall Temperature	IV-23
b. Shielding Factor	IV-23
4. Parallel Spreading of Disturbances	IV-24
5. General Effect of Conduction on MLI Performance	IV-27
6. Effect of Variable Foil Emissivity	IV-29
7. Thermal Diffusion in Superinsulation	IV-31

Table of Contents (continued)

		Page
	a. Diffusion Parallel to Foils	IV-31
	b. Diffusion Normal to Foils	IV-31
8.	Comments Regarding the Location of Multilayer Insulation	IV-32
	a. Simplicity	IV-32
	b. Ground-hold	IV-32
	c. Ascent	IV-34
	d. Venting During Space Storage	IV-34
	e. Payload Factor Improvement	IV-34
	f. Others	IV-34
IV-B.	MULTILAYER INSULATION AS A UNIFORM BLANKET OVER A TANK	IV-35
1.	Uniform Incident Power--Any Foil System	IV-35
2.	Non-Uniform Incident Power--Pure Radiating Foils	IV-35
	a. Single Relationship Giving the Total Heat Flow	IV-36
	b. Calculation of the Temperature Distribution Within the Foils	IV-37
3.	Non-Uniform Incident Power--Foils With Normal Conduction	IV-38
IV-C.	PENETRATIONS AND DISCONTINUITIES IN MULTILAYER INSULATION	IV-39
1.	Basic Effect of a Penetration or a Discontinuity	IV-39
2.	Radiative Heat Leaks Through a Gap	IV-41
3.	Gradation of Thermal Shorts	IV-45
4.	Limits to Weak or Linear Shorts	IV-48
5.	Strong or Non-Linear Shorts	IV-48
6.	Design of Thermal Shorts When a Choice is Possible	IV-52
7.	Decoupling of Thermal Shorts	IV-55
8.	Penetrations with Temperature-Dependent Thermal Conductivity	IV-62
IV-D.	GENERAL SCALING RELATIONSHIPS	IV-66
1.	Insulation Blanket	IV-66

Table of Contents (continued)

		Page
	2. Penetrations	IV-69
IV-E.	METHODS OF TEMPERATURE FIELD AND HEAT FLOW COMPUTATIONS	IV-71
IV-F.	CORRELATION OF THEORY WITH EXPERIMENT	IV-73
	1. Geometrical Considerations	IV-73
	a. Boundary Conditions	IV-73
	b. Case of Axial Symmetry	IV-73
	2. Interpretation of Tests on a Uniform Blanket of Multilayer Insulation in a Uniform Radiation Environment	IV-73
	3. Variation in Incident Flux	IV-77
	a. Calculations Based on Radiative Heat Transfer Normal to the Layers	IV-78
	b. Calculations Based on Average Values of the Conductivities	IV-83
	4. Copper Penetration	IV-85
	5. General Program	IV-89
APPENDIX A--SHROUD RADIATION TO A TANK		A-1
APPENDIX B--ANALYSIS OF INTERNAL PIPE RADIATION		B-1
APPENDIX C--VENTING OF MULTIFOIL INSULATION DURING ASCENT		C-1
APPENDIX D--TEMPERATURE PERTURBATIONS IN MULTILAYER INSULATION		D-1
APPENDIX E--HEAT FLOW THROUGH A BLANKET OF PURE RADIATION FOILS		E-1
APPENDIX F--EQUATIONS FOR THE GENERAL CYLINDRICAL THERMAL SHORT IN PURE RADIATION FOILS		F-1
APPENDIX G--BIBLIOGRAPHY		G-1

List of Figures

Figure		Page
III-1	ILLUSTRATION OF THE RADIATIVE ENVIRONMENT ON INTEGRAL TANKS	III-1
III-2	ILLUSTRATION OF THE RADIATIVE ENVIRONMENT ON SHROUDED TANKS	III-4
III-3	GENERAL BEHAVIOR OF A PENETRATION WHEN DECOUPLED FROM FOIL EDGES	III-6
III-4	TYPICAL VEHICLE CONFIGURATION	III-8
IV-A-1	MEAN FREE PATH BETWEEN TWO PLATES	IV-2
IV-A-2	RADIATION TRANSFER THROUGH PERFORATED SHIELD	IV-7
IV-A-3	ONE-WAY ENERGY FLUX BETWEEN TWO FOILS VS.GAP WIDTH	IV-10
IV-A-4	HEAT FLUX THROUGH 100 PERFORATED SHIELDS AS A FUNCTION OF PERFORATION FACTOR FOR VARIOUS HYDROGEN GAS FLOW RATES	IV-14
IV-A-5	DIRECT VENTING OF LEAKING GAS BY DOUBLE-WALLED TANK CONSTRUCTION	IV-16
IV-A-6	GAS FLOW PATTERN FOR CLOSELY SPACED PERFORATIONS	IV-18
IV-A-7	RADIATION FLOW PATTERN FOR CLOSELY SPACED PERFORATIONS	IV-18
IV-A-8	GAS FLOW PATTERN FOR WIDELY SPACED PERFORATIONS	IV-19
IV-A-9	RADIATION FLOW PATTERN FOR WIDELY SPACED PERFORATIONS	IV-19
IV-A-10	EFFECT OF MECHANICAL LOADING ON HEAT FLUX THROUGH MULTILAYER INSULATIONS	IV-22
IV-A-11	SPREADING OF DISTURBANCES IN MULTILAYER INSULATION	IV-26
IV-A-12	TWO ALTERNATIVE METHODS OF INSULATING A SHROUDED TANK (SCHEMATIC ILLUSTRATION)	IV-33
IV-C-1	USE OF RESISTANCE CONCEPT TO ILLUSTRATE THE EFFECT OF PENETRATIONS	IV-40

List of Figures (continued)

Figure		Page
IV-C-2	GRAPHICAL ILLUSTRATION OF THE EFFECT OF PENETRATIONS	IV-42
IV-C-3	GAP BETWEEN TWO PANELS OF MULTIFOIL INSULATION. THE TANK TEMPERATURE IS T_o. THE OUTER TEMPERATURE IS T_s	IV-43
IV-C-4	EFFECTIVE GAP δ IN UNITS OF THE INSULATION THICKNESS B, FOR VARIOUS VALUES OF THE SHIELDING FACTOR $n\left(\frac{2}{\epsilon} - 1\right)$.	IV-44
IV-C-5	TEMPERATURE DEPRESSION IN MULTILAYER INSULATION DUE TO A THERMAL TEST	IV-46
IV-C-6	PROPERTIES OF CYLINDRICAL THERMAL SHORTS FOR $\Delta T_{max} < 0.1\ T_a$ (WEAK SHORTS) IN 0.002" ALUMINUM FOIL INSULATION	IV-49
IV-C-7	PROPERTIES OF CYLINDRICAL THERMAL SHORTS FOR $\Delta T_{max} < 0.1\ T_a$ (WEAK SHORTS) IN INSULATION FOILS OF MYLAR WITH 10^{-2} IN. VACUUM DEPOSIT OF ALUMINUM	IV-50
IV-C-8	THE MAXIMUM WIDTH OF VARIOUS MATERIALS PENETRATING MULTILAYER INSULATIONS AND CONSTITUTING WEAK THERMAL SHORTS ($T_a = 300^oK$)	IV-51
IV-C-9	LIMITS BETWEEN WEAK AND STRONG THERMAL SHORTS SHOWN IN GENERALIZED PARAMETRIC FORM	IV-53
IV-C-10	TECHNIQUES FOR DECOUPLING STRONG THERMAL SHORTS FROM FOIL EDGES	IV-56
IV-C-11	EXAMPLES OF THE USE OF INTERMEDIARY INSULATION FOR STRUCTURAL STRIPS OR SEAMS	IV-59
IV-C-12	EXAMPLES OF THE USE OF INTERMEDIARY INSULATION FOR PIPING	IV-60
IV-C-13	EFFECT OF DECOUPLER GEOMETRY ON HEAT FLOW-THROUGH	IV-61
IV-C-14	EFFECT OF A PENETRATION WITH TEMPERATURE DEPENDENT THERMAL CONDUCTIVITY	IV-64
IV-F-1	SCHEMATIC OF THE ENVIRONMENTAL TANK WITH INSULATION AND THERMAL ENVIRONMENT	IV-74

List of Figures (continued)

Figure		Page
IV-F-2	DEVELOPMENT OF A GORE STRIP FOR ANALYZING MULTI-LAYER INSULATION IN THE CASE OF AXIAL SYMMETRY	IV-76
IV-F-3	INCIDENT FLUX NEAR THE MID-PLANE OF THE TANK IN THE HOT-COLD TEST	IV-79
IV-F-4	TEMPERATURE DISTRIBUTION IN THE TOP FOIL NEAR THE LIP SEPARATING UPPER AND LOWER BAFFLES	IV-82
IV-F-5	CALCULATED TEMPERATURE DISTRIBUTION IN FIVE LAYERS OF ALUMINIZED MYLAR AROUND A THREE-INCH DIAMETER COPPER PENETRATION (ABSOLUTE SHORT)	IV-86
IV-F-6	TEMPERATURE DISTRIBUTION IN FIVE-FOIL SYSTEM, ALUMINIZED MYLAR AROUND A THREE-INCH DIAMETER-COPPER PENETRATION	IV-88
A-1	MODEL FOR SHROUD ANALYSIS	A-2
A-2	A SIMPLIFIED ILLUSTRATION FOR SHROUD ANALYSIS	A-7
B-1	RADIATION INSIDE A PIPE, CONSIDERING ONLY THE EMISSION FROM THE WARM END PROPAGATING DIRECTLY TO THE PLANE OF THE COLD END	B-2
B-2	RADIATIVE HEAT LEAK WHEN WALL CONDUCTIVITY IS NEGLIGIBLE, FUNCTION OF ϵ_{ends} BUT INDEPENDENT OF ϵ_{wall}	B-3
B-3	RADIATION PATTERN FOR $\epsilon_{wall} = 0$, THE SAME AS FOR FIGURE B-2, CONDUCTIVE HEAT LEAK IS ADDED DIRECTLY TO THE RADIATIVE HEAT LEAK	B-5
B-4	HEAT BALANCE FOR A CYLINDRICAL ELEMENT OF PIPE	B-7
B-5	TOTAL HEAT LEAK (DIMENSIONLESS) TO A TANK VIA A STRAIGHT PIPE, VERSUS ϵ_{wall}, FOR VARIOUS ϵ_{end} AND μ ; L/D = 3	B-11
B-6	AXIAL TEMPERATURE DISTRIBUTION OF PIPE WALLS UNDER VARIOUS CONDITIONS	B-13
D-1	MODEL FOR ANALYZING THE TEMPERATURE FIELD NEAR A WEAK THERMAL SHORT (k_1 ASSUMED CONSTANT)	D-2
F-1	MODEL FOR ANALYZING THE GENERAL CYLINDRICAL THERMAL SHORT	F-2

DESIGN AND OPTIMIZATION OF SPACE THERMAL PROTECTION FOR CRYOGENS--ANALYTICAL TECHNIQUES AND RESULTS

by

J. M. Bonneville

ABSTRACT

19847

The results of analyses and relevant experiments dealing with multilayer insulation, performed during the last four years, are presented in a logical sequence. Emphasis is placed on the experimental fact that in a carefully designed and applied insulation system, the foils will act as intended, i.e., as pure radiative shields. Several relationships useful for determining the heat flow to a cryogenic tank are developed on that basis.

Penetrations through the insulation are discussed in detail. Methods for ascertaining their effect, and for decoupling them from the edges of foils, are presented, along with criteria to determine the usefulness of decoupling in a given case.

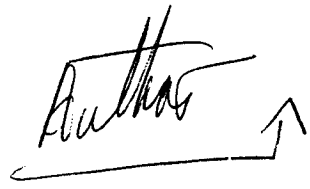

DESIGN AND OPTIMIZATION OF SPACE THERMAL PROTECTION FOR CRYOGENS--ANALYTICAL TECHNIQUES AND RESULTS

by

J. M. Bonneville
Arthur D. Little, Inc.

SUMMARY

The object of this report is to assemble the significant results of all the analytical work performed to date on the subject of multilayer insulation (MLI).

In the introduction, the basis for the organization of the report is laid down in terms of (i) the role played by various insulation schemes and (ii) the steps involved in solving the thermal problem. The scope of the report is then made clear: to present the analytical aspects of the work involved in choosing, designing and optimizing a thermal protection system, with emphasis on MLI.

The environment of space is first treated, by way of an outline of the analytical procedure required to account for that environment. Previous work on the subject is referred to. The environment external to a tank is next discussed; this will differ from the space environment in the case of a shrouded tank. A shroud appears to be mandatory, in view of the requirements of ascent aerodynamic heating and space micrometeoroid protection; it would be most useful during groundhold also.

Section IV, which is divided into six parts, treats in detail multilayer insulation. Part A is a general, though quantitative, discussion of the thermal behavior of real multilayer insulation necessary for an understanding of MLI. Part B justifies and discusses the treatment of MLI as a continuous blanket over the tank. This approach is valid because penetrations will affect the heat flow through the MLI blanket only slightly, whereas the converse is not true (the MLI blanket affects the heat flow through penetrations).

In Part C, the thermal effect of penetrations and discontinuities in MLI is discussed in detail. First, concepts are developed for an understanding of the basic effect. Following this, various types of thermal shorts are graded according as they permit simple analysis or not. Methods for designing shorts for minimum heat leak are introduced. The very important matter of decoupling penetrations from the edges of foil is treated in detail. Some cases appear where decoupling is useless, or worse.

Parts D and E deal with analytical methods and relationships. Part D treats of scaling laws that can be applied to the MLI blanket, and to the penetrations. Part E summarizes the methods of computation recommended in determining the temperature field within MLI.

Part F discusses those parts of the experimental work done at Arthur D. Little, Inc., to investigate the validity of the analytical approach.

A series of six appendices deal in detail with: shroud radiation; internal pipe radiation; venting during ascent; the spreading of perturbations in MLI; the heat flow through a blanket of pure radiating foils (which is independent of conduction parallel to foils); and the general cylindrical thermal short.

NOMENCLATURE

a	thickness between shields; a_t, thermal diffusivity, $k/\rho C_p$; distance
A	area; general constant
B	thickness of insulation; general constant
c	velocity; $\bar{c}$, average molecular velocity
C	general constant; C_p, heat capacity at constant pressure; C_i, conduction heat input into i^{th} element, see Eq. B-5
D	diffusion coefficient; representative dimension
f	parameter Eq. IV-C-33
F	parameter defined in Eq. III-4; molecular flux through shield
G	parameter defined in Eq. III-5; parameter defined in Eq. IV-C-32
I	incident radiation flux
k	thermal conductivity; $k_\perp$, perpendicular to plane of insulation; $k_\parallel$, parallel to plane of insulation; k_f, foil
k	Boltzmann's constant
kt	product of thermal conductivity times thickness
K	general constant
l	length
L	length
n	number of shields; n_s, shields; n_p, number of penetrations
N	molecular density
p	exponent in Eq. IV-C-30
P	loading or pressure; ΔP, pressure difference
q	heat flow; q_r, radiation heat flow

Q	heat flux; Q_{pen}, due to penetration
r	radius of penetration; distance
R	gas constant; radiosity (see Appendix A); general symbol for resistance
S	stress
t	thickness; t_f, of foil
T	temperature; T_a, adiabatic; T_s, surface; T_{liq}, liquid
u	dimensionless parameter relating lengths
w	solid angle, $2\pi \sin\theta \, d\theta$; width of penetration; $\dot{w}$, mass flow rate
x	distance
X	perturbation decay characteristic length
Δy	B/n
Z	distance
α	absorptivity; α_o, of surface; α_{ij}, parameter in Eq. A-2; α_n, parameter in Eq. F-15
β	$4 \epsilon_o T_a^3$
γ	parameter in Eq. IV-D-2
δ	gap width
ϵ	emissivity; ϵ_o, of surface
ζ	Z/D
θ	angle; $T/T_{a,max}$, time
Θ	parameter in Eq. D-12
κ	$\epsilon/2n\epsilon_o$
λ	parameter proportional to conductivity of penetration
μ	parameter in Eq. B-9
ν	molecular flux from walls

ξ	X/D
ρ	density
σ	Stefan-Boltzmann constant
τ	characteristic time for heat conduction; perforated fraction in insulation
ϕ	temperature parameter in Eq. IV-C-6
ψ	parameter defined in Eq. F-15

I. INTRODUCTION

By definition, the temperature of a cryogenic substance at normal pressure is below 100°K. On the other hand, the temperature of a body in equilibrium with the thermal radiation environment of the inner solar system (the adiabatic, or equilibrium temperature) can reach several hundred degrees Kelvin, the actual value depending on the geometry of the body, its distance from the sun, and its absorbtance and emittance. At the latter temperatures, a cryogen either would experience a high pressure rise, requiring containing walls of excessive mass, or a large fraction would boil off, requiring an excessive initial amount for a desired useful amount. It follows that the space storage of cryogenic propellants in the inner solar system presents a thermal problem; this problem must be solved in order to reduce dead mass in space vehicles.

A number of methods (thermal protection schemes) are available for dealing with this problem. Each of these methods involves additional mass, so that in considering their application, attention must be paid to the effect this mass has on the payload ratio. Unless this effect is small, an optimization procedure is required, both in the choice of method and in the choice of parameters associated with the method chosen. It must be remembered also that any thermal protection scheme must be consistent with the physical requirements of groundhold, earth ascent and micrometeoroid protection in space, as well as those of overall system performance, since any scheme that is not so consistent cannot be accepted, regardless of its merits as regards thermal protection in space. Also, simplicity of operation, leading to reliability, and consonance with other systems aspects (e.g., life, structural, propulsion, guidance, communication) are required of any scheme.

A. Role Played by Various Thermal Protection Schemes

The role played by the various schemes can be illustrated by considering three cases: two extremes and the intermediate case. At one extreme, one can consider the case of a large amount of propellant to be stored for a relatively short period. The thermal problem might then conceivably be so slight as to be solved by mere containment in bare tanks, with boil-off losses made up during groundhold and boil-off and/or pressure rise acceptable during boost-out and space flight.

At the other extreme, relatively small amounts of cryogenic propellants are to be stored in space for very long periods in orbits that pass close to the sun. In such cases only the most minute net heat input rates to the propellant can be tolerated. One scheme to solve this problem would be to combine shadow-shields, radiators and attitude control to maintain the adiabatic temperature of the propellant tank at, or not far above, the normal boiling point of the cryogen. In this

way the propellant could be contained easily without any net heat absorption. We note that again the tank can be bare (in principle), but is shaded from the sun. The shadow-shields can also be used in combination with a refrigerator that extracts whatever heat has been absorbed by the propellant. A refrigerator implies the presence of a power source or a solar energy converter aboard the vehicle.

Between the two extremes there exists a wide range of cryogenic propellant storage problems where the heat absorbed on bare tanks is not tolerable but a finite amount of heat input would be. Here, insulation can play a major role in controlling the heat input, provided it can compete with shadow shields, radiators and refrigerators.

During the last few years, the concept of multiple radiation shields has been developed to practical reality, in what is now called MLI. This consists in a number of highly reflective foils laid layer upon layer on the surface to be protected. Because of the high effectiveness of these foils, it is possible with their use to reduce the heat flow to a cryogenic tank in vacuum to very low values. So much so, that incidental heat inleakage through pipes, insulation seams, tank support and other penetrations can very easily predominate, and must be carefully controlled if they are not to nullify the effectiveness of the insulation system.

Of course, the use of MLI need not preclude the use of other methods in conjunction with it: shadow-shields, radiators, refrigerators, or pre-flight sub-cooling to augment the heat absorption capacity of the liquid cryogen. On the other hand, because of the effectiveness (per unit mass) of MLI, there will be few intermediate cases where its total replacement by some other scheme is justified.

B. Steps Involved in Solving the Thermal Problem

It is useful to delineate the solution of the thermal problem previously discussed, by subdividing it into four sequential logical steps. Although each detail of each step need not be performed in the given order, each step must be taken if the best solution is to be found.

The first step in determining the thermal protection system for cryogenic propellants is to obtain information regarding the following:

(1) Characteristics of the trajectory and orientation of the vehicle in space during the storage period, as determined from over-riding non-thermal considerations.

(2) The space thermal environment, as determined from (1).

(3) The configuration of the vehicle: dimensions and relative positions of components, details of any component, e.g., electronics, living space, etc., whose

temperature is fixed for operational reasons; internal heat sources if any, method of tank support, and propellant transfer.

(4) Groundhold and launch characteristics.

(5) The thermal environment of the tanks, as determined from (3) and (4).

(6) The manner in which mass additions, due to the thermal problem and its solution, will affect over-all mission performance. This determines the criterion to be adopted in selecting and optimizing a thermal protection scheme.

The second step, which can only be based on the first, is the assessment of the possible thermal protection schemes, singly and in combination, and a selection of one scheme. One basis for assessment and selection is the criterion found from (6) above. However, questions of practicality and reliability, micrometeoroid protection, groundhold and ascent requirements, and other non-thermal aspects, must enter at this point as well; in fact they may prevail over questions of payload delivery performance.

The third step consists in optimizing the parameters associated with the chosen scheme, using the criterion found from (6). This optimization is not purely mathematical; it consists also in using all the potentialities of the chosen scheme to reduce heat inleakages to the cryogenic propellant.

The fourth step consists in fully evaluating the performance of the thermal protection system in its final form. This evaluation may include testing (prototype or model) under simulated conditions. It should include a calculation, in as much detail as necessary, of the total heat leak to the cryogenic tanks. This calculation will correct any errors that have crept into the analysis of the third step due to simplifications made in optimizing the system. The calculation will include heat leaks through piping, tank supports and other penetrations through insulation, as well as heat leaks through the insulation itself.

C. Organization of This Report

During the last four years, Arthur D. Little, Inc., has been actively engaged on behalf of NASA in work on the thermal protection of cryogenic tanks for storage in space. This report brings together the results of the analytical portion of this work, in the form of principles, theorems, guidelines, simplifications, recommended procedures, formulae and charts.

Because analytical work has been performed in all the four categories or steps outlined for the solution of the thermal problem, this work is presented in the order shown for those steps. Where a procedure, analytical result, etc., can belong in more than one category, it appears under only one, but mention is made of this plurality of roles.

A large fraction of our analytical work has centered on MLI. As a consequence, this area is more deeply analyzed than others. Nevertheless, this report, taken as a whole, presents a fairly complete tableau of present-day techniques for dealing with the thermal protection problem. In addition, it can serve as a basis for launching studies into promising areas.

Some topics of relevance to this report have been covered adequately in separate topical reports (not merely in progress reports). Such will be treated here only to such depth as is necessary to point out their relevance and to extract the conclusions useful to the present work. The separate publications will, of course, be quoted and included in the bibliography.

D. Acknowledgments

Some items discussed in this report, and not referenced in topical reports, were developed by persons other than the author. Acknowledgment is made of the contributions of Alfred E. Emslie on gas conduction, radiation within multifoils and gas leakage; also that of Arthur A. Fowle on insulation venting during ascent. Frank Gabron provided background information on foil emissivity. Luciano L. Mazzola performed the computer programming and solution of the pipe radiation, and the "absolute-short", and the "hot-cold" environment problems in support of the insulated tank experimental program.

Thanks are due to James Kramer, of NASA Lewis, as well as Richard B. Hinckley, Norman N. Wiederhorn, and Arthur A. Fowle for their support and cooperation in the work as originally presented and in the preparation of the present report.

II. THE SPACE THERMAL ENVIRONMENT

The thermal environment of space is considered to be purely radiative, the radiating sources being the sun and the planets. The natural satellites (moons) also radiate, but in a manner similar to planets and in the present discussion they are treated as planets.

During interplanetary travel, solar thermal radiation is the only significant thermal input from space. During the escape and capture maneuvers, the incident flux from planets can be appreciable, but its time-integral can be neglected compared to solar flux integrated over the transfer period. On the other hand, if propellant is to be stored in orbit around a planet for an extended period of time, planetary radiation--emitted and reflected (albedo)--must be taken into account in addition to solar radiation.

The two types of radiation differ in wavelength and directionality. The latter point of difference lies in the fact that solar radiation will be essentially collimated at expected distances (in solar radii) of vehicles from the sun; whereas the same is not true of planetary radiation at planetary radii. It is, of course, much easier to analyze the input from a collimated beam; in fact, the fundamental method of analyzing planetary radiation consists in breaking down the planetary surface into a number of parts, each approximately flat and subtending a small solid angle at the vehicle, so that incident radiation can be considered as made up of a number of collimated beams, one from each planet part.

In the present context, the meaning of the difference just discussed will depend on the aim of the radiation calculations.

A. Total Incident Power

It will be shown later (Appendix E) that the total heat flow through multilayer insulation consisting of pure radiating foils, may be calculated in a simple manner from a knowledge of the total radiation flux absorbed on the insulation, independently of conduction in the plane of the insulation foils. If the absorptivity is independent of angle of incidence, the total absorbed flux is proportional to the total incident flux.

If the tank is integral with the structure, the flux incident upon it comes directly from space. It will also appear later that the total flux on a shrouded tank can often be deduced from the total flux from space incident on the shroud; moreover, in many other instances an inference can be made with good approximation. Finally, an isothermal shroud presents to a tank a black-body environment at a temperature determined by total incident flux (see Appendix A). The notion of total incident flux is, therefore, of great use in a screening analysis (steps 1 to 3 of Introduction).

The total flux incident on a vehicle from a collimated beam is merely the beam intensity times the projected area of the body in a plane normal to the beam. Total incident solar radiation can thus be calculated simply, once the required projected area is known. Total incident planetary radiation can, in general, be obtained only by summing up the products, "projected area x intensity" associated with beams from the radiating planet parts, since each beam arrives from a different direction with a corresponding different vehicle projected area.

A method has been developed [1]* for calculating the projected area of a convex body of revolution as a function of beam direction. The results can, of course, be applied to solar or planetary radiation; in the latter case, a projected area is calculated for each beam. In addition, total planetary radiation has been calculated [2,3,4,5] for simple shapes: sphere, cylinder, flat plate; the results are usually available in tabular form.

B. Incident Power Distribution

At some point in the solution of the thermal problem (particularly step 4 of Introduction), the heat flow through penetrations in multi-layer insulation must be determined accurately. Also, it may be possible to select for some of the major penetrations (e.g., pipes and struts) a location for least heat flow. For these purposes, knowledge of total radiation input does not suffice; it is necessary to know in detail the distribution, over the vehicle surface, of radiant flux from space. Moreover, complex vehicle shapes can be conceived where a determination of the surface flux distribution followed by a summation over the surface is just as efficient a method of determining total flux as is that previously discussed (i.e., summation of products involving projected areas and elemental beam intensities).

The intensity of thermal radiation flux incident on a surface from a parallel beam is simply the beam intensity multiplied by the cosine of the angle of incidence. Hence, the distribution of incident solar radiation over the surface of a vehicle of given shape is not difficult once its location and orientation are known.

Local incident planetary radiation can be calculated on the same basis, except that each point on the vehicle (or each elemental vehicle surface part--sufficiently small and flat) has incident on it a number of collimated beams, one from each planet part; each beam arrives from a particular point on the planet and, hence, has its own intensity and direction of incidence; the effect of each must be added. It will be recalled that the receiving vehicle surface part was to be chosen small enough to be considered flat; this simplifies calculations by allowing use of the concept of planetary radiation incident on a flat plate. This case has already been analyzed in the literature and the results are available in tabular, [2,3,4,5] graphical, [6] and partly in analytical form [1,2].

* Numbers in parenthesis refer to the bibliography in Appendix G.

C. Accounting for Vehicle Movements

Excepting interplanetary travel with a fixed orientation toward the sun, vehicle movement in space introduces a complication in radiant input calculations. As the vehicle moves, its position and orientation with respect to the sun and planets vary with time. Therefore, the following will be time-variant: the vehicle projected area as seen from the sun and various points on a planet; the angle of incidence of radiation beams from the sun and planet parts on various parts of the vehicle surface; and, the beam intensities.

In order to express the changing space thermal environment, with reasonable control over all variables, there is need of a method to account systematically for vehicle location and attitude. Such a method has been developed;[1] it involves the transformation of coordinates by matrix multiplication, parts of the matrix depending on vehicle orbit and mode of orientation, hence, varying with time. The method will be described briefly in the following paragraphs.

The vehicle surface is divided into a finite number of parts. The parts must be of sufficient flatness to ensure the accuracy of the ensuing calculations of incident power; they must also be small enough in surface dimensions so that the subsequently assumed functional temperature variation within the part (linear, polynomial, etc.) will give result of the required accuracy.

The thermal radiation arriving at a small part of a vehicle's surface depends on the distance of the vehicle from the radiating source, and, for each source, on the relative directions of the source-vehicle line, the surface normal at the source, and the surface normal at the vehicle part. These quantities must be described in a single set of coordinates, in terms of the vehicle position and orientation.

The direction of the surface normal at a vehicle part can always be given as a vector in a coordinate system fixed on the vehicle (vehicle coordinates). The surface normal can then be expressed in the coordinate system most useful for the thermal radiation calculations. This is done by multiplying the surface normal vector by a matrix that represents the rotations which would be necessary to bring the vehicle coordinates into coincidence with those of the useful system. The vehicle coordinates themselves should have been previously chosen so that the matrix is the simplest possible.

The choice of transformation (rotations) depends on the type of orbit and the form of orientation stabilization (e.g., spinning, fixed in solar space, aligned toward a planet, etc.). This is given in detail in Reference (1).

In Reference (1) is also given a method of accounting for the shadowing of one vehicle part by another during vehicle motion. It

involves the measurement of shadowing factors, for instance by shining a parallel beam of light from various angles at a model of the vehicle, and measuring for each angle the unshadowed fraction of each part. These fractions can then be incorporated in the calculation of the radiation incident on each vehicle part from the sun and from the planet parts. This method, of course, becomes unnecessary in the case of fully convex vehicles.

III. THE ENVIRONMENT EXTERNAL TO A TANK

In defining and discussing this environment, we adopt a point of view that has been found to be valid. It is most useful in screening and optimization studies, and often applicable in detailed heat flow evaluations.

A propellant tank installed aboard a space vehicle is subjected to an environment that will be broken down into a radiative and a conductive part. The radiative part is the thermal radiation incident on the outer surface of the tank insulation, or on the tank itself, if bare. The conductive part consists of the temperature differences existing between the ends of the elements connecting the tank to the other components of the vehicle: the transfer lines, tank supports, control feedthroughs, and any others.

One reason for this subdivision is the near-independence between the two parts as defined, at least insofar as major heat inputs are concerned. The important conductive elements (e.g., pipes, tank supports) will have their surfaces shielded from the radiation environment and are very nearly independent of it. Conversely, because the conductive elements do not generally present large lateral surface areas, and (more importantly) because they will be shielded, their effect on the radiative part is small. Pipe internal radiation is generally coupled to pipe conduction; however, both will be independent of the radiative environment, and controlled only by end temperatures and pipe configuration; for that reason, the pipe enters into the conductive part of the environment (or as a separate third part, if desired).

It will be noted that pins, seams, gaps, overlaps, foam, penetration decouplers (see later), and any other penetrations within the insulation, are part of the insulation and not of the environment. It is the task of the designer to minimize the effect of these and enhance the effectiveness of the insulation. On the other hand, a pipe or a support cannot be considered by the designer as part of the insulation since (i) these obviously do not insulate the tank but rather have the opposite effect; and (ii) they will be thermally decoupled from multilayer insulation.

In defining the radiative environment, the possibility of a bare tank was mentioned. This possibility exists when the tank is surrounded by a shroud; in such a case, insulation might be applied on the inner side of the shroud rather than on the tank. This point will be discussed later.

A. The Radiative Environment

We consider two main cases: integral and shrouded tanks.

1. Integral Tanks

Figure III-1 illustrates schematically an integral tank. It is seen that its radiative environment is (i) direct space radiation to the tank sides; this can be made negligible in interplanetary space by aligning the vehicle axis toward the sun; (ii) radiation to the tank ends from emission and reflection between elements 1, 2, and 3; here the sources are parts 1 and 2, viz., the bulkhead and sides; the sides (2) are really the tank supports and generally would be shielded with multilayer insulation (inside and outside if the sun shines broadside, inside only if end-on).

Integral tanks do not appear promising for long-term missions. First, their sides (and the insulation thereon) must be protected against the environment of groundhold and ascent as well as against micrometeoroids; this will necessitate some protective outer surface. In effect they will be completely surrounded by some sort of shroud, and so, even if designed as integral tanks, from the present point of view they may be treated as shrouded tanks.

2. Shrouded Tanks

Figure III-2 illustrates a shrouded tank. In this case the tank does not view space directly from any direction. Its radiative environment will, however, depend on space radiation as well as on the type of vehicle orientation, conduction around the shroud and geometry of shroud and tank. It will also depend on the temperatures of adjacent elements: payload, engines, adjacent tank, and on the manner in which these elements are insulated.

The elements adjacent to the tank form part of its environment with the shroud proper. In fact, the elements can be considered as part of the shroud in a thermal sense, even in the case where some of these elements contain heat sources.

We again refer to a later part of this report (Appendix E) showing that the total heat flow through a blanket of insulation on a tank depends on the total absorbed radiation alone. Now, if the total shroud (including elements) were to fit rather closely over the tank so that the view factor between the two (shroud and tank) were nearly unity, then a good approximation for the total power incident on the tank could be obtained from a knowledge of the surface-integral of the fourth power of the shroud temperature. In fact, a close-fitting shroud acts simply as one shield to be added to those of the insulation. The fourth-power integral over the surface of the total shroud is easily obtained from a heat balance with space and with internal heat sources (see Appendix A).

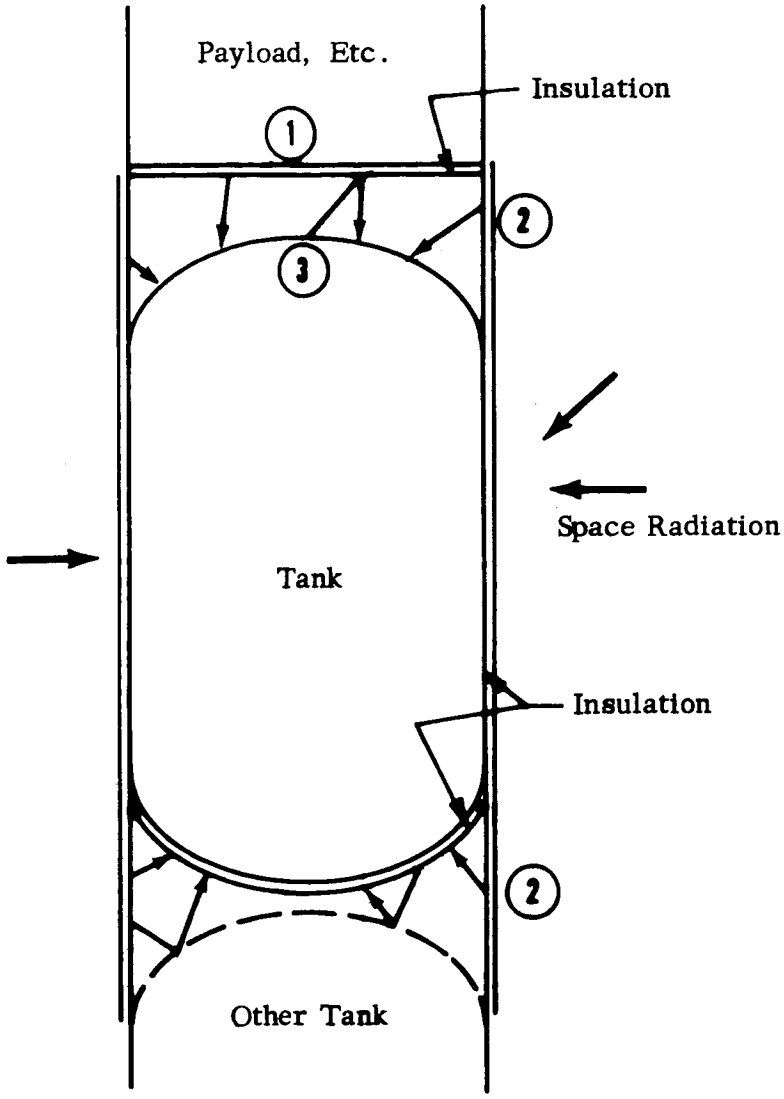

Note: Schematic only - Piping omitted for clarity.

FIGURE III-1 ILLUSTRATION OF THE RADIATIVE ENVIRONMENT ON INTEGRAL TANKS

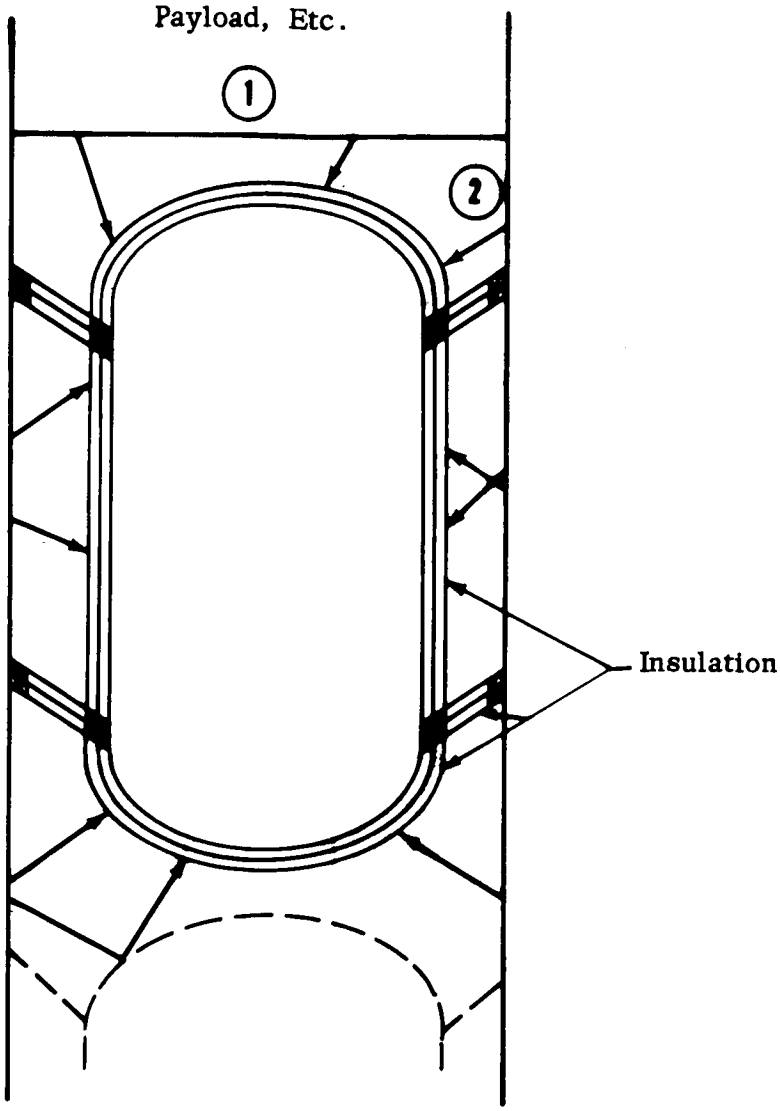

Note: Schematic only - Piping omitted for clarity.

FIGURE III-2 ILLUSTRATION OF THE RADIATIVE ENVIRONMENT ON SHROUDED TANKS

For a more loosely-fitting shroud (e.g., a cylindrical shroud containing spherical tanks), the view factor from shroud to tank is less than unity. This alters the relationship and brings in a dependence on geometry, and internal surface emissivities. However, for reasonable geometries the dependence on geometry itself is rather weak, and the dependence on emissivities is weaker still. This weak dependence is explained by the small amount of total heat leaking into the tank through the insulation, as compared with the total radiative power incident on the tank insulation; almost all this incident power is re-radiated toward the shroud, the net result being the same regardless of emissivities. Therefore, the total power incident on the tank can be estimated with rather good accuracy by setting equal to unity the emissivities of the shroud inner surface and of the insulation outer surface.

B. The Conductive Environment, Inter-Component Heat Flow

Tank supports and pipes can be considered as conducting heat to a propellant tank from two regions: (i) their warmer end and (ii) the edges of foils where they penetrate insulation. Usually, the thermal conductance of these elements is such that if they experienced the same temperature gradient as does the insulation, they would conduct heat to the tank in amounts far greater than that flowing through the entire insulation blanket, thus defeating the purpose of insulation.

High temperature gradients can occur in penetrating elements if the edges of the foils are allowed to come into thermal contact with the penetration. Therefore, such thermal contact must be avoided. This can be achieved by inserting a decoupler (or "buffer zone", or "thermal separator") of isotropic, low-k material between the penetration and the foil edges (see section IV-C). Such a decoupling procedure has two results: to separate regions (i) and (ii) discussed above, and to render the heat flow from (ii)--the foil edges--much smaller than that from (i). Figure III-3 illustrates the general effect of decoupling; this matter will be taken up in more detail later. Thus, the necessary decoupling permits a separation of the conductive environment from the behavior of the insulation.

Major penetrations, laterally shielded against radiation exchange, can be treated as cases of uni-dimensional heat flow, which makes the problem simple once the geometry and end temperatures are specified.

We wish at this point to show that conductive heat flow to tanks through decoupled major penetrations can be kept reasonably low using presently available materials and techniques. To illustrate this, we choose a typical vehicle and mission, defined by the following situation. It should be stressed that these are chosen for illustrative purposes only. The sample situation has further been simplified in that the boil-off losses are arbitrarily specified a priori rather than being optimized as part of the system. However, the conclusions that are derived can be shown to be quite general. In this analysis

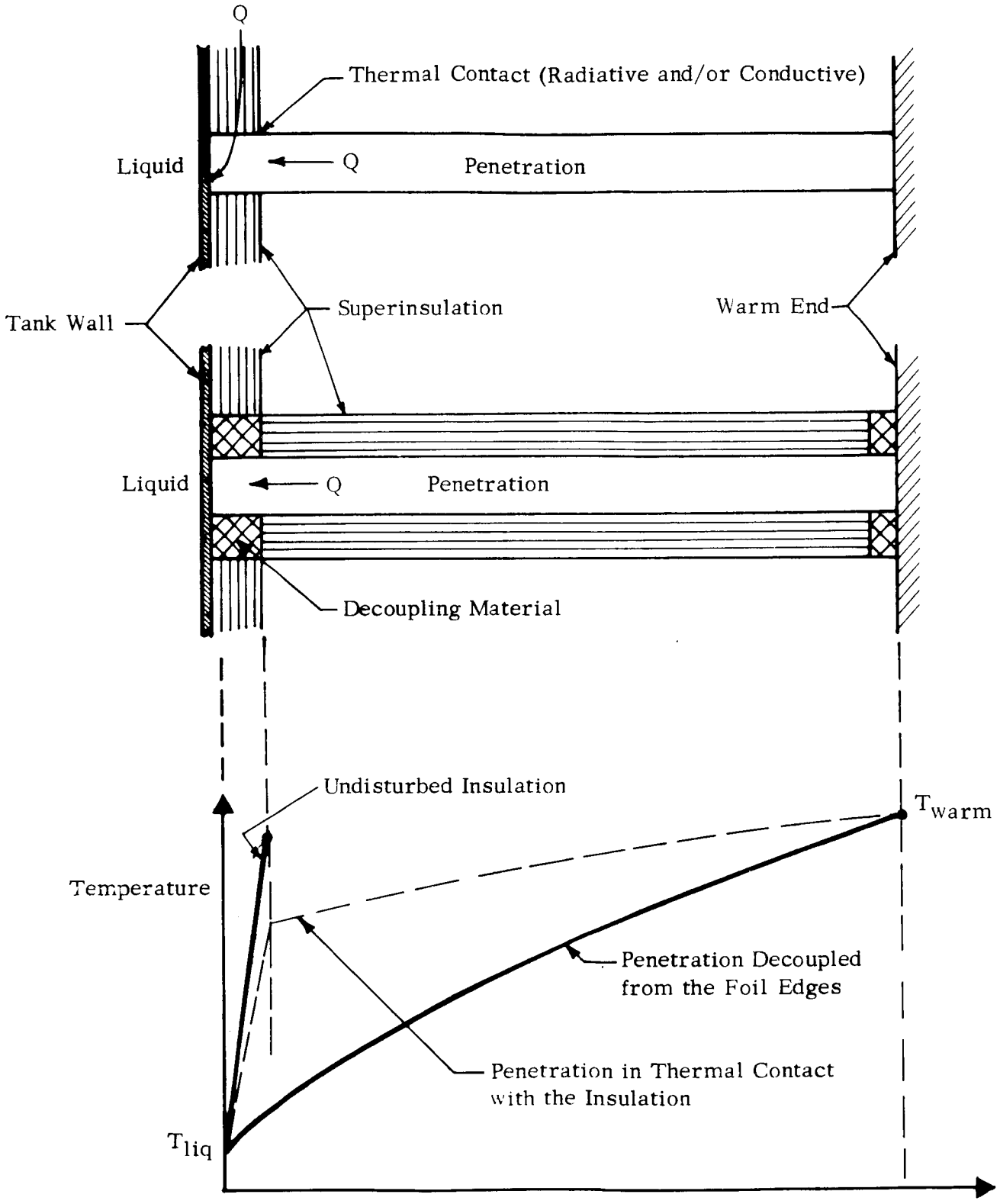

FIGURE III-3 GENERAL BEHAVIOR OF A PENETRATION WHEN DECOUPLED FROM FOIL EDGES

we do not consider internal pipe radiation, which will be treated in III.C.

1. Typical Situation

Payload	9,500	pounds
Power plant	2,500	"
Structure	2,500	"
Tankage	500	"
LH_2	5,000	"
LO_2	25,000	"
TOTAL	45,000	pounds

A 400-day mission.

A 10 g maximum launch acceleration.

Allowable boil-off during the mission:
5% of initial LH_2 and 5% of initial LO_2.

A configuration is shown in Figure III-4. The LH_2 tank is forwardmost in the vehicle, followed by the LO_2 tank, payload and engine, in that order. The relative positions of the tanks are justified on two counts: a minimization of pipe internal pressures during acceleration, and a minimization of heat leaks.

Consistent with this situation is a heat leak of 3.6 watts to the LO_2 tank and 1.5 watts to the LH_2 tank. One might apportion one-third of these leaks to piping and support on an equal basis. Hence, our estimate of a reasonable heat leak to the LO_2 tank would be 0.6 watts through piping and 0.6 watts through supports; similarly, for the LH_2 tank we would have 0.25 watts through piping and 0.25 watts through supports.

2. Supports

Considering Figure III-4, heat leakage would occur through the supports separating the two tanks and those separating the LO_2 tank from the payload or engine. The latter support presents the greater problem because of (i) a larger temperature difference, and (ii) a greater cross-section for heat transfer, since this support must withstand greater loads. Therefore, we have considered only the support from the payload or engine to the LO_2 tank since a solution of this case implies a solution of the other, easier case.

The support must withstand a maximum compressive load to accelerate about 30,000 lbs. of propellants at 10 g, i.e., the loading will be

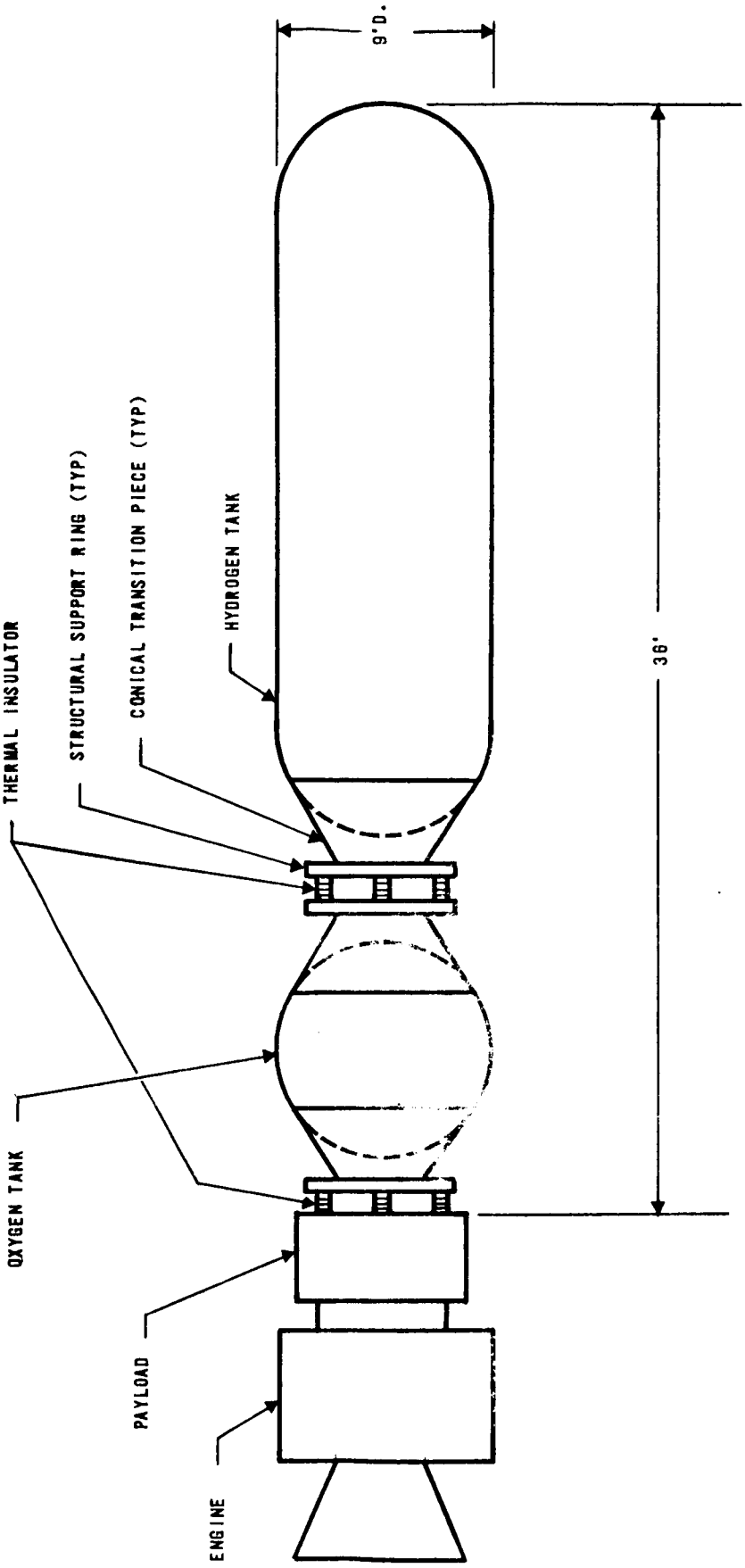

FIGURE III-4 TYPICAL VEHICLE CONFIGURATION

P = 300,000 lbs. For a given material, this will impose a minimum cross-section area A equal to P/S, where S is the allowable stress.

The heat leak will be

$$q = (A/L) \int_{90^\circ K}^{300^\circ K} k\,dT \qquad \text{(III-1)}$$

where k is the thermal conductivity. Hence, the minimum length L of support for a given maximum q is

$$L = (A/q) \int k\,dT \qquad \text{(III-2)}$$

The weight of the support will be

$$\text{Weight} = \rho\, AL$$

$$= \frac{\rho A^2}{q} \int k\,dT = \frac{P^2}{q} \frac{\rho}{S^2} \int k\,dT \qquad \text{(III-3)}$$

where ρ is the density of the support material. The quantity P^2/q is fixed for the particular vehicle and mission. The weight of the supports will vary with the remaining factor in (III-3), namely

$$\text{Weight} \sim \frac{\rho}{S^2} \int_{90^\circ K}^{300^\circ K} k\,dT \equiv F \qquad \text{(III-4)}$$

which contains only material properties and thus may be used as a figure of merit for comparison of materials. Values of the factor F are given in Table III-1, for several possible support materials, including a stack of stainless steel washers, 0.001" thick. The values of F shown are relative, the value unity having been assigned to the washers.

As was shown in Equation (III-2), the required length of support varies with the heat leak. However, this may lead to unreasonable lengths. Supposing the length to be fixed, then since A_{min} is still given by P/S, the heat leak will be determined by substituting for A in (III-1)

TABLE III-1

PARAMETERS F AND G FOR SUPPORT MATERIALS

(Integrals From 90 to 300 K)

$$F = \frac{\rho}{S^2} \int_{90^\circ K}^{300^\circ K} k\,dT \qquad G = \frac{1}{S} \int_{90^\circ K}^{300^\circ K} dk\,T$$

Material	(Weight Factor,* Heat Leak Given)	(Heat Leak Factor,* Length Given)
Stainless Steel	670	670
Nylon	13	30
Micarta	7	24
Mylar	13	25
Teflon	3,140	380
Stacked Stainless Steel Washers	1	1

* Values given are relative to Stacked Stainless Steel Washers. The effective thermal conductivity of the washers was assumed to be (1/670) that of solid stainless steel; this value may vary with loading and surface treatment but is indicative of the values which have been measured experimentally.

$$q = \frac{P}{LS} \int kdT \qquad \text{(III-5)}$$

In this case, the quantity P/L is fixed by the vehicle and, therefore, the parameter $G = \frac{1}{S} \int kdT$, representing the heat leak when the length is fixed, may be used as a figure of merit. Relative values of G are also given in Table III-1.

Considering Table III-1, the stacked stainless steel washers appear to be the best by far. Calculations show that for our sample vehicle and mission, six stacks of washers each 1 and 1/16-inch in diameter and 0.9 inch long, with a total weight of 1.37 lbs., will allow a leak rate of 0.6 watts. Moreover, the washers would have to be supplemented by a structural transition piece to transmit the load across to the LO_2 tank, over a length of from 3 to 5 feet (see Figure III-4). The six stacks of washers as insulating support, combined with a less efficient insulation for a transition piece, will give a heat leak lower than 0.6 watts. If the elements must resist stress in two directions, stacked cups (axes normal to the loads) can be used instead of the washers.

3. Piping

Based on reasoning similar to that employed for the supports, one obtains, for piping, the same weight parameter, F, (see Table III-1), if the piping is to be designed to withstand internal pressures only. Thus, we would expect that the plastics would be superior to steel, giving less weight for a given thermal resistance, or providing greater thermal resistance at a fixed length.

Using the configuration of Figure III-4, the pressures at the "bottom" of the pipes, i.e., the point nearest to the engine, can be calculated. The heights of the liquid columns producing the pressures are based on full liquid tanks. Table III-2 gives the dimensions and the internal pressures arrived at, for both LO_2 and LH_2, under a 10 g acceleration.

TABLE III-2

DATA GIVING MAXIMUM INTERNAL PRESSURES
IN FEED PIPING FROM TANKS TO ENGINE

Liquid	Height - Feet			Liquid Density	Base Pressures
	Tank	Piping	TOTAL	lb/ft^3	(psi) at 10g
O_2	9	3	12	71.2	60
H_2	22	14	36	4.37	11

From the above table appears an important advantage to placing the LO_2 tank nearest to the engine; if it is separated from the engine by the LH_2 tank, the LO_2 column pressure becomes 180 psi for our sample configuration.

Stainless steel would be a desirable material to use for piping. Although its thermal properties do not appear the most promising, a sample calculation indicates that it is still a useful material for pipes. If we assume a 10-inch pipe diameter, uniform wall thickness, and an allowable stress of 100,000 psi, the results for the LO_2 pipe are: a required thickness of 0.003 inches (paper-thin); a weight of 0.96 lbs; and a heat leak of 0.16 watts. For the LH_2 pipe, the thickness required is 0.0006 inches, the weight is 0.88 lbs., and the heat leak 0.008 watts. It is seen that there is no materials problem here. In fact, using 0.010-inch stainless steel pipe throughout, the resulting heat leaks are 0.56 watts for the LO_2 pipe and 0.14 watts for the LH_2 pipe. The total weight of piping would be 18 lbs. Reinforced plastics such as polyester or epoxy glass laminates could be used for the LH_2 to reduce the total heat leak even further. Therefore, piping made of useful structural materials for low temperature service installed with permanent connections, can be used without causing an unacceptable heat inleakage to the cryogenic storage vessel.

4. Conclusions

The heat leaks through the required tank supports and piping (decoupled from foil edges and from the radiative environment) can be kept small with reasonable weights, using stainless steel or plastics. The design of these elements is within the present state-of-the-art. If necessary, stacked stainless steel washers or cups can be used to limit the heat leaks through the supports.

C. A Special Problem: Internal Pipe Radiation

The thermal coupling through a transfer line joining a cryogenic tank to a relatively warm body (e.g., the engine) involves internal heat radiation as well as conduction along the pipe wall. If thermal radiation were absent or negligible, the heat flow to the tank could be kept within reasonable limits with the use of realistic pipe wall materials and thicknesses, as we have seen in III.B.3. Thermal radiation from the warm end adds to the heat leak not only by contributing a radiative inleakage, but by increasing the conductive flow as well. Energy emitted at the warm end is partly absorbed by the walls at points nearer the cold end; some of the absorbed energy is conducted and some re-radiated toward the cold end. The resulting radiation and increased pipe wall gradients can lead to heat leaks greater than that flowing through the blanket of superinsulation over the entire cryogenic tank.

An analysis of this radiative-conductive effect is presented in Appendix B. A straight pipe is considered, with attention centered on an L/D ratio of three. The results of the analysis are also presented in the Appendix, and indicate that a transfer line must be designed with thermal radiation in mind; otherwise, a heat inleakage of many watts can occur. The effective end emissivities should be low. However, this may be difficult to achieve except with shiny baffles near the ends.

Some variations in the design of the pipe, to decrease the heat leak to values of the order of a watt or less, are possible: higher L/D ratios, baffles at selected points, curved pipes.

When the pipe itself is in a surrounding of low radiation intensity (i.e., in the shade), part of its outer surface near the warm end can be left bare. In this way, the internally absorbed heat can be bled by emission to the cold environment, and the temperature of the pipe can fall off to low values over most of its length. The cold end then receives radiation only from the distant circle of the warm-end cross-section, and the radiative interchange is effectively kept low, and is de-coupled from the conductive heat flow.

When the pipe is in a warm exterior surrounding, the same results can be obtained by ducting some of the vaporized hydrogen to a point near the warm end, and using the sensible heat of the vapor to cool the pipe, i.e., to remove the absorbed radiation, there. This technique is called vapor-shielding.

IV-A. MULTILAYER INSULATION--GENERAL DISCUSSION

The concept underlying multilayer insulation (MLI) is that of a number of highly reflective radiation shields placed between the radiation environment and the surface to be protected, i.e., the cryogenic tank wall. Conceptually, there is no other agent of heat transfer through multilayer insulation but radiation impeded by many reflective barriers.

Another feature of MLI generally implied is that adjacent shields are spaced close enough together so that (i) the net interspacial radiation in the direction parallel to the foils is zero in a region where there are no "breaks" or discontinuities in the foils; and (ii) the view factor from one foil to an adjacent one is unity.

1. Disturbing Influences

Where the conditions postulated above are met, many concepts developed in the past (and some recently) become available to simplify thermal analysis and insulation design calculations. Since also the idealized conditions represent minimal heat leak to the tank, it is desirable to eliminate any disturbances that detract from these conditions. We will now discuss these disturbing influences with the aim of understanding them in order to avoid them.

a. Gas Conduction

Multilayer insulations must be evacuated to at least 10^{-4} torr for adequate performance. Two approaches are possible. The first method is to produce a pre-evacuated or cryopumped insulation by using a flexible outside shield. There is considerable doubt that the required high vacuum could be maintained at the various joints during the severe vibration and acceleration of the launching. Unless the outside skin can be removed at altitude, any noncondensible gases which might diffuse through the outer skin or through the tank wall would increase the gas pressure within the insulation. Also, in view of the possible outgassing of metal surfaces as a result of bombardment by high energy radiation, it is questionable whether the required vacuum could be maintained in space, unless adequate means for venting were provided.

The second approach is to exclude atmospheric gases by purging with a noncondensible gas such as helium. In this case, the insulation is not subjected to atmospheric pressure; however, reliance must be placed on rapid venting at altitude.

Venting to the space environment is required in both approaches. Such venting will depend on the geometric arrangement of the insulation layers (e.g., exposure of the edges to the external vacuum or perforation of the shields) which will be designed to enhance the pumping speed for gas molecules.

i. Edge Pumping

To determine the equilibrium pressure when a panel of multilayer insulation is pumped only at the edges, we must first calculate the mean free path of a molecule confined in the space between two parallel plates separated by a distance a. If the molecule leaves the lower plate (Figure IV-A-1) with a cosine distribution in angle, then the mean radial distance that the molecule travels before hitting the other plate is

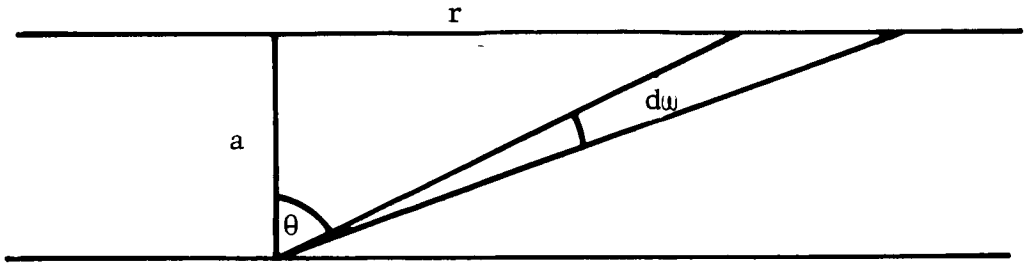

FIGURE IV-A-1 MEAN FREE PATH BETWEEN TWO PLATES

$$\bar{r} = \frac{1}{\pi} \int^{\pi/2} r \cos \theta \, dw \qquad \text{(IV-A-1)}$$

where dw is an element of solid angle and θ is the angle of the path with respect to the normal to the plates.

Since $dw = 2\pi \sin \theta \, d\theta$ and $r = a \tan \theta$, the integral can be evaluated to give

$$\bar{r} = \frac{\pi}{2} a \qquad \text{(IV-A-2)}$$

The corresponding two-dimensional diffusion coefficient for motion parallel to the plane of the plates is

$$D = \frac{1}{2} \bar{c} \bar{r} = \frac{\pi}{4} \bar{c} a \qquad \text{(IV-A-3)}$$

Now assume that the two plates are in the form of a long strip of width ℓ and that molecules are outgassing from the interior surfaces at a net rate of ν cm^{-2} sec^{-1}. Then the diffusion equation for the equilibrium density of molecules is

$$D \frac{\partial^2 N}{\partial x^2} = - \frac{2\nu}{a} \qquad \text{(IV-A-4)}$$

where N is the density of the molecules and x is measured from the center of the strip.

The solution for the case of a perfect vacuum along each edge of the strip is

$$N = \frac{\nu}{Da} \left(\frac{\ell^2}{4} - x^2 \right) \qquad \text{(IV-A-5)}$$

The maximum density occurs at the center of the strip and is

$$N_{max} = \frac{\nu \ell^2}{4Da} = \frac{\nu \ell^2}{\pi \bar{c} a^2} \qquad \text{(IV-A-6)}$$

If the pressure is to be less than 10^{-5} mm Hg at 25°K, the gas density must be less than 4×10^{12} molecules cm^{-3}. Now assume, as a typical example, that the shield consists of panels 1 meter wide composed of radiation shields 0.002 cm thick and stacked 40 to the cm, with spacers that occupy effectively 90% of the spaces between the foils.

Then we can substitute the following values in Equation (IV-A-6):

$$\ell = 100 \text{ cm}$$

$$\bar{c} = 3 \times 10^4 \text{ cm sec}^{-1}$$

$$a_{effective} = 0.0023 \text{ cm}$$

$$N_{max} = 4 \times 10^{12} \text{ cm}^{-3}$$

The maximum allowable outgassing rate is therefore

$$\nu = 2 \times 10^8 \text{ molecules cm}^{-2} \text{ sec}^{-1}$$

This corresponds to the removal of one monomolecular layer from all exposed surfaces every two weeks. Much higher outgassing rates than this are likely to be encountered if the radiation shields and spacers are exposed to atmospheric pressure at the time of launching. In which case, adequate venting must be provided to prevent destructive effects due to sudden pressure reduction.

Another difficulty with edge-pumping is that at the pumping areas, the innermost foils must be brought into contact with the vacuum outside. This provides places where incident thermal radiation can bypass most of the shields and penetrate almost directly to the insulated tank.

ii. Broadside Pumping of Perforated Radiation Shields

Let τ be the perforated fraction of the surface of each radiation shield, so that τ is the molecular transmission coefficient. Thus, if N is the density of molecules on one side of a shield and N' the density on the other side, the net flux F of molecules through the shield is

$$F = \frac{1}{4} N\bar{c}\tau - \frac{1}{4} N'\bar{c}\tau \qquad \text{(IV-A-7)}$$

For a stack of shields, this equation can be written in the form

$$F = -\frac{\bar{c}\tau}{4} \frac{\partial N}{\partial n_s} \qquad \text{(IV-A-8)}$$

where n_s is the series number of the shields.

As before, let ν be the outgassing rate per cm^2 of actual shield surface. Then the number of molecules emitted per cm^2 per second into the space between two shields is $2\nu(1 - \tau)$. Thus, for steady-state flow,

$$\frac{\bar{c}\tau}{4} \frac{\partial^2 N}{\partial n_s^2} = -2\nu(1 - \tau) \qquad \text{(IV-A-9)}$$

If the array of shields is in contact with a perfect vacuum on one side and an impervious wall on the other side, the boundary conditions are

$$\frac{\partial N}{\partial n_s} = 0 \quad \text{for } n_s = 0$$

$$N = 0 \quad \text{for } n_s = n$$

Equation (IV-A-9) gives for the maximum allowable molecular density, assuming $\bar{c}$ is constant;

$$N_{max} = \frac{4\nu(1-\tau)n^2}{\bar{c}\,\tau} \qquad \text{(IV-A-10)}$$

It is of interest to consider under what conditions broadside and edge-pumping are equally efficient. On equating the values of the outgassing rates given by Equation IV-A-6 and IV-A-10, we find for the required relationship

$$\frac{\ell}{a} = n\sqrt{\frac{4\pi\tau}{1-\tau}}$$

If $n = 100$, $\tau = 0.1$, and $a = 0.0023$ cm, we find that $\ell = 2.3$ cm. This means that for edge-pumping to be as efficient as broadside pumping with 10% perforated shields, the edge-pumping must be applied along lines separated by only 2.3 cm. The excessive exposure of the innermost foils in such a design appears to be quite impractical. We, therefore, conclude that the method of broadside pumping is much preferred.

The allowable outgassing rate with broadside pumping may be calculated from Equation IV-A-10 with the following values:

$$N_{max} = 4 \times 10^{12}\ \text{cm}^{-3},\ \tau = 0.1,\quad n = 100,\ \bar{c} = 3 \times 10^{4}\ \text{cm sec}^{-1}$$

Then

$$\nu = 3 \times 10^{11}\ \text{cm}^{-2}\ \text{sec}^{-1}$$

Actually, the allowable outgassing rate must be considerably less than this, because τ must be well below 0.1 to prevent excessive radiation transfer through the perforations in the shields.

iii. Effects of Static Gas Density

Consider two adjacent radiation shields at temperatures T and T + ΔT. The number of molecular impacts on each surface per unit area per second is $N\bar{c}/4$, where N is the number of molecules per unit volume and $\bar{c}$ is the mean molecular velocity. If the accommodation coefficient is unity and the mean free path of the molecules is large compared with the spacing of the shields, the average kinetic energy of the molecules

striking one shield is $c_v T$ and that striking the other shield is $c_v(T + \Delta T)$. The heat transfer rate is therefore

$$q_c = \frac{N\bar{c}}{4} c_v \Delta T \qquad \text{(IV-A-11)}$$

$$= \frac{3}{8} N\bar{c} k \Delta T$$

since c_v is approximately equal to the translational kinetic energy per degree at the low temperatures where conduction is important. *

The radiation transfer rate is

$$q_r = \frac{\Delta(\sigma T^4)}{\frac{2}{\epsilon} - 1} \qquad \text{(IV-A-12)}$$

where ϵ is the emissivity of the surfaces.

The total heat flux is therefore

$$q = \frac{3}{8} N\bar{c}k \Delta T + \frac{\Delta(\sigma T^4)}{\frac{2}{\epsilon} - 1} \qquad \text{(IV-A-13)}$$

We must now sum this difference equation over the set of n successive gaps between the shields. In doing this, we assume that ϵ is constant and that $N \propto 1/T$ and $\bar{c} \propto \sqrt{T}$, since the pressure is constant. The result of the summation is:

$$nq = \frac{3}{4} N_1 \bar{c}_1 k \left(\sqrt{T_1 T_2} - T_1\right) + \frac{\sigma(T_2^4 - T_1^4)}{\frac{2}{\epsilon} - 1} \qquad \text{(IV-A-14)}$$

where N_1, $\bar{c}_1$, T_1 refer to the low-temperature side of the shield and T_2 refers to the high-temperature side.

---

* In reality the energy carried is not c_v but $(c_v + k/2)$ if one accounts for the fact that those molecules with the higher velocities will travel between the shields in a shorter time. Also c_v is (3/2) k only if the temperature is sufficiently low that no internal energy modes are excited (or if the gas is monatomic). Eq. (IV-A-11) is, however, a good approximation in most cases.

b. Radiation Transfer Within Multilayer Insulations

In addition to the transmission of heat by gas conduction through multilayer insulations, the following radiation transfer conditions arise:

i. Radiation Transfer Through Perforated Radiation Shields

Figure IV-A-2 shows the radiation entering and leaving on the two sides of a perforated shield of emissivity ϵ, transmission coefficient τ, and temperature T. The energy balance equations are

$$I'_+ = \tau I_+ + (1 - \tau)(1 - \epsilon) I'_- + (1 - \tau) \epsilon \sigma T^4 \qquad \text{(IV-A-15)}$$

$$I'_- = \tau I_- + (1 - \tau)(1 - \epsilon) I_+ + (1 - \tau) \epsilon \sigma T^4 \qquad \text{(IV-A-16)}$$

$$I'_+ - I'_- = I_+ - I_- = q_r \qquad \text{(IV-A-17)}$$

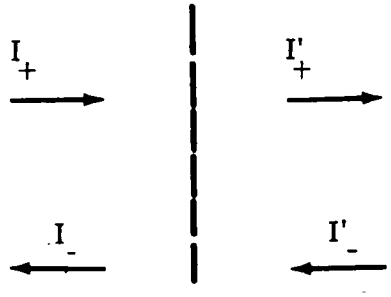

FIGURE IV-A-2 RADIATION TRANSFER THROUGH PERFORATED SHIELD

Equations IV-A-15, 16, and 17 are satisfied by relations of the form

$$I_+ = A - kn_s \qquad \text{(IV-A-18)}$$

$$I_- = B - kn_s \qquad \text{(IV-A-19)}$$

$$\sigma T^4 = C - kn_s \qquad \text{(IV-A-20)}$$

where A, B, C, and k are constants and n_s, as before, is the series number of a given shield. To get I'_+ and I'_- we replace n_s by $n_s + 1$. The constant k is the gradient $\Delta(\sigma T^4)/\Delta n_s$.

On substituting equations IV-A-18, 19 and 20 into equation IV-A-15 and 16 and noting that A - B is the net radiation flux q_r, we find that

$$q_r = \frac{\epsilon + (2 - \epsilon)\tau}{(2 - \epsilon)(1 - \tau)} \quad \frac{\Delta \sigma T^4}{\Delta n_s} \qquad \text{(IV-A-21)}$$

Now suppose that a stack of n shields is placed between two black sheets at temperatures T_2 and T_1. Then, on adding the radiative impedances of the two outer gaps to that given in IV-A-21, we find for the flux:

$$q_r = \frac{\sigma(T_2^4 - T_1^4)}{1 + \frac{(2 - \epsilon)(1 - \tau)}{\epsilon + (2 - \epsilon)\tau} n} = \frac{\sigma(T_2^4 - T_1^4)}{1 + (\frac{2}{\epsilon'} - 1)\, n} \qquad \text{(IV-A-22)}$$

where ϵ' is the effective emissivity of the perforated foils:

$$\epsilon' = \epsilon + (2 - \epsilon)\tau \qquad \text{(IV-A-23)}$$

Note that equation IV-A-22 gives correct results for $\epsilon' = 0$ and 1.

Let $\epsilon = 0.05$ and $\tau = 0.1$. Then $\epsilon' = 0.245$. Thus, a transmission factor that is large enough to give an appreciable molecular pumping speed increases the effective emissivity of the shields by a factor of five.

ii. Radiation Transfer by Closely Spaced Shields

The usual formula for radiation transfer through a stack of radiation shields does not apply when the spacing of the shields is less than the wavelength of the peak of the black-body spectral distribution corresponding to the temperature of the shields. Two effects set in at these close spacings--wave interference and radiation tunneling. Wave interference of the emitted radiation occurs in the narrow gaps between the shields and may increase or decrease the energy transfer, depending on the spacing. Radiation tunneling allows transfer of radiation that ordinarily suffers total internal reflection inside the shield material; the resulting energy transfer increases exponentially as the spacing decreases. The two effects together give an energy transfer rate per unit area which becomes, in the limit of zero spacing,

$$q = \frac{n^4}{n^2 + k^2} \sigma (T_2^4 - T_1^4)$$

where n and k are the real and imaginary parts of the complex refractive index, σ is the Stefan-Boltzmann constant, and T_2 and T_1 are the temperatures on the two sides of a gap.

The formula implies that the radiation density ϵ' and velocity of propagation c' in the shield material are:

$$\epsilon' = \frac{n^2 \sigma T^4}{c}$$

$$c' = \frac{n^2 c}{n^2 + k^2}$$

For moderate values of the absorption index k, the flux formula predicts a transfer rate between two close shields greater than that between two black surfaces.

In the case of metal shields, when the spacing between the two shields is increased from zero, the radiation transfer rate at first rises sharply to a high maximum and then falls below the usual value for widely spaced shields. The flux returns to the normal level when the spacing exceeds about one half of the wavelength of the black-body peak. (See Figure IV-A-3)

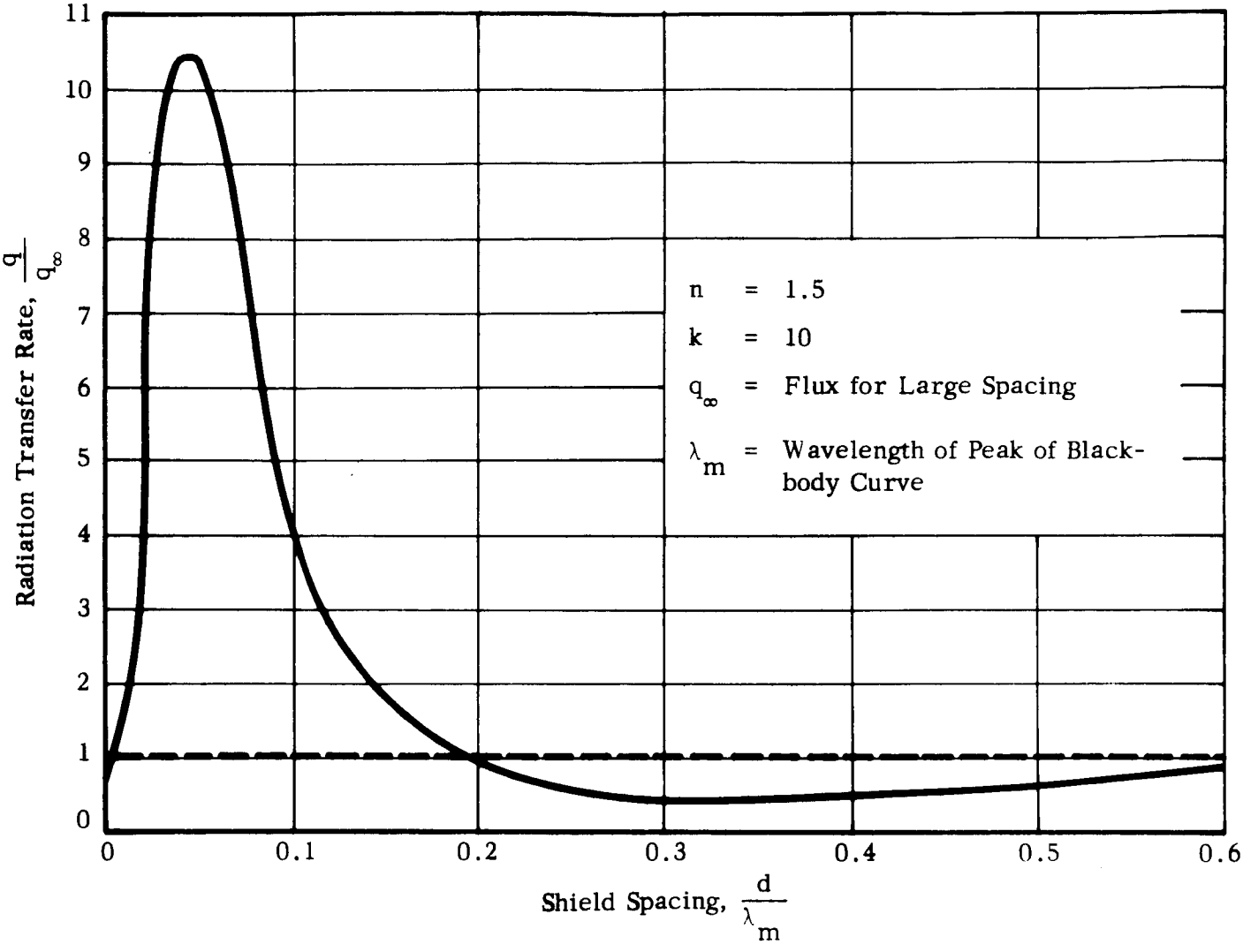

FIGURE IV-A-3 ONE-WAY ENERGY FLUX BETWEEN TWO FOILS VS GAP WIDTH

c. Gas Leakage from Cryogenic Fuel Tanks

With present technology, it is practically impossible to make large tanks for liquid hydrogen with gas-tight welds. The leak rates from large tanks may be so high that the performance of multilayer insulations will be seriously degraded unless proper allowance can be made in the design of the thermal protection system. Similar problems may arise when the helium-purged gas is vented.

i. Minimum Heat Flux Through a Stack of Perforated Radiation Shields

The analysis of the minimum heat flux through a series of perforated radiation shields can be based on the preceding calculations, and the heat transfer rates due to both conduction and radiation can be obtained for any given value of the perforation coefficient τ. It is clear that the total heat flux must pass through a minimum as τ varies from 0 to 1, since the radiation is very large when τ is near unity and the conduction is very large when τ is near zero. It is, therefore, of interest to find that best value of τ and the corresponding minimum value of the flux.

The flux due to gas conduction near the cold side of the stack of shields, where the gas density is highest, is, from Equations IV-A-10 and IV-A-11,

$$q_c = \frac{3}{2} \frac{n^2 \nu (1 - \tau) k \Delta T}{\tau}$$

where ΔT is the temperature difference across a single gap. We will make no appreciable error in assuming that this expression holds over the whole set of shields, since the effect of conduction is negligible except near the cold side of the stack, due to the rapidity with which the radiation factor σT^4 rises with T.

The radiation rate can be written with sufficient accuracy, from equations IV-A-21, 22, and 23, as

$$q_r = \frac{\epsilon + (2 - \epsilon)\tau}{\tau} \sigma \Delta T^4$$

where ΔT^4 refers to one gap. We have omitted the 1 in the denominator of equation IV-A-22 to facilitate further calculations. Since n is large and ϵ' small, this makes no appreciable difference.

The sum of these two expressions is the total flux q across a given gap and is a difference equation in ΔT and ΔT^4. When this

equation is summed over all the gaps and the result divided by n, we obtain for the total flux

$$q = \frac{\epsilon + (2 - \epsilon)\,\tau}{(2 - \epsilon)\,(1 - \tau)} \cdot \frac{\sigma (T_2^4 - T_1^4)}{n} + \frac{3}{2}\,\nu k (T_2 - T_1) \cdot \frac{(1 - \tau) n}{\tau}$$

$$= \frac{\sigma (T_2^4 - T_1^4)}{\left(\frac{2}{\epsilon} - 1\right) n} + \left(\frac{2}{2 - \epsilon}\right) \sigma (T_2^4 - T_1^4) \cdot \frac{\tau}{(1 - \tau) n} + \frac{3}{2}\,\nu k (T_2 - T_1) \cdot \frac{(1 - \tau) n}{\tau}$$

(IV-A-24)

The first term in equation IV-A-24 is the radiation flux without perforations. The second term is the increase in radiation due to the perforations. The third term is the flux due to conduction by the gas molecules in the spaces between the shields.

For any fixed value of n, this expression goes through a minimum for a certain value of the perforation coefficient τ. The optimum value of τ is given by

$$\frac{\tau}{1 - \tau} = n \left[\frac{\frac{3}{2}\,\nu k (T_2 - T_1)}{\sigma (T_2^4 - T_1^4)} \left(\frac{2 - \epsilon}{2}\right) \right]^{1/2} \qquad \text{(IV-A-25)}$$

The corresponding minimum value of q is

$$q_{min}(n) = \frac{\sigma (T_2^4 - T_1^4)}{\left(\frac{2}{\epsilon} - 1\right) n} + \left[6\,\nu k (T_2 - T_1)\,\sigma (T_2^4 - T_1^4) \left(\frac{2}{2 - \epsilon}\right) \right]^{1/2} \qquad \text{(IV-A-26)}$$

Equation IV-A-26 shows that, no matter how large n may be, the flux can never be less than the value

$$q_{min}(\infty) = \left[6 \nu k (T_2 - T_1) \sigma (T_2^4 - T_1^4) \left(\frac{2}{2 - \epsilon}\right) \right]^{1/2} \qquad \text{(IV-A-27)}$$

Table IV-A-1 shows how $q_{min}(\infty)$ depends on the outgassing rate under the following conditions:

$$T_2 = 300^{\circ}K$$

$$T_1 = 25^{\circ}K$$

$$\epsilon = .05$$

$$k = 1.38 \times 10^{-16} \text{ erg deg}^{-1}$$

For comparison, when n = 100, the first term in Equation IV-A-26 is 118 erg cm^{-2} sec^{-1}.* This value corresponds to the optimum heat flux for an interplanetary mission, with only radiation transfer through the shield. Table IV-A-1 indicates that this optimum flux cannot be obtained with practical shielding if the outgassing rate is higher than 10^{10} molecules cm^{-2} sec^{-1}.

TABLE IV-A-1

MINIMUM HEAT FLUX AS A FUNCTION OF OUTGASSING RATE

Outgassing Rate (molecules cm^{-2} sec^{-1})	$q_{min}(\infty)$ (erg cm^{-2} sec^{-1})	Watts/ft^2 x 10^2
10^{10}	33	0.31
10^{11}	105	0.95
10^{12}	330	3.1
10^{13}	1,050	9.5

The flux q, as given by equation IV-A-24, is plotted in Figure IV-A-4 in Btu/ft^2-hr as a function of the perforation factor $\mathcal{T}$ for various assumed values of the hydrogen gas flow rate ν_o (expressed in

* 118 erg cm^{-2} sec^{-1} = 1.09×10^{-2} watts/ft^2.

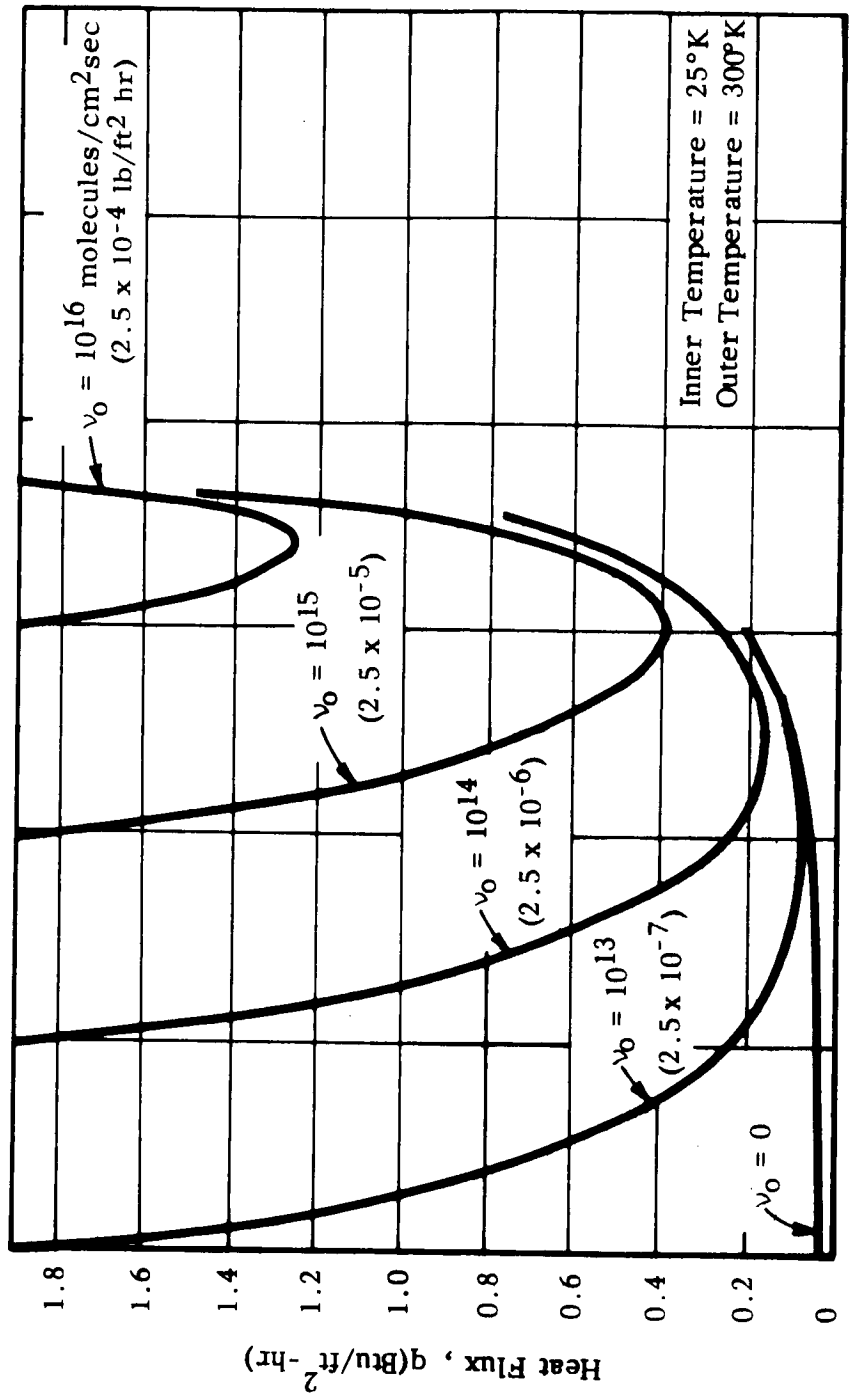

FIGURE IV-A-4 HEAT FLUX THROUGH 100 PERFORATED SHIELDS AS A FUNCTION OF PERFORATION FACTOR FOR VARIOUS HYDROGEN GAS FLOW RATES

both molecules/cm^{-2} -sec and lb/ft^2-hr). The graph refers to the case of 100 shields of emissivity 0.05, with outer and inner temperatures of 300°K and 25°K, respectively.

Figure IV-A-4 shows that an optimum perforation factor exists for any given gas flow rate. Table IV-A-2 gives the optimum value of τ and the corresponding minimum heat flux q for various values of the gas flow rate ν_o. The table shows that a hydrogen flow rate of 2.5×10^{-7} lb/ft^2-hr impairs the insulation by a factor of about two. This leakage rate corresponds to only 1 lb per year from a tank of 500 ft^2 surface area.

TABLE IV-A-2

OPTIMUM PERFORATION FACTOR τ_{opt} AND MINIMUM HEAT FLUX q_{min} FOR VARIOUS GAS FLOW RATES ν_o

ν_o ($lb\ H_2/ft^2$- hr)	τ_{opt}	q_{min} (Btu/ft^2 - hr)
0	0	0.04
2.5×10^{-7}	0.01	0.07
2.5×10^{-6}	0.03	0.14
2.5×10^{-5}	0.11	0.38
2.5×10^{-4}	0.27	1.24

For the leakage rate of 2.5×10^{-4} lb/ft^2-hr, which corresponds to a loss of 3 lb/day from the 500 ft^2 tank, the total heat input is 600 Btu/hr, which would boil off all the hydrogen in two months. Actual leak rates may be even larger than 3 lb/day.

These calculations indicate clearly that the gas leaking through the seams of the tank should not be pumped by the external vacuum through the insulating blanket. Instead, the gas should be vented directly to the external vacuum by means of a double-walled arrangement, shown schematically in Figure IV-A-5. The leakage of gas into the insulating layers will be greatly reduced if the outer tank wall is reasonably gas-tight.

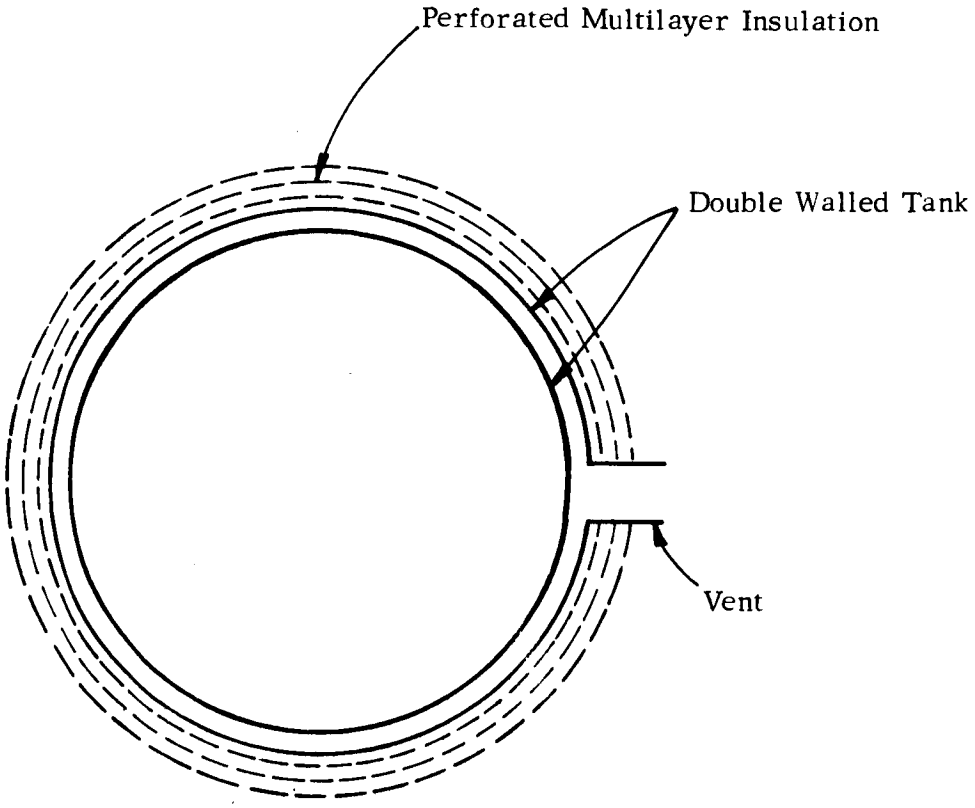

FIGURE IV-A-5 DIRECT VENTING OF LEAKING GAS BY DOUBLE-WALLED TANK CONSTRUCTION

The vent pipe will probably have to extend well beyond the insulation to prevent diffusion of the vented gas back into the perforated shields from the outside. The static pressure at the exit of a pipe of cross section 1 cm^2 that transmits 3 pounds of hydrogen per day is about 5 mm-Hg; thus, aerodynamic rather than free molecular flow occurs at the exit.

A much better solution to the gas conduction problem than the double-walled tank arrangement would, of course, be the development of a method for making vacuum-tight welds. It is likely that successful long-term cryogenic storage in space will depend on this development.

The configuration of the perforations in the multilayer insulation is of considerable importance. For a given perforation ratio, the highest gas-pumping performance, relative to the inward radiation leakage, is obtained with a large number of small holes with an average spacing much less than the shield separation. This perforation arrangement was assumed in the derivation of Equation IV-A-24. The reason why this is the best arrangement is that the net flow pattern for both gas molecules and radiation is then in the form of straight lines perpendicular to the shields, except in the immediate vicinity of the shields themselves. The two flow patterns are illustrated in Figures IV-A-6 and -7. The only difference is that some of the radiation flow lines start and terminate on unperforated parts of the shields, whereas the molecular flow lines cannot do this.

On the other hand, when the perforations are widely spaced relative to the shield separation, as in Figures IV-A-8 and -9, the radiation flow is much more nearly perpendicular to the foils than is the gas flow. The reason is that the gas can flow only through the holes, whereas the radiation can also flow directly through the non-perforated regions by the process of absorption on one side of a foil and re-emission on the other side. Since the gas must take longer paths through the foils than the radiation, the pumping efficiency, relative to the radiation leakage, is much less for very widely spaced holes.

Calculation of the flow patterns of Figures IV-A-8 and -9 would be very difficult; but one can see qualitatively that not much change from the conditions of Figures IV-A-6 and -7 will occur if the hole spacing is of the same order as the shield spacing. On the other hand, for very large hole spacings, the gas flow rate approaches zero, while the radiation rate drops to a limiting value. For the case of regularly spaced holes that are staggered from shield to shield as in Figures IV-A-8 and -9, the radiation flux has the limiting value:

$$q = \frac{\sigma (T_2^4 - T_1^4)}{n \left(\frac{2}{\epsilon} - 1\right)\left(\frac{1}{1 + 2\tau}\right) + 1} \qquad \text{(IV-A-28)}$$

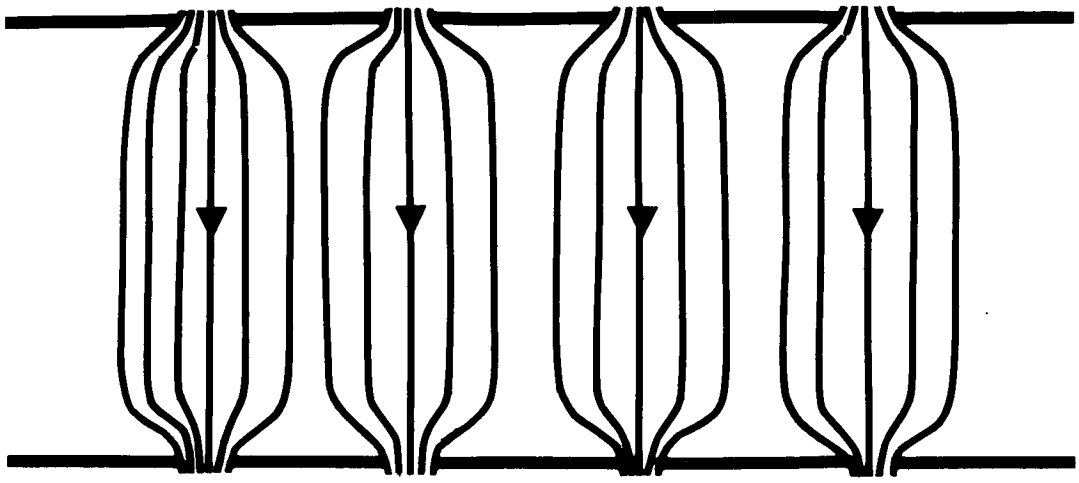

FIGURE IV-A-6 GAS FLOW PATTERN FOR CLOSELY SPACED PERFORATIONS

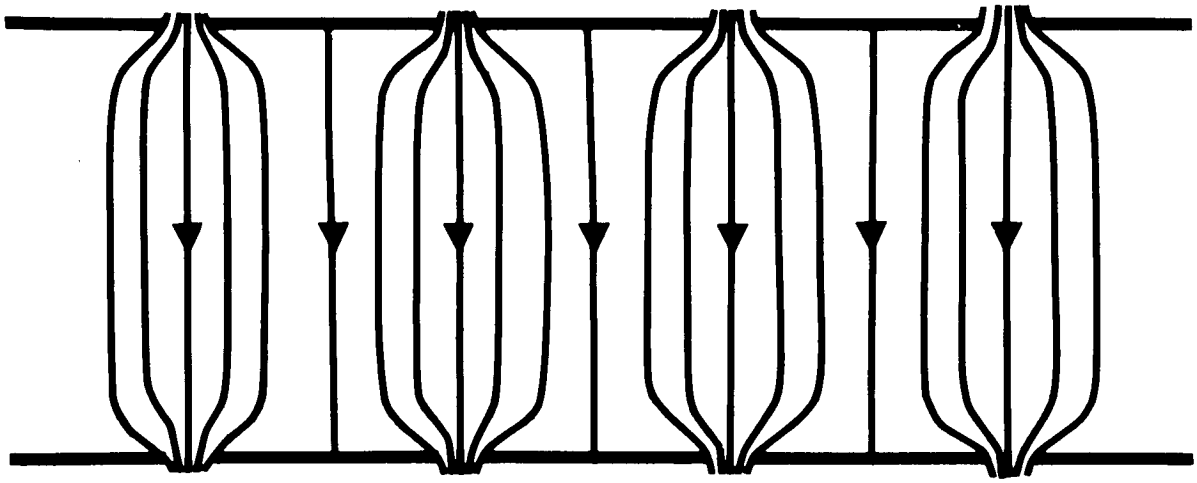

FIGURE IV-A-7 RADIATION FLOW PATTERN FOR CLOSELY SPACED PERFORATIONS

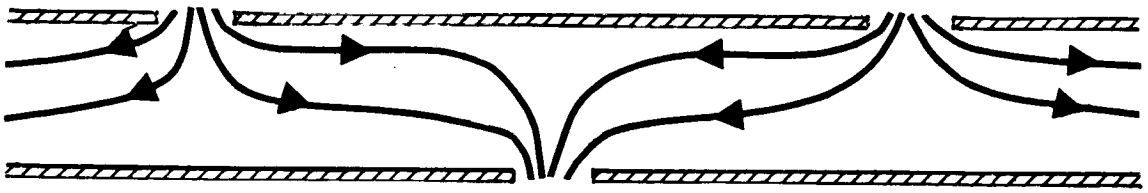

FIGURE IV-A-8 GAS FLOW PATTERN FOR WIDELY SPACED PERFORATIONS

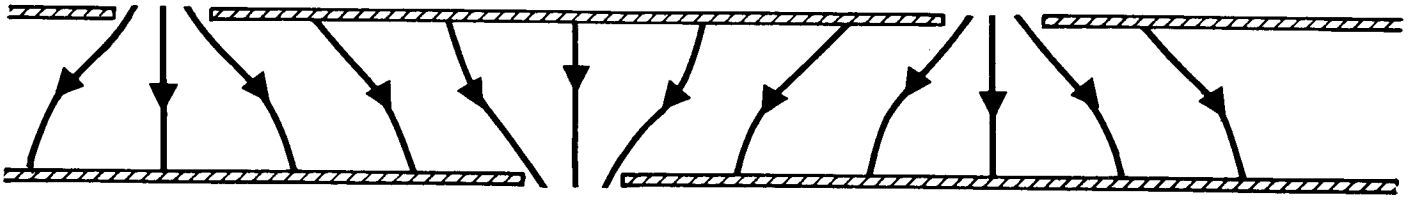

FIGURE IV-A-9 RADIATION FLOW PATTERN FOR WIDELY SPACED PERFORATIONS

For randomly distributed holes the limit is

$$q = \frac{\sigma (T_2^4 - T_1^4)}{n \left(\frac{2}{\epsilon} - 1\right)\left(\frac{1 - \tau}{1 + \tau}\right) + 1} \qquad \text{(IV-A-29)}$$

For small values of τ these two expressions are almost identical.

On the other hand, the radiation flux for closely spaced holes, as shown in Equation IV-A-22, is:

$$q = \frac{\sigma (T_2^4 - T_1^4)}{n \left[\frac{2}{\epsilon + (2 - \epsilon)\tau} - 1\right] + 1} \qquad \text{(IV-A-30)}$$

A comparison of (IV-A-29) and (IV-A-30) shows that, for constant τ, the radiation flux increases considerably as the hole spacing is decreased, but the gas conduction flux decreases by a still larger amount.

Production problems impose a practical lower limit on the diameter of the perforations as well as their spacing. New production techniques will have to be devised to obtain the desired perforations and thus increase the insulating performance of multilayer insulations in an actual installation.

d. Venting During Ascent

Multilayer insulation may be immersed in a non-condensable gas at a pressure of one atmosphere at launch. As the vehicle ascends through the atmosphere the interstitial gas vents to a milieu of constantly reducing pressure. Accordingly, during ascent a pressure gradient from inside-to-outside exists within the foil system and the question arises as to the ability of the insulation system to withstand these differences without damage. The analysis presented in Appendix C is intended to shed some light on the nature of this problem, and to provide some guidance to the design of experiments which should be made to prove the adequacy of the insulation system to withstand ascent decompression.

e. Solid Conduction

The concept of radiation shielding with radiative heat transfer dominating implies the absence of mechanical contact between adjacent foils or between foils and spacers. Contact will occur when mechanical pressure is applied in the direction normal to the tank wall. This

pressure is due to gravity, differential thermal contraction, stressing on application, or externally applied loading.

The effect of mechanical load on the density and thereby on the heat flux through a sample of a multilayer insulation is of considerable practical significance. An increase in mechanical load will cause the radiation shields and spacers to be compressed into a thinner sandwich of higher density. A subsequent decrease in mechanical load will allow the radiation shield and spacers to return to their original density, provided that no permanent deformation has taken place.

We examined the capability of several insulation systems to withstand compressive mechanical loading.

The results of the tests, which appear in Figure IV-A-10 illustrate the following:

As the mechanical load increases, the solid-conduction contribution to heat transfer becomes dominant.

The differences in heat flux at zero load are the result of differences in the spacer materials. Spacers consisting of oriented fibers have a high contact resistance, which impedes solid conduction. With no external load on the insulation, the closeness of the packing of these fibers (and hence the contact resistance) depends upon the previous history, such as number of load applications, method of manufacture, and storage conditions.

2. Conclusions from Experimental Evidence

Experiments both with the thermal conductivity apparatus and with an insulated tank system (see Section IV-F) show that it is possible to design and apply multilayer insulation so that radiation is indeed the dominant mode of heat leakage into the tank. Therefore, the concept of idealized MLI as defined on page IV-1 is realistic.

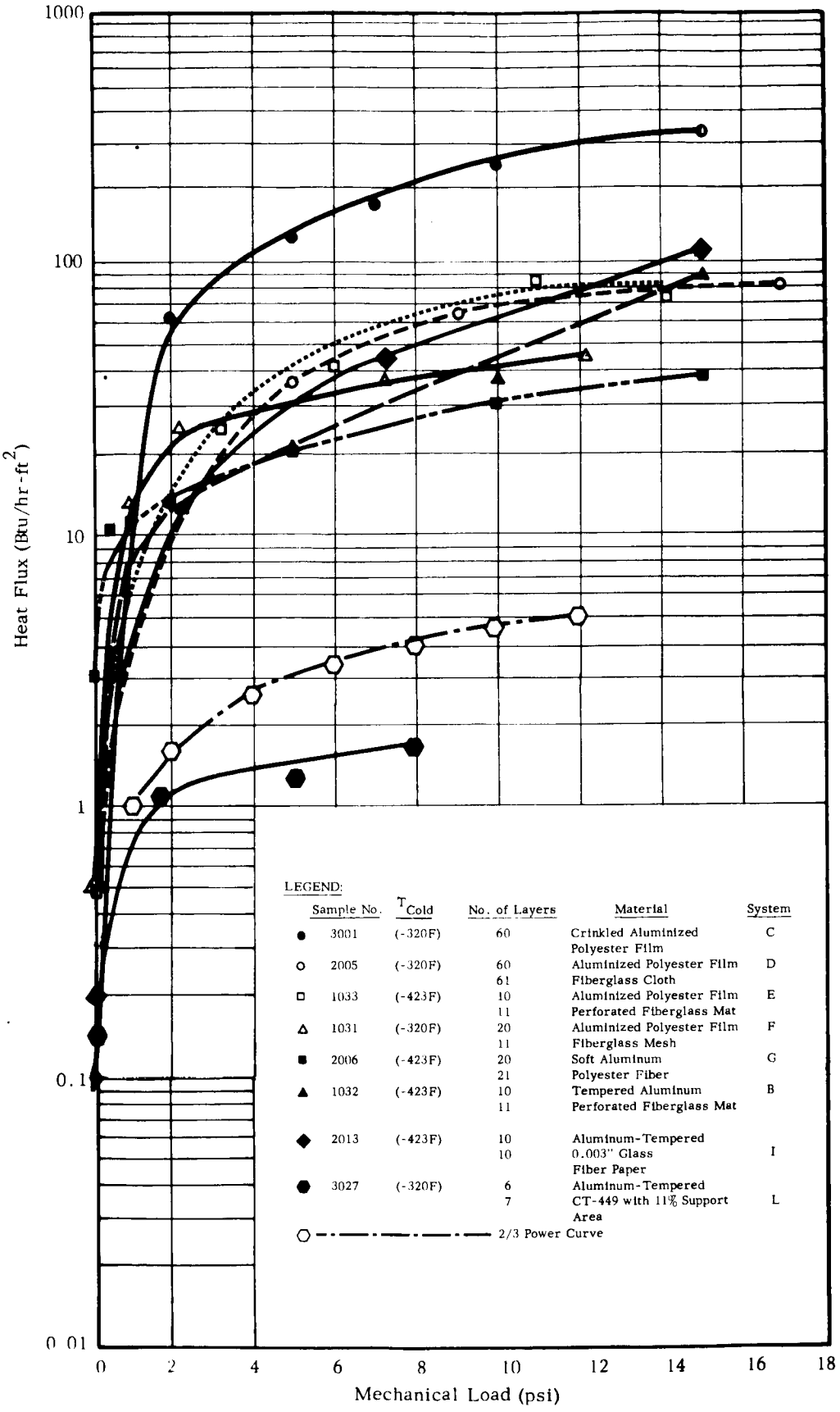

FIGURE IV-A-10 EFFECT OF MECHANICAL LOADING ON HEAT FLUX THROUGH MULTILAYER INSULATIONS

3. Concepts Based on Truly Radiative Shielding

Consider a portion of the surface of a cryogenic liquid tank covered with multilayer insulation having uniform thermal radiation of intensity I incident upon its outer foil. A steady-state heat balance equation may be written, equating the absorbed incident power to the sum of the re-radiated and tank input powers, in terms of temperatures and radiative properties;

$$\alpha_o I = \sigma \epsilon_o T_s^4 + (Q/A)_{tank} \qquad \text{(IV-A-32)}$$

where α_o is the absorptivity of the outer foil surface for the incident radiation, ϵ_o is the emissivity of that surface and T_s is its temperature. The terms in the equation all have units of power per unit of surface area.

a. Adiabatic Wall Temperature

Suppose the last term in Equation (IV-A-32) were zero; this is the so-called adiabatic case, in which all absorbed incident power is re-emitted. From the simplified equation, the temperature at which this emission occurs can be calculated; let this be T_a. Then from (IV-A-32),

$$T_a^4 = \frac{\alpha_o I}{\epsilon_o \sigma} \qquad \text{(IV-A-33)}$$

The concept of an adiabatic wall temperature is extremely useful in evaluating the heat flow into a tank, even in cases where the incident flux is not uniform, or when the foils are not pure radiators but also conduct heat through contacts and penetrations, as will be seen later. At this point we still consider the simplifying conditions to introduce another concept.

b. Shielding Factor

From the definition of T_a, Equation (IV-A-33), we re-write (IV-A-32):

$$\sigma \epsilon_o (T_a^4 - T_s^4) = (Q/A)_{tank} \qquad \text{(IV-A-34)}$$

But for pure radiating foils in a uniform environment, an expression can be found and substituted for $(Q/A)_{tank}$:

$$\sigma \epsilon_o (T_a^4 - T_s^4) = \frac{\sigma (T_s^4 - T_{liq}^4)}{\left(\frac{2}{\epsilon} - 1\right) n} \qquad \text{(IV-A-35)}$$

where ϵ is the emissivity of the foils (assumed independent of temperature) n is their number, and T_{liq} the liquid tank temperature.

For cases of interest, (i.e., T_{liq} a cryogenic temperature), $T_a^4 \ll T_s^4$. Also, $\epsilon < 0.05$, so that $2/\epsilon \gg 1$. Therefore (IV-A-35) can be simplified to

$$(T_a^4 - T_s^4) = \frac{\epsilon}{2n\epsilon_o} T_s^4 \equiv K T_s^4 \qquad \text{(IV-A-36)}$$

Solving for T_s we find

$$T_s^4 = \frac{T_a^4}{1 + K} \qquad \text{(IV-A-37)}$$

We also have

$$T_a^4 - T_s^4 = \frac{K}{1 + K} T_a^4 \qquad \text{(IV-A-38)}$$

a relation that can be substituted into (IV-A-34) to obtain

$$(Q/A)_{tank} = \frac{K}{1 + K} \epsilon_o T_a^4 \qquad \text{(IV-A-39)}$$

which, from the definition of T_a, can be written

$$(Q/A)_{tank} = \frac{K}{1 + K} \alpha_o I \qquad \text{(IV-A-40)}$$

The pure number, K, is generally very small. For example, with $\epsilon = 0.05$, $n = 30$, $\epsilon_o = 0.8$, K is about 0.001. This means, first of all, that it can be neglected compared with unity. Once this is done, the physical significance of K becomes evident. It is the reciprocal of a shielding factor. This is clear from the last equation, which states that the heat flux into the tank equals the absorbed flux divided by the shielding factor. Also, from Equation (IV-A-38) we see that the outer foil temperature is very nearly equal to the adiabatic temperature:

$$\frac{T_a^4 - T_s^4}{T_a^4} = \frac{K}{1 + K} \cong K \qquad \text{(IV-A-41)}$$

4. Parallel Spreading of Disturbances

The spreading of disturbances brings into play the ratio of thermal conductivities parallel and perpendicular to the foils. The concept of conductivity, in either of these directions, has to be applied with some care. First it is necessary to consider as a continuum a set of discrete foils separated by spacers and/or vacuum; of course, this can be justified when enough foils are involved. An

effective parallel (i.e., in the plane of the foils) conductivity may then be defined in terms of some mean foil material conductivity, thickness and number density. A similar statement may be made about an effective perpendicular conductivity, except for the strong temperature dependence and hence variation in a direction normal to the foils, of a conductivity so defined, especially for foils that act as true radiation shields (i.e., without conductive contacts between foils and/or spacers).

In spite of the complication just outlined, it has been found most useful in discussing the spreading of temperature perturbations to use the concept of effective conductivities in the two perpendicular directions, defined by over-all behavior, although this concept will not be useful for other applications (e.g., in defining shielding factors). We define these quantities as $k_{\parallel}$ and $k_{\perp}$.

In the discussion presented in Chapter IV-A-3, the behavior of insulation was treated as a uni-dimensional problem, with distance normal to foils as the independent variable. We define a disturbance as a deviation from this uni-dimentionality; this definition implies parallel conduction and some non-uniformity causing such conduction.

There are two main causes giving rise to parallel conduction: variation in incident flux over various portions of the tank surface, and penetrations due to piping, structural supports, seams, etc. This is illustrated in Figure IV-A-11. The first can introduce local parallel variations in T_a (and hence in foil temperature) over the tank; the second can introduce local sources of variations in foil temperature, which can spread over the tank surface to distances that depend on the ratio $k_{\parallel}/k_{\perp}$. This spreading is discussed in Appendix D.

There is another basic difference between these two main causes. Variation in surface flux can spread less in depth because the heat transfer coupling between foils is mainly radiative, and, inherent to the design of the multifoil insulation, the coupling between foils is made weak, whereas the conductance parallel to the foils is relatively large. Therefore the spreading of the effect is localized to outer layers. In the case of penetrations, all the foils are involved in the temperature perturbation, by thermal contact at the material penetration (e.g., at a pipe). Therefore, parallel conduction involves all the foils in this case. One exception to this is the gap, which is a discontinuity in the insulation that leads to additional heat leaks by radiation alone.

The discussion of Appendix D leads to the conclusion that the distance of perturbation decay is

$$X_{decay} \sim B\sqrt{\frac{k_{\parallel}}{k_{\perp}}} \qquad \text{(IV-A-42)}$$

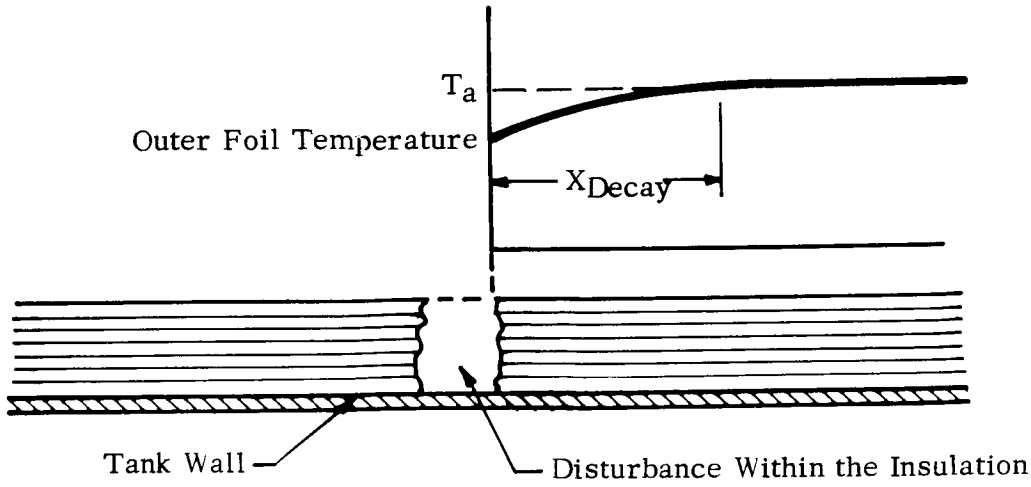

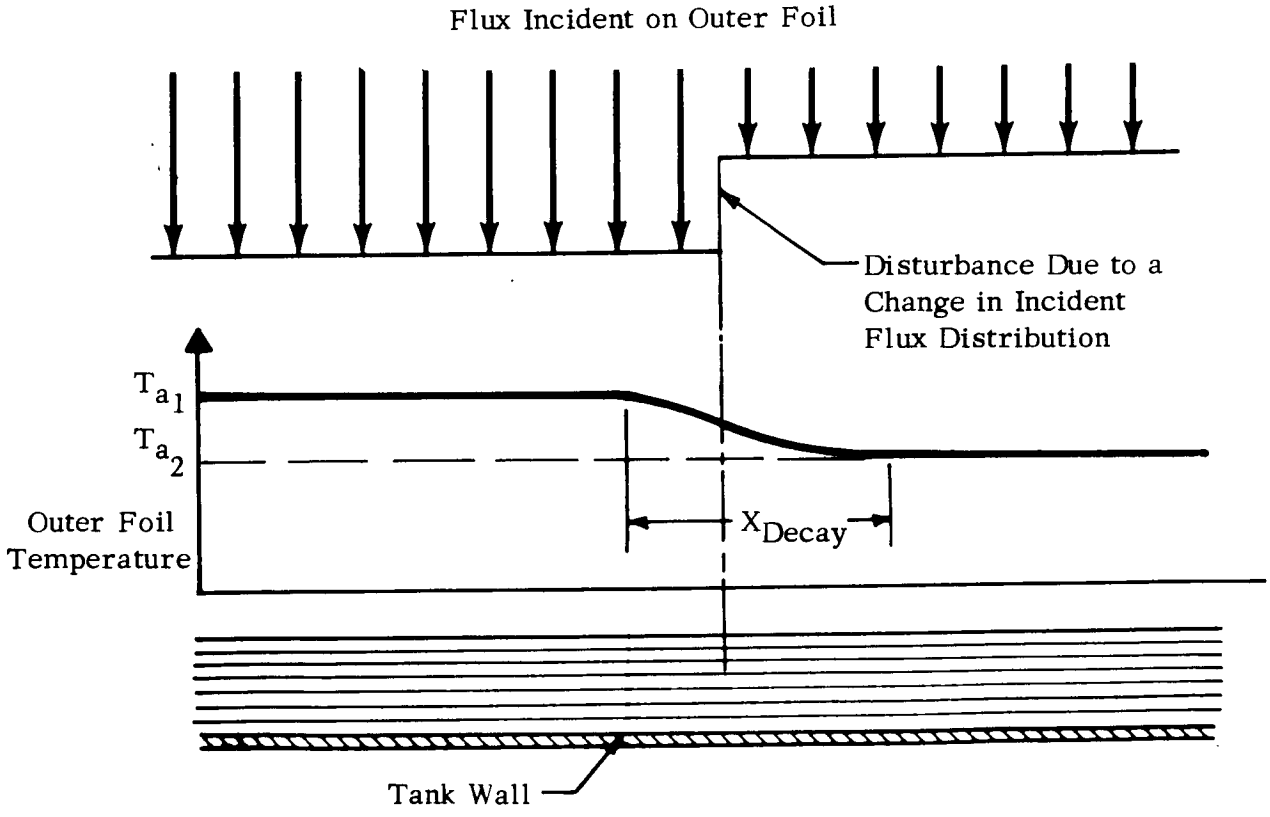

FIGURE IV-A-11 SPREADING OF DISTURBANCES IN MULTILAYER INSULATION

Now if we define the two conductivities according to the concepts introduced in this section:

$$k_{//} \equiv k_f t_f \, n/B \qquad \text{(IV-A-43)}$$

$$k_{\perp} \equiv \text{(measured constant)} \; \frac{B}{n} \qquad \text{(IV-A-44)}$$

where k_f is the conductivity of foil materials

t_f is the thickness of the foils

n is the number of foils

B is the thickness of insulation

Note that n/B has a limit imposed by the desirability of avoiding large conductive heat flow to the tank (viz. Figure IV-A-10). From the last three equations we can express the decay distance as

$$X_{decay} = \text{(constant)} \; n\sqrt{k_f t_f} \qquad \text{(IV-A-45)}$$

When the foils act as pure radiators at a constant emissivity ϵ, the constant can be evaluated, to give, approximately,

$$X_{decay} = n\sqrt{\frac{2k_f t_f}{\sigma \epsilon T_s^3}} \qquad \text{(IV-A-46)}$$

Where T_s is the outer foil temperature.

The last equation illustrates a weakness of the concept as applied to pure radiation foils: assuming T_s given, the local value of $k_{\perp}$ varies as T^3_{foil} and the local X_{decay} varies as $T_{foil}^{-3/2}$. The last formula implies that X_{decay} is the same for all foils, whereas it will be longer for the colder foils. Nevertheless, even for pure radiation foils the decay distance varies directly as $n\sqrt{k_f t_f}$. The idea of using an effective n suggests itself; this corresponds to the physical phenomenon previously alluded to, namely, that only a portion of the foils, near the top, participate in conducting heat absorbed from the radiation environment toward a penetration or toward a region of less intense incident radiation.

The expression in equation (IV-A-46) assumes a much more precise meaning in the analysis of thermal shorts though pure radiation foils, given in Appendix F.

5. General Effect of Conduction on MLI Performance.

It is of interest to determine the effect of the internal perpen-

dicular conduction component within foils, due to compressive contacts, large numbers of small attachment pins or threads, etc., which are not truly thermal shorts leading to local temperature perturbations, but are disposed throughout the insulation and have an effect everywhere within the insulation. In particular, it is important to ascertain whether these will cause an appreciable change in the temperature of the outer foil. To form some idea of this effect we consider a blanket of insulation in a uniform radiation environment, hence, once again a uni-dimensional situation.

In the absence of such conductive elements we have, as in Equation (IV-A-34), for pure radiation heat transfer through the foils.

$$\sigma \epsilon_o (T_a^4 - T_{s_o}^4) = (Q/A)_{rad} \qquad \text{(IV-A-47)}$$

In the presence of the conductive elements we must add a term to the right-hand side of this equation:

$$J \epsilon_o (T_a^4 - T_s^4) = (Q/A)_{rad} + (Q/A)_{cond} \qquad \text{(IV-A-48)}$$

By subtraction we obtain

$$J \epsilon_o (T_{s_o}^4 - T_s^4) = (Q/A)_{cond} \qquad \text{(IV-A-49)}$$

A combination of (IV-A-37, 39) gives

$$(Q/A)_{rad} = \eta J \epsilon_o T_{s_o}^4, \qquad \text{(IV-A-50)}$$

which, by division into (IV-A-49) gives

$$\frac{Q_{cond}}{Q_{rad}} = \frac{T_{s_o}^4 - T_s^4}{\eta T_{s_o}^4} \qquad \text{(IV-A-51)}$$

In these equations T_s and T_{s_o} are the outer foil temperature with and without the conductive component, respectively.

As an example, consider 20 foils of emissivity 0.04, with ϵ_o equal to unity; then η equals 0.001. To produce a one-percent change in the fourth power of the outer foil temperature (or one-quarter

percent change in its first power), the conductive heat leak must be ten times as large as the radiative heat leak; this would hardly be tolerated. The required ratio of conductive to radiative heat leak increases with the number of foils.

We conclude that in a properly designed system the internal conductive component of heat leak through foils will not alter the outer foil temperature appreciably.

6. Effect of Variable Foil Emissivity

The emissivity of the foils is temperature-dependent. This dependence is not usually taken into account, the function $\epsilon(T)$ being rather uncertain in the absence of laboratory-controlled surface purity. Hence, an estimate of the error involved in assuming ϵ to be constant is useful. To obtain such an estimate we assume a power dependence, which is reasonable according to theoretical and experimental results reported in the literature. (7,8)

Let the outer foil temperature of multilayer insulation on a tank be T_1, and the tank temperature T_o, and let this be true out to large distances (uni-dimensional case). We have, for the heat flow between two adjacent foils, a and b:

$$Q = \frac{\sigma (T_a^4 - T_b^4)}{\frac{2}{\epsilon} - 1}$$

$$\simeq \frac{\sigma \epsilon}{2} (T_a^4 - T_b^4)$$

$$= \frac{\sigma \epsilon}{2} \Delta (T^4) \qquad \text{(IV-A-52)}$$

When the number n of foils is large, it is a good approximation to write

$$\Delta (T^4) = 4 T^3 \Delta T \qquad \text{(IV-A-53)}$$

so that

$$Q = 2 \sigma \epsilon T^3 \Delta T \qquad \text{(IV-A-54)}$$

If we now assume a power dependence for ϵ,

$$\epsilon = \epsilon_1 (T/T_1)^{\ell} \qquad \text{(IV-A-55)}$$

where ϵ_1 is the emissivity at temperature T_1, then

$$Q = \frac{2\pi\epsilon_1}{T_1^{\lambda}} T^{(3+\lambda)} \Delta T \qquad \text{(IV-A-56)}$$

The differential process can now be reversed to give

$$Q = \frac{2\pi\epsilon_1}{(4+\lambda)T_1^{\lambda}} \Delta (T^{(4+\lambda)}) \qquad \text{(IV-A-57)}$$

At steady-state, the same amount of heat flows across each space between foils, so that equations similar to (IV-A-57) can be added once for each space, namely n times:

$$n\,Q = \frac{2\pi\epsilon_1}{(4+\lambda)T_1^{\lambda}} (T_1^{4+\lambda} - T_o^{4+\lambda})$$

or

$$Q = \frac{2\pi\epsilon_1}{(4+\lambda)n} T_1^4 \left[1 - (T_o/T_1)^{4+\lambda}\right] \qquad \text{(IV-A-58)}$$

Now if the emissivity were constant at a value ϵ_1, (i.e., if λ were zero), we would have

$$Q_{\lambda=0} = \frac{\pi\epsilon_1}{2n} T_1^4 \left[1 - (T_o/T_1)^4\right] \qquad \text{(IV-A-59)}$$

At cryogenic temperatures, the second term in brackets of both (IV-A-58) and (IV-A-59) can be neglected. Hence, we can form the ratio

$$\frac{Q_{\lambda=0}}{Q_\lambda} = \frac{4+\lambda}{4} = 1 + \frac{\lambda}{4} \qquad \text{(IV-A-60)}$$

If the number of foils were truly infinite, the results above would be exact. It is seen that the fractional error is $\lambda/4$. Common values for λ are between one-half and unity, giving an error between 12 to 25%.

Of course, if the emissivity is assumed constant at some intermediate value, the error can be reduced; in fact, the value of ϵ_1 can be so chosen that the error is eliminated.

7. Thermal Diffusion in Superinsulation

The transients in superinsulation will be highly complex, involving as they do radiation and conduction (gas as well as solid), in a truly three-dimensional medium. However, it is our purpose to consider here only simple concepts such as diffusion parallel and transverse to the insulation foils. In particular, we wish to form an estimate of the transient time for heat flow in each of these two directions.

The transient time may be characterized by τ:

$$\tau \simeq X^2/a_t \qquad \text{(IV-A-61)}$$

where X is a characteristic dimension in the direction of heat flow, a_t is the thermal diffusivity of multifoils in that same direction.

a. Diffusion Parallel to Foils

For flow parallel to foils the characteristic dimension will be the tank size, for instance the diameter D of a spherical tank. The transient time will be

$$\tau_{\parallel} = \frac{D^2}{a_{foils}} = \frac{D^2 \rho_f c_f}{k_f} \qquad \text{(IV-A-62)}$$

where the subscript f refers to foil materials. ρ, c and k are density, heat capacity and thermal conductivity, respectively. For pure aluminum foils, the transient time has the order of magnitude

$$\tau_{\parallel} \doteq 2\,(D/_{10})^2 \text{ days} \qquad \text{(IV-A-63)}$$

where D is in feet. Note that neither the thickness nor the number of foils enters into the relationship.

b. Diffusion Normal to Foils

For flow across the foils the characteristic dimension will be the thickness B of the insulation. The density and normal conductivity of foils are

$$\rho = \rho_f\, t_f n/B \qquad \text{(IV-A-64)}$$

where t_f is the foil thickness; and

$$k_{\perp} = \frac{\sigma \epsilon T^3 B}{2n} \qquad \text{(IV-A-65)}$$

so that the characteristic time may be expressed as

$$\tau_{\perp} = \frac{2n^2}{\sigma \epsilon T^3} \rho_f c_f t_f$$

where T is some characteristic temperature, say that of the outer insulation foil, T_s. For pure aluminum foils with $T_s = 300^{\circ}K$, $\epsilon = 0.04$, $t_f = 0.001$ inch, we have, approximately,

$$\tau_{\perp} = n^2 \text{ hours} \qquad \text{(IV-A-66)}$$

This estimate is undoubtedly rough, since k varies as T^3 within the insulation.

8. Comments Regarding the Location of Multilayer Insulation

In the present report as in other works, multilayer insulation is considered as being applied directly on a cryogenic tank, implying that that location is the best. Such may not be the case in a shrouded tank. An alternative location is on the inside of the shroud, as illustrated in Figure IV-A-12.

Placing the insulation inside the shroud and away from tanks, with the tanks left bare, is not expected to decrease the heat flow through the insulation blanket. However, it does offer several advantages:

a. Simplicity

Manhole covers and other protuberances that must remain accessible on the launch pad need not be covered with foils, eliminating the necessity for complex joints in insulation.

b. Ground-hold

If the shroud is made reasonably (not absolutely) gas-tight, the volume between tank and shroud can be filled with helium slightly above one atmosphere, with a controlled slow leak to the atmosphere, to prevent condensation of air components on the tank. It is possible that some amount of insulation (e.g., foams) will be required at the shroud to prevent condensation there.

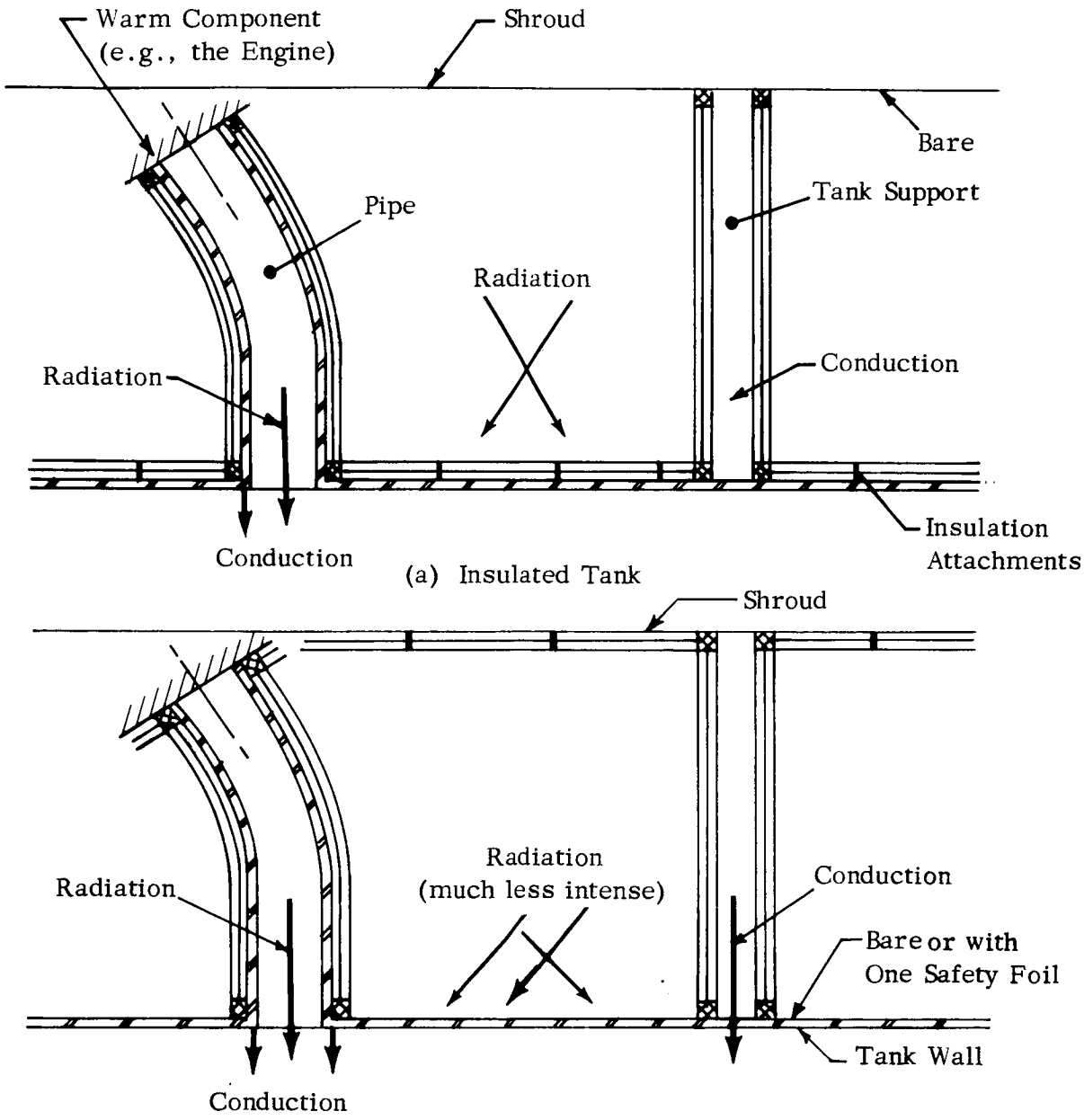

FIGURE IV-A-12 TWO ALTERNATIVE METHODS OF INSULATING A SHROUDED TANK (SCHEMATIC ILLUSTRATION)

c. Ascent

With a gas-tight shroud, ascent decompression can be controlled without an excessive amount of perforation in the foils (see chapter IV-A-1 and Appendix C).

d. Venting During Space Storage

Any leaks through the cryogenic tank walls can be vented to space without going through the insulation and degrading its performance. Of course, the effect of foil outgassing remains.

e. Payload Factor Improvement

It is possible to jettison all insulation and all structure no longer needed, just prior to the terminal maneuver in which the stored propellant is to be used. It is known [9] that such a procedure leads to important improvements in payload factor.

f. Others

Other advantages are: better control over contact stresses between foils due to differential thermal contraction; a decrease in heat flow through insulation attachments and other internal penetrations because of the smaller temperature difference. (The innermost foil on the shroud would be at about $90^{\circ}K$.)

One problem associated with insulating inside the shroud is due to aerodynamic heating during ascent from earth. This problem is also present when the insulation is on the tank. Foam or other types of insulation placed just inside the shroud to prevent condensation can be designed for protection against aerodynamic heating as well (and jettisoned along with shroud and MLI prior to terminal maneuver if desired).

IV-B. MULTILAYER INSULATION AS A UNIFORM BLANKET OVER A TANK

We analyze in this section the behavior of insulation independently of major penetrations such as pipes and structural supports, but not independently of penetrations internal to the insulation, which affect the behavior of the latter in its detail, and can be considered to form part of it. The reason for separating out the major penetrations has been suggested in preceding sections (viz., Section III) and anticipates Section IV-C, where it is shown that such major penetrations can be effectively decoupled from the insulation; when this is done, as it should be, these two major components can be analyzed separately to determine the heat-inleakage contribution of each, for a subsequent superposition.

Before proceeding to the general case of arbitrary distributions of incident power on the tank insulation, the simple case of uniform incident power, which is of some importance, will first be dealt with.

1. Uniform Incident Power--Any Foil System

Uniform incident thermal radiation flux intensity is more likely to occur in the presence of a shroud surrounding the tank. As previously suggested, such a shroud (i) will be necessary for protection against ascent aerodynamic heating and micrometeoroids in space; (ii) can easily be incorporated as part of the structure (from which the tanks can be supported); and (iii) permits considering the "insulated-shroud " alternative (see Section IV-A-8), which offers many advantages in the design, application, and behavior of MLI systems. A shroud, even though it receives a non-uniform space radiation flux over its outer surface, will tend, by multiple reflections within the tank-shroud space and by conduction along both the MLI foils and the shroud itself, to have an inner surface (i.e., facing the tank), at uniform radiosity; this will result in a more uniform flux incident on the tank insulation (see Appendix A). Another cause that tends to render the flux incident on the tank more uniform is the spinning or tumbling of a vehicle. It is probable that the incident power will not be perfectly uniform; however, uniformity may be assumed with acceptable accuracy in some circumstances represented by the above examples.

The calculation of the total heat flow to a tank through a uniformly irradiated insulation blanket is simple. In the case of pure radiation foils, use is made of the concepts of T_a and K developed in IV-A. Since T_a is uniform (if the ratio α_o/ϵ_o is uniform over the outer foil) the total heat flow will be

$$Q = A_{tank} \frac{K}{1+K} \alpha_o I \qquad \text{(IV-B-1)}$$

When there is conductive as well as radiative heat flow across the foils, use can be made of an experimentally determined thermal conductance $k_\perp$

$$k_\perp \equiv \frac{(Q/A)_{experimental}}{T_s - T_{liq}} \quad , \qquad \text{(IV-B-2)}$$

and the total heat flow is given by

$$Q = A_{tank}\, k_\perp\, (T_s - T_{liq}) \qquad \text{(IV-B-3)}$$

where, for the usual values of K,

$$T_s = \frac{T_a}{(1 + K)^{1/4}} \doteq T_a \qquad \text{(IV-B-4)}$$

2. Non-Uniform Incident Power--Pure Radiating Foils

a. Single Relationship Giving the Total Heat Flow

The analysis presented in Appendix E brings to light a most useful relationship (theorem) for the case of pure radiating foils in an incident flux environment of arbitrary distribution: the heat flow through the foils and into the cryogenic tank is independent of thermal conduction in the plane of the foils. That analysis assumes that there is no net radiative parallel flow in the spaces between foils. As mentioned in the opening statements of Section IV, this assumption is equivalent to another one, that the radiative view factor between adjacent foils is unity. For closely-spaced foils as contemplated for application in MLI for cryogenic space tanks, the assumption is very nearly correct. Calculations based on this assumption lead to predictions of detailed temperature distributions that are verified satisfactorily by experiment (see Section IV-F). Note again that the double assumption regarding MLI, i.e., only radiation normal, and only conduction parallel, implies a carefully designed and applied insulation system.

Based on the independence of the total heat flow on $k_\parallel$, that heat flow can be calculated simply according to the relationships given in Appendix E, or by assuming that $k_\parallel$ is either zero or infinite; the resulting total heat flow will be the same.

b. Calculation of the Temperature Distribution Within the Foils

The decoupling of thermal shorts, to be discussed in IV-C, does not eliminate the heat leak around the short entirely, though it renders the heat flow through the insulation and the short independent of one another. One part that remains dependent on the MLI temperature distribution is the heat flowing from the foils into the intermediate insulation employed to effect the decoupling. This part may have some importance, in which case it will be necessary to evaluate it; for this purpose, the temperature distribution in the locality of the short must be known. Usually this requires a calculation of the entire temperature field within the MLI.

The need for calculating the temperature field may also arise in the evaluation of heat flow through certain small internal penetrations which, although they do not interfere seriously with the assumption of pure radiation foils (and, therefore, allow the use of the theorem of Appendix E), still provide a contribution to the heat flow that must be evaluated. The evaluation of such heat leaks depends on first-power temperature differences rather than on fourth-power, and thus requires some knowledge of the temperature field.

The calculation of the temperature distribution within MLI in the general case will be discussed in Section IV-E. In addition, if certain scaling laws are obeyed (see Section IV-D), the temperature distribution within pure radiating foils around a tank can be deduced from the known (by test or calculation) distribution on another, geometrically similar tank in a geometrically similar radiation environment. Two simplifying conditions can occur, however, that may permit of a rapid calculation.

The distance for the decay of a perturbation was given as $B\sqrt{k_{\parallel}/k_{\perp}}$ in chapter IV-A-4. The ratio between this distance and a representative tank dimension D, can be used as a criterion in two extreme cases.

When $B\sqrt{k_{\parallel}/k_{\perp}}/D >> 1$, then for the purpose of calculating heat flow through penetrations, the foils may be taken to be isothermal. In such a case, a heat balance between the incident and re-radiated powers suffices to establish the value of the (isothermal) outer foil temperature $T_s = T_a$. This value is used as the warm-end temperature of the penetrations or decouplers.

When $B\sqrt{k_{\parallel}/k_{\perp}}/D << 1$, the foils may be assumed not to conduct in their own plane, and the value of T_s at a point is established from a heat balance between the local incident and local re-radiated powers at that point. In such a case, the calculation of the warm-end temperatures for the penetrations depends on a knowledge of the distribution

of incident power, which is a more demanding requirement than when $\frac{B}{D}\sqrt{k_{\parallel}/k_{\perp}} >> 1$. Nevertheless, for this case also, there is no need to calculate the entire temperature field within the MLI.

3. Non-Uniform Incident Power--Foils With Normal Conduction

If the conductive heat flow normal to foils cannot be neglected nor separated from the radiative heat flow, the problem of determining either the total heat flow or the temperature distribution becomes, in principle, much more difficult to solve. Usually in such cases (e.g., compressed foils) the "thermal conductance" of the conductive component is unknown, and the ratio between the local heat flux and the local temperature gradient (i.e., the "local $k_{\perp}$") is an unknown function of the local temperature within the foils.

If knowledge of the temperature distribution in such a case is critical, it would be best to design the system once more, for reliance cannot be had on calculations except within a large error. Moreover, tests can have little meaning, for controlled tests under realistic conditions imply a knowledge and control over the operational conditions, which is contrary to the situation postulated.

IV-C. PENETRATIONS AND DISCONTINUITIES IN MULTILAYER INSULATION

1. Basic Effect of a Penetration or a Discontinuity

Suppose there is a "break" or discontinuity in the multifoil insulation. The immediate result is that, whereas with continuous layers the energy was forced to flow from layer to layer by radiation (and conduction), there is now in the gap between adjacent ends of foils a path for radiation to bypass one or more layers. This radiation can be emitted from the uppermost layer that may not be broken, or from the space between layers. Consequently, more heat flows toward the tank wall than if there were no discontinuity. An example of this class of problem is analyzed in Reference 10.

A similar effect occurs if a piece of material penetrates through the insulation. The edge of the multifoil insulation will be in some thermal contact with that piece of material. Additional heat can flow to the tank by radiation from upper multifoil layers toward the tank, with partial reflection from the piece of material toward the tank wall, and partial absorption by the piece, with re-emission and conduction toward the tank. If the ends of the foil are in mechanical contact with the piece, and if, as is usual, the piece is of thermal conductivity greater than $k_{\perp}$, there will be a heat inleakage by conduction, from the ends of the foils into the piece, as well as radiation from the space between foils absorbed by the piece, and conducted into the tank.

It is thus clear that any penetration in the multifoil insulation leads to an increase in heat leak into the tank over that which would exist if the penetration and foils were thermally decoupled. The problem is to assess the importance of such leaks and minimize the important ones. An appreciation of the mechanism and general behavior of penetrations is useful for this purpose.

The sketch at the top of Figure IV-C-1 illustrates the path followed by the heat leak added due to a penetration, as just now explained. The sketch at the bottom of the same figure represents the resistances to this additional heat flow along its path: (i) from the environment to the outer foil, (ii) through and along the foils and (iii) along the penetration. The heat actually flows in a complex pattern, so that the representation in terms of three resistances is not exact; however, the concept is useful for delineating between various penetrations. In practical cases, the resistance R_E is very low; equivalently, the outer foil is very nearly at the adiabatic wall temperature T_a (see Section IV-A) over most of its surface. Consequently, the heat leak may be said to be controlled by two resistances: $R_{//}$ and R_P. One may immediately classify a penetration within three categories, according as the ratio $R_{//}/R_P$ is small, near unity or large. In anticipation of Chapter IV-C-3, penetrations so classified are defined as weak, strong, or absolute thermal shorts, respectively.

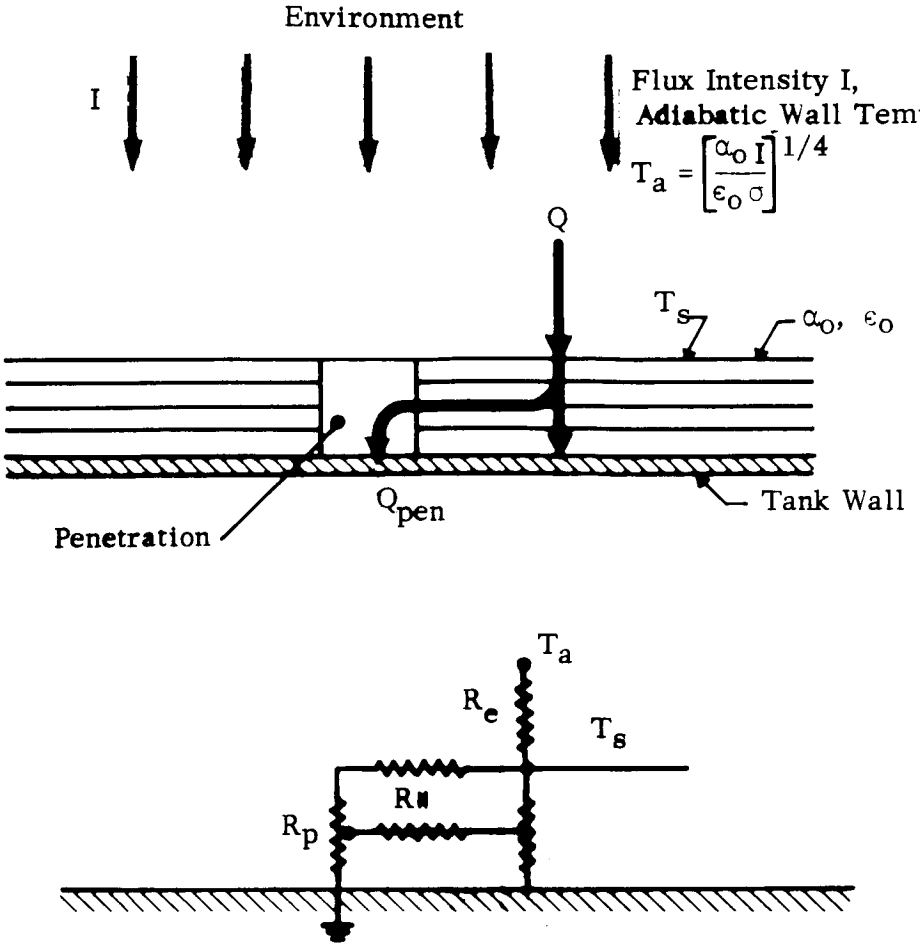

R_e: Resistance to Environment: Usually Very Low ($T_a \simeq T_s$)

R_{11} : Resistance to Parallel Flow Along Foil

R_p: Resistance of Penetration

Weak Shorts:	$R_p \gg R_{11} + R_e$:	R_p Controls Q_{pen}
Strong Shorts:	$R_p \approx R_{11} + R_e$:	$R_p + R_{11} + R_e$ Controls Q_{pen}
Absolute Shorts:	$R_p \ll R_{11} + R_e$:	$R_{11} + R_e$ Controls Q_{pen}

FIGURE IV-C-1 USE OF RESISTANCE CONCEPT TO ILLUSTRATE THE EFFECT OF PENETRATIONS

Suppose we now fix the value of $R_{\parallel}$, that is, we consider insulation consisting of a given number of foils of specified type. Let us also fix the geometry of the penetration (e.g., the diameter of a pipe, pin, thread, etc.), and vary the thermal conductivity, k, of the penetration material. The resulting variation in the heat leak is illustrated in Figure IV-C-2. At low values of kA/B, (where A is the penetration cross-section, B is the thickness of insulation), the heat leak varies directly as kA/B, which is the conductance of the penetration, $1/R_P$. Eventually, at high values of kA/B (low values of R_P), the resistance $R_{\parallel}$ controls, and the heat leak reaches an asymptotic value. At the same time, the temperature drop across the penetration, which is nearly constant when R_P controls, decreases to zero as kA/B attains large values (as R_P vanishes).

A measure of the ratio $R_{\parallel}/R_P$ can be found in terms of the foil and penetration properties.

$$R_{\parallel}/R_P \sim \sqrt{\frac{wk/B}{k_{\parallel}\, k_{\perp}}} \qquad \text{(IV-C-1)}$$

where w is the width of the penetration (e.g., pipe wall thickness, width of straight strip, etc.). This parameter will appear several times in subsequent analyses.

2. Radiative Heat Leaks Through a Gap

Radiative heat leaks through various discontinuities in multilayer insulation have been treated in a previous topical report [10]. We present here the important results for a gap in the insulation. The geometry and nomenclature describing such a gap are shown in Figure IV-C-3. The important variable is the gap width, δ.

The resulting heat leak into a tank is given graphically in Figure IV-C-4, as a function of δ/B, the ratio of gap width to insulation thickness. The heat leak is represented by an effective width, δ_{eff}, of insulating panel that would transmit the same flux as does the gap for the same temperatures. An example will illustrate the use of the graph.

We consider a cylindrical tank 10 feet long, 10 feet in diameter, with flat ends and insulated with 80 layers of metal foil having an emissivity of 0.04 and total thickness of one inch. If the insulation is applied in four sections, namely, two end disks, and two halves of a cylindrical shell, the total length of seam is 80 feet. The total area of the tank surface is 450 ft^2. The shielding factor $n\left(\frac{2}{\epsilon} - 1\right)$ is about 4000.

If we allow a gap width at the seams of $\delta = 0.1$ inch, then $\delta/B = 0.1$, and from the upper curve in Figure IV-C-4, we find that $\delta_{eff}/B = 102$.

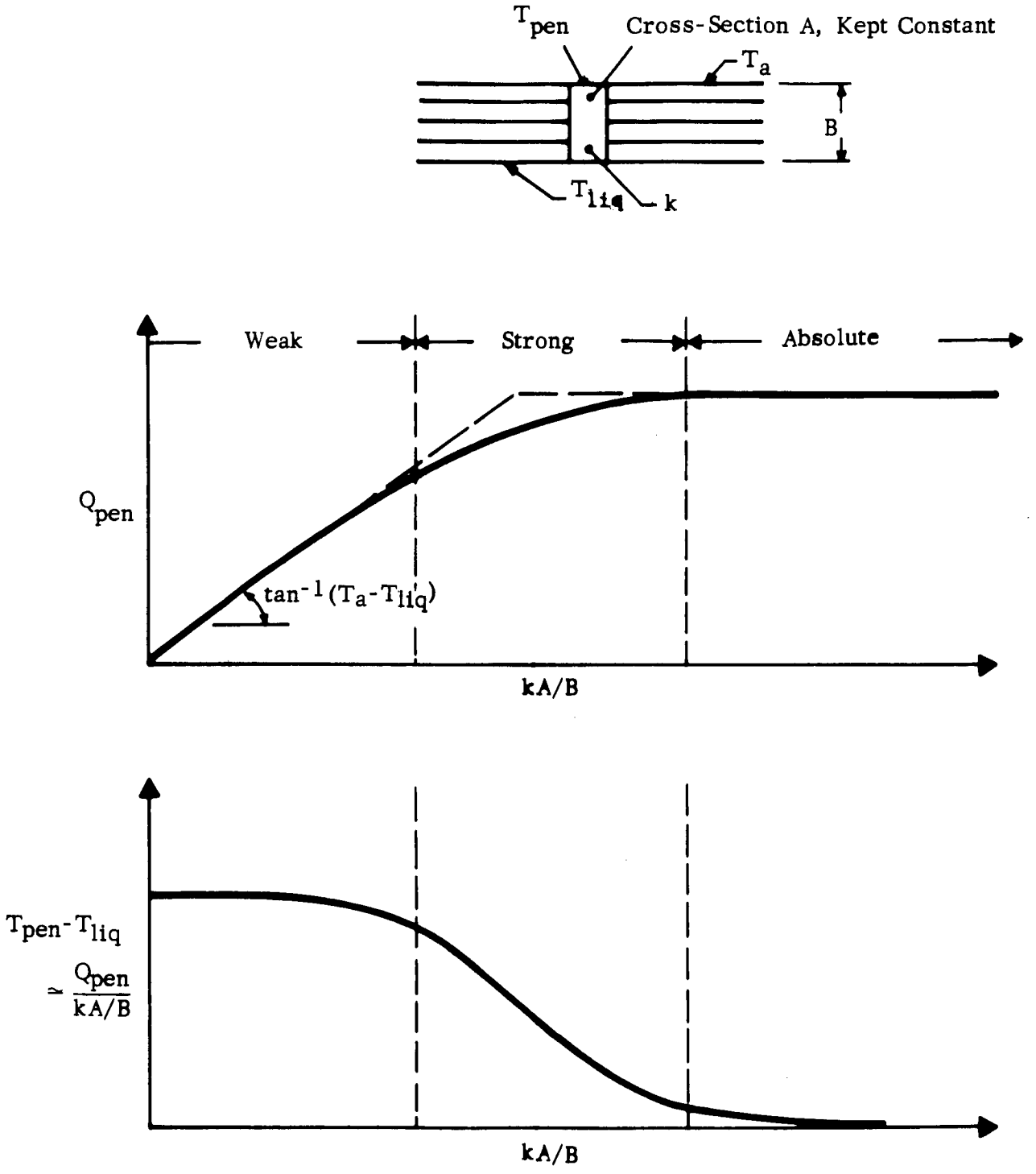

FIGURE IV-C-2 GRAPHICAL ILLUSTRATION OF THE EFFECT OF PENETRATIONS

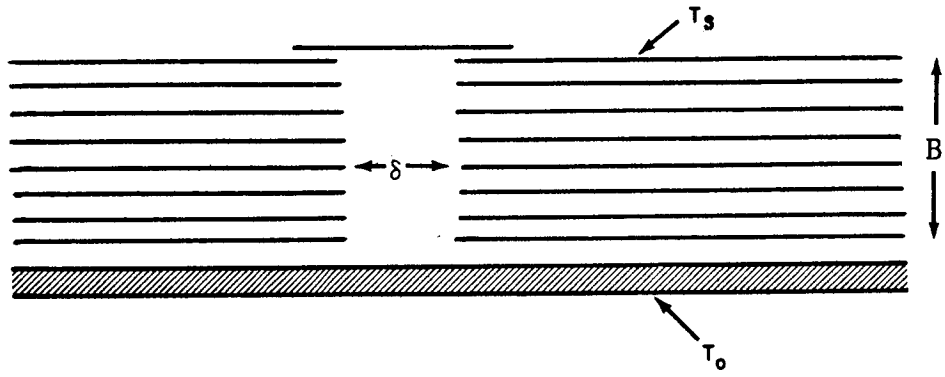

FIGURE IV-C-3 GAP BETWEEN TWO PANELS OF MULTIFOIL INSULATION. THE TANK TEMPERATURE IS T_o. THE OUTER TEMPERATURE IS T_s

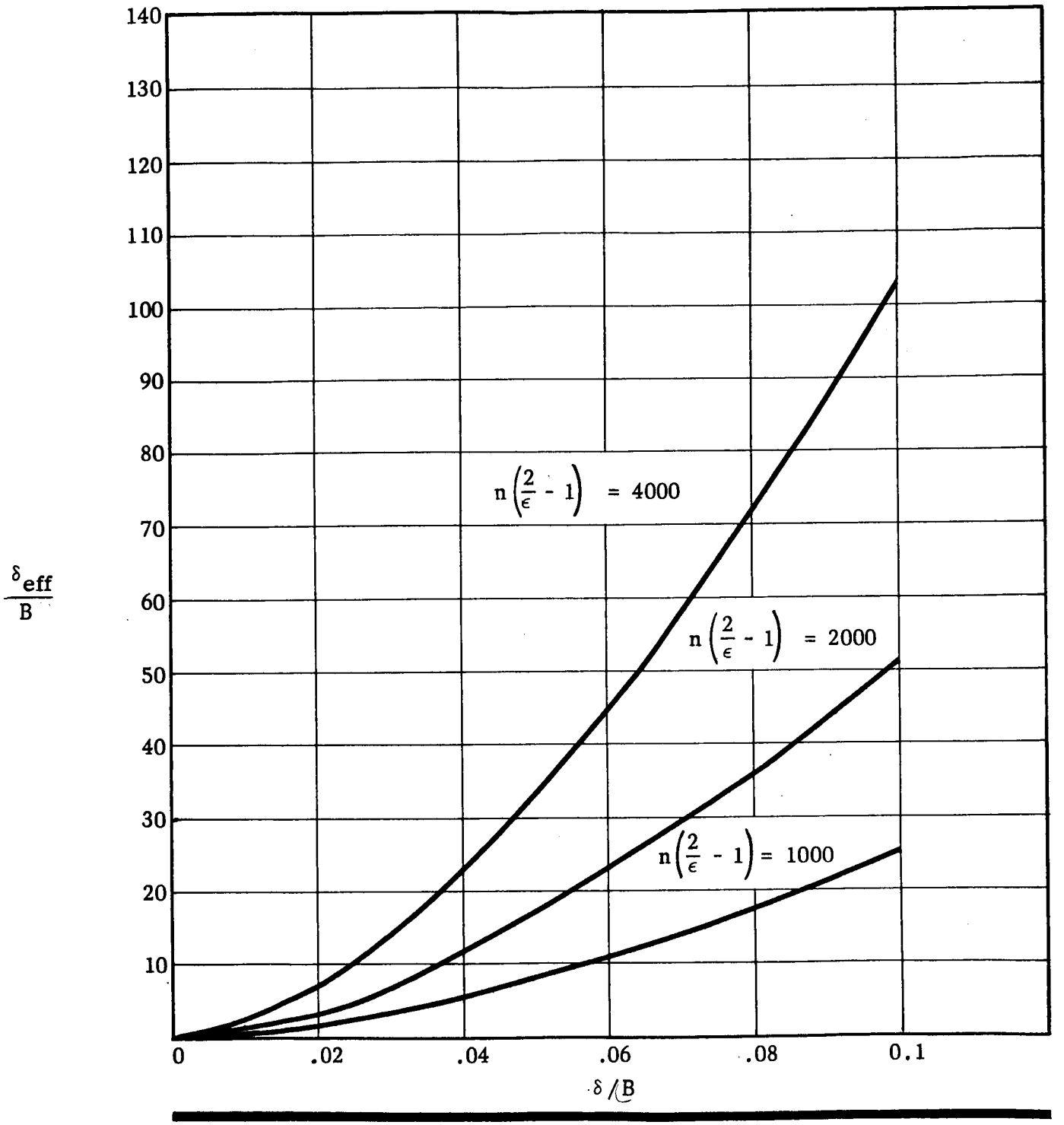

FIGURE IV-C-4 EFFECTIVE GAP δ IN UNITS OF THE INSULATION THICKNESS B, FOR VARIOUS VALUES OF THE SHIELDING FACTOR $n\left(\frac{2}{\epsilon} - 1\right)$.

Therefore, δ_{eff} = 102 inches = 8.5 feet, and the effective area of the seams is 8.5 ft x 80 ft = 680 ft^2. Since the total area of the tank is 450 ft^2, the seams cause an additional heat input of 150%.

3. Gradation of Thermal Shorts

The additional energy that flows to the tank through a penetration originates from the radiation environment. Since, as we have seen in Section IV-A, the net heat input arises from a difference $T_a^4 - T_s^4$, then where the heat inleakage is increased locally, that difference must increase. Therefore, the outer foil temperature T_s must be depressed in the neighborhood of a penetration. This depression, ΔT, will be largest right at the penetration. This maximum depression is defined as ΔT_{max}; an illustration is given in Figure IV-C-5. In a given insulation and for a given geometry, ΔT_{max} depends on the amount of heat inleakage, and, therefore, on the conductance of the penetration. If the latter is high, so will be the depression. In a certain range of conductances, ΔT_{max} will be small enough so that the calculation of the additional conductive or radiative heat leak can be made assuming that the full temperature gradient of the undisturbed insulation is applied across the conductance, without serious error.

The calculation of the heat flow through a penetration in MLI is a complicated affair in the general case, involving both radiation and conduction, with some uncertainties regarding thermal contact resistance. Therefore, it will be extremely useful to be able to recognize those cases where the complication can be avoided. As suggested in the previous paragraph, it can be avoided when ΔT_{max} is small, for then a good approximation to the heat leak through the penetration is simply

$$Q_{PENETRATION} \cong \frac{kA}{B} (T_s - T_{liq}) \qquad \text{(IV-C-2)}$$

where T_s is the outer foil temperature in the undisturbed insulation. The error in $(T_s - T_{liq})$ is ΔT_{max}, and it is on the conservative side. Actually, T_s can be replaced by T_a since we have seen in Section IV-A that $T_a - T_s$ is very small in undisturbed insulation. However, in order to recognize that the simplified equation (IV-C-2) can be applied for a given penetration, we still need to know what is the value of ΔT_{max} produced by that penetration. This requires a relation that can only be obtained from analysis.

The linearized analysis of Appendix D is of aid in this respect. In that appendix, there are two linearizations. The first is based on the assumption that $k_\perp$ is uniform at some mean value; it was useful in determining decay distances for perturbations, and it can be used here in obtaining a good estimate of ΔT_{max}. The second is a linearization in the boundary condition at the outer foil, the latter condition being expressed as

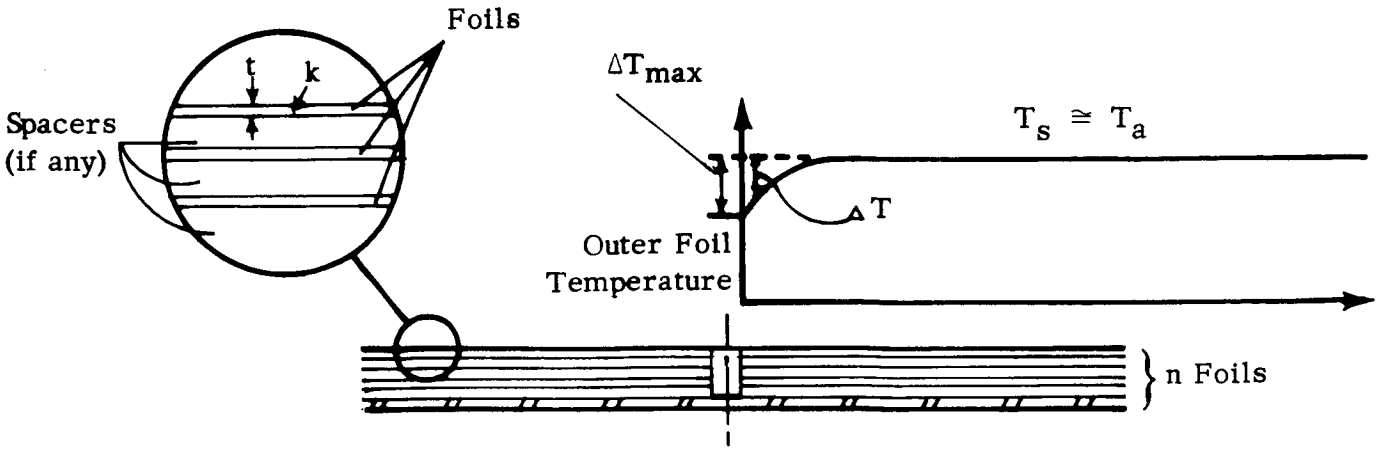

(a) Thermal Short, Foils of Low kt

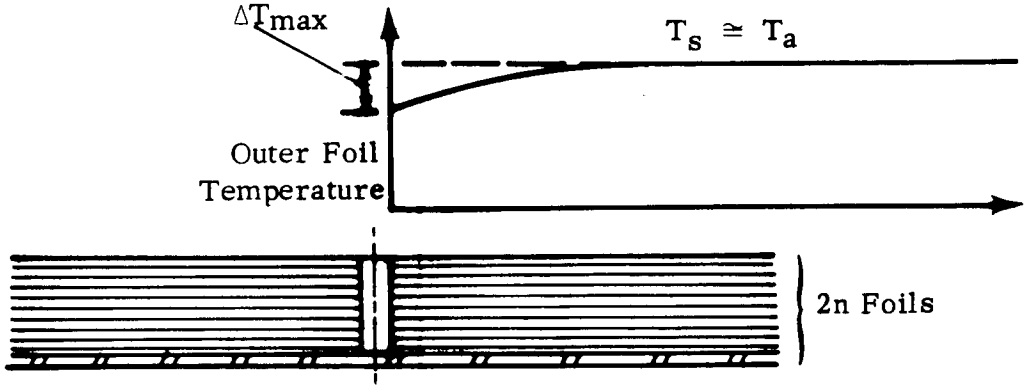

(b) Increased Number of Same Foils as in (a) (Short of Same k_1, A, but Twice as Long)

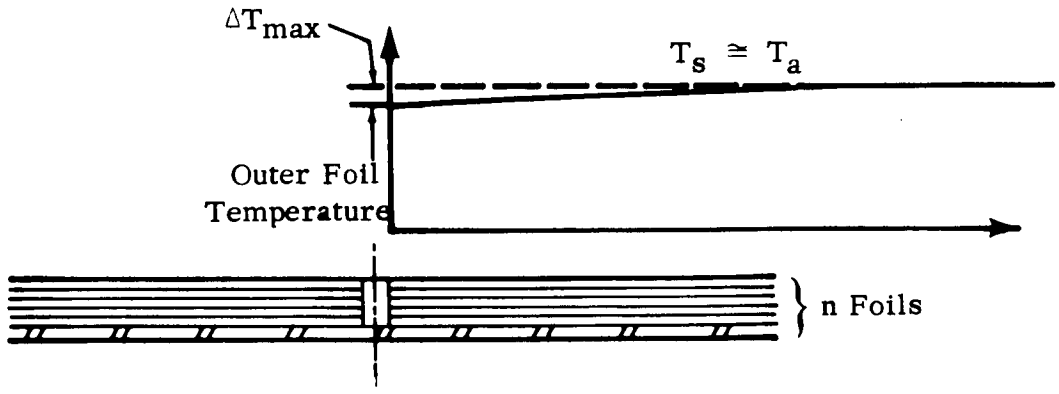

(c) Same Short and Number of Foils as in (a) Foils of High kt

FIGURE IV-C-5 TEMPERATURE DEPRESSION IN MULTILAYER INSULATION DUE TO A THERMAL TEST

$$(Q/A)_{in} = \text{const } (T_a - T_s) \qquad \text{(IV-C-3)}$$

instead of

$$(Q/A)_{in} = \sigma \epsilon_o (T_a^4 - T_s^4) \qquad \text{(IV-C-4)}$$

which is the exact expression for the net heat flux into the insulation. Now Equation (IV-C-4) can be re-written as

$$(Q/A)_{in} = 4 \sigma \epsilon_o T_a^3 (T_a - T_s) \phi \qquad \text{(IV-C-5)}$$

with

$$\phi = \frac{1}{4} \left(1 + \frac{T_s}{T_a} + \frac{T_s^2}{T_a^2} + \frac{T_s^3}{T_a^3}\right) \qquad \text{(IV-C-6)}$$

The limiting values of ϕ are: unity when $T_s = T_a$ and 0.25 when $T_s = 0$. Suppose $\Delta T_{max} = 0.1\ T_a$. Then the lowest value of T_s, on the outer foil will be $0.9\ T_a$, and the lowest value of ϕ will be 0.86. If ϕ is maintained between 0.86 and unity, equation (IV-C-5) can be replaced by (IV-C-3) with an error no greater than 14% (actually less). Maintaining $\Delta T_{max} < 0.1\ T_a$ allows this. It also allows the use of equation (IV-C-2) within 10%.

We arbitrarily define a <u>weak</u> thermal short as one for which

$$\frac{\Delta T_{max}}{T_a} < 0.1 \qquad \text{(IV-C-7)}$$

A <u>strong</u> thermal short is one for which

$$0.1 < \frac{\Delta T_{max}}{T_a} < 1 \qquad \text{(IV-C-8)}$$

Finally, an <u>absolute</u> thermal short is one for which

$$\frac{\Delta T_{max}}{T_a} \simeq 1 \qquad \text{(IV-C-9)}$$

It will be noted that this generalized definition in no way implies that a weak thermal short necessarily leads to a low heat leak. A thermal short can be defined as weak or otherwise only in terms of the insulation which it penetrates. In fact, the same penetration (of given geometry and properties) can be a weak short and produce a high heat leak in certain insulations and be a strong one, producing a low heat leak in others. Figure IV-C-5 shows ΔT_{max} as varying from one insulation to another for a given penetration. Obviously if ΔT_{max} is large, the actual temperature drop across a given penetration will be low, giving a low heat leak.

A weak short should be thought of as one permitting a linearized analysis and a simple heat flow calculation. The properties associated with weak shorts will now be discussed.

4. Limits to Weak or Linear Shorts

An analysis similar to that of Appendix D was performed to analyze the thermal behavior of the general cylindrical penetration.

Figure IV-C-6 shows maxima of the parameter wk_1/B for which penetrations of various radii remain in the weak thermal short category, as defined by Equation (IV-C-7). The curves have n, the number of foils, as parameter, and are for penetrations in two-mil aluminum foils. Figure IV-C-7 gives the same results for penetrations in aluminized Mylar foils.

The quantity w, representing penetration width, or cylinder wall thickness, has of course a physical maximum in the latter case. This maximum is $r_o/2$, representing a full cylinder. In fact, for full cylinders, in both figures the parameter wk_1/B can be replaced by $k_1 r_o/2B$.

In both figures, the curves tend to asymptotic values of wk_1/B as r_o becomes large. These asymptotic values are therefore applicable to straight strips, such as might be used on the edges of panels of insulation. The results for such straight strips have been interpreted in terms of various penetration materials, for two thickness of each of the two types of insulation, in Figure IV-C-8.

5. Strong or Non-Linear Shorts

The analysis of the general cylindrical short, without linearizations, presented in Appendix F, reveals the dependence of the added heat flow due to the penetration on three parameters: K, ψ and v_o. The determination of this dependence is left to future work. However, it is possible

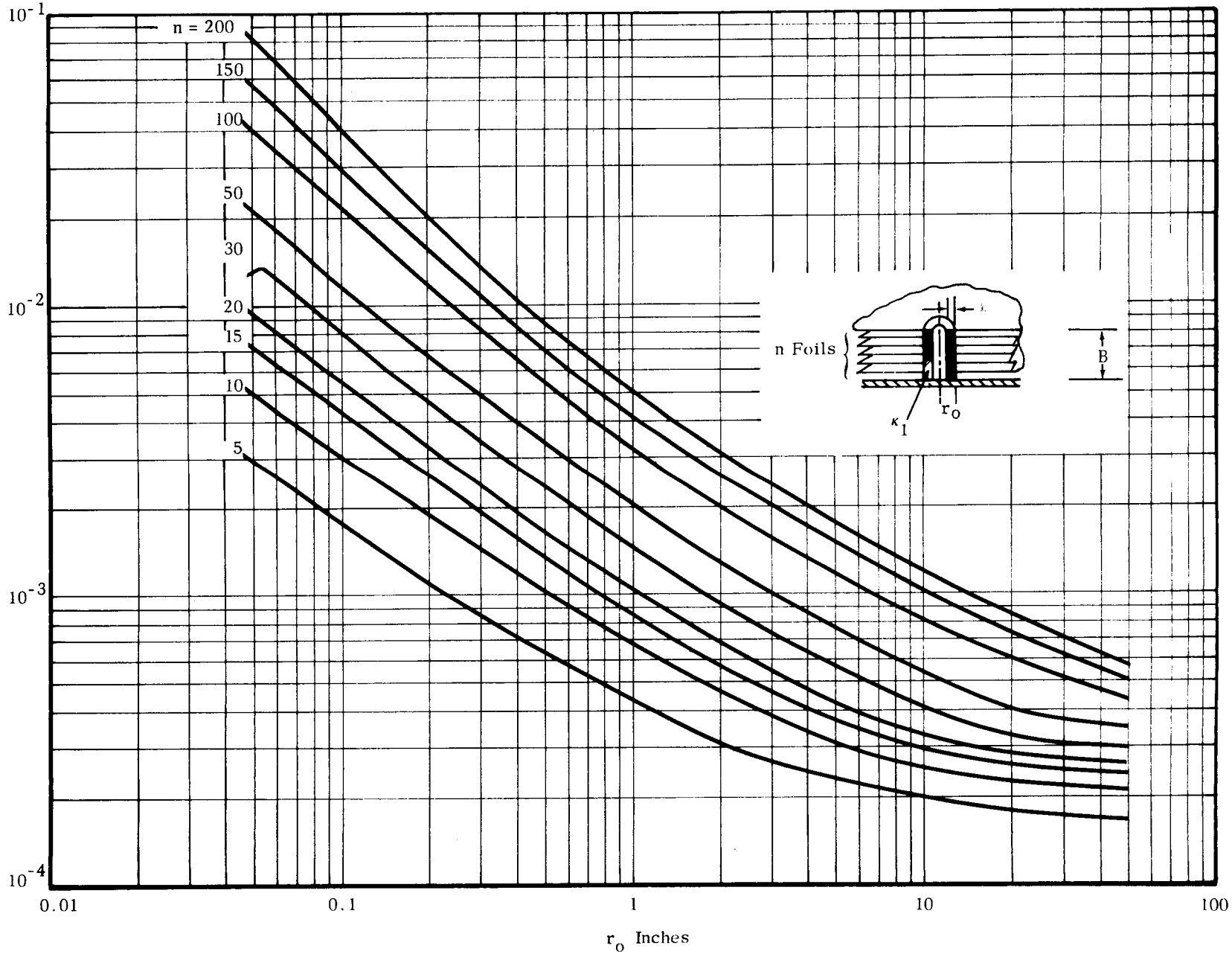

FIGURE IV-C-6 PROPERTIES OF CYLINDRICAL THERMAL SHORTS FOR ΔT_{max} $<0.1\ T_a$ (WEAK SHORTS) IN 0.002" ALUMINUM FOIL INSULATION

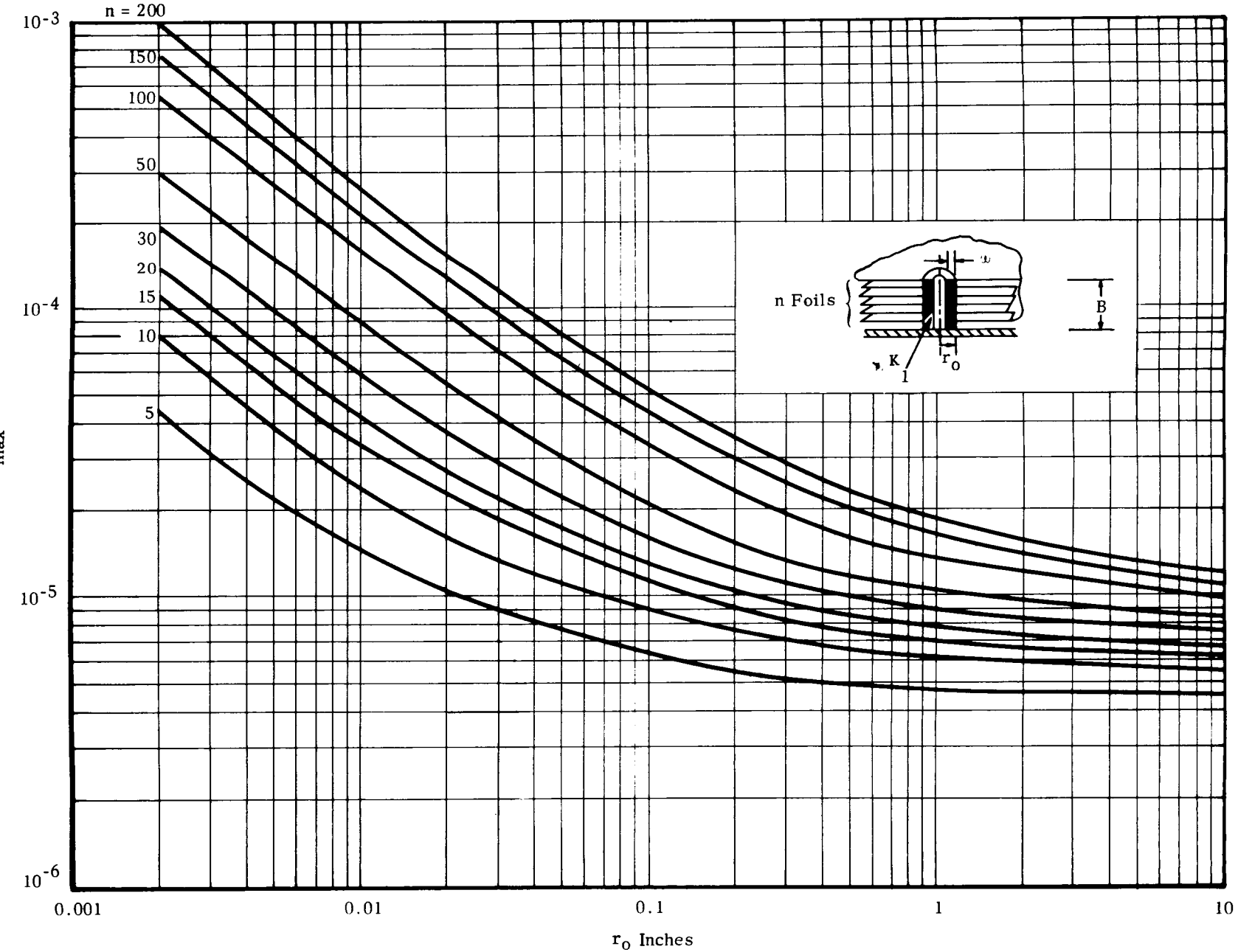

FIGURE IV-C-7 PROPERTIES OF CYLINDRICAL THERMAL SHORTS FOR ΔT_{max} <0.1 T_a (WEAK SHORTS) IN INSULATION FOILS OF MYLAR WITH 10^{-2} IN. VACUUM DEPOSIT OF ALUMINUM

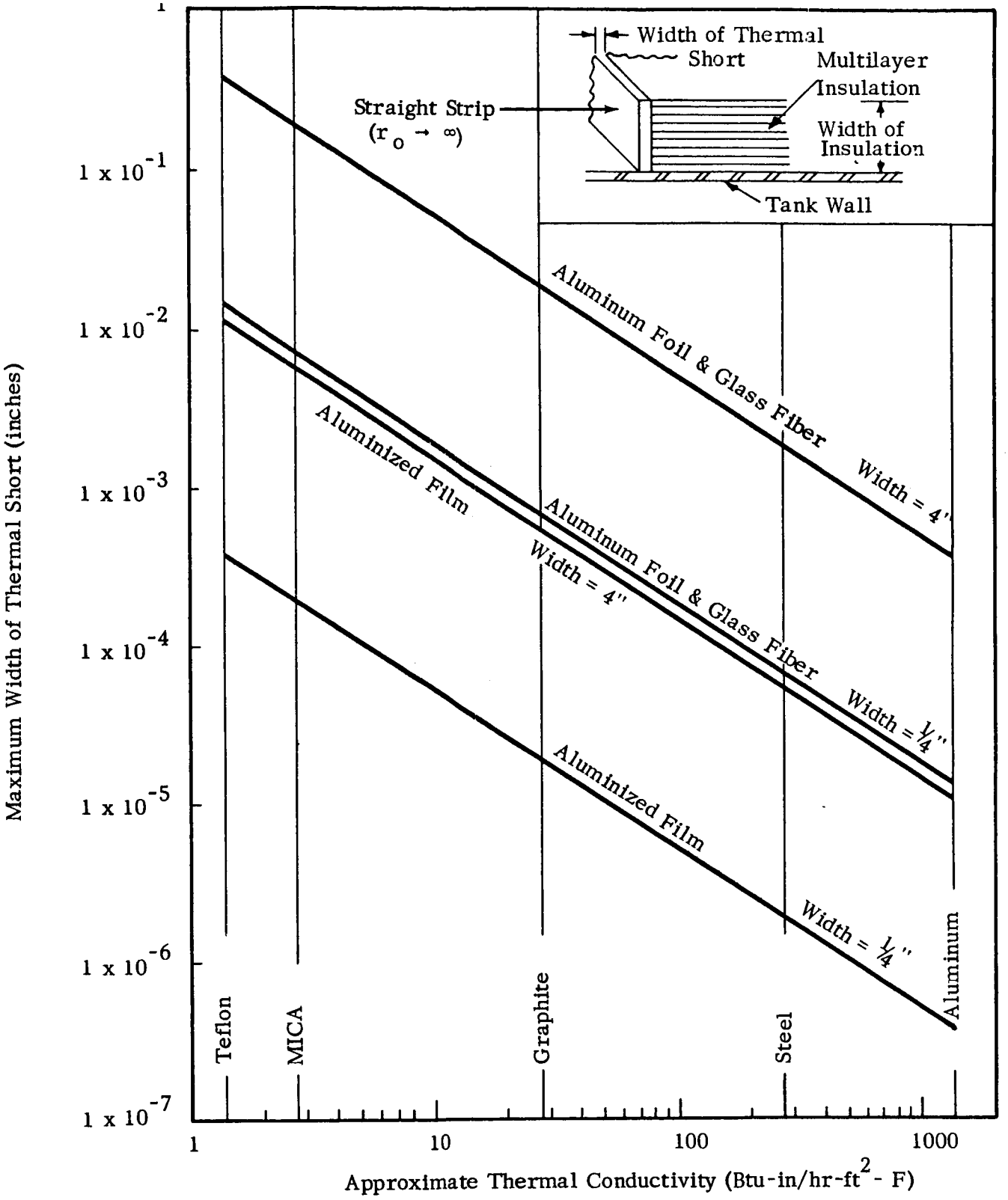

FIGURE IV-C-8 THE MAXIMUM WIDTH OF VARIOUS MATERIALS PENETRATING MULTILAYER INSULATIONS AND CONSTITUTING WEAK THERMAL SHORTS (T_a = 300°K)

to locate, in this significant group of parameters, the limits between weak and strong thermal shorts. The limits are shown in Figure IV-C-9. The curves presented there are applicable to any type of foil, in any number (down to about five), and for penetration of all radii, thermal conductivities and wall thicknesses.

The three parameters κ, ψ and v_o are defined in Appendix F. With reference to the resistance concept introduced in Chapter IV-C-1, ψ and κ can be shown to have the following significance:

$$\psi = R_{\parallel} / R_P \qquad \text{(IV-C-10)}$$

$$\kappa = R_E / R_{\parallel} \qquad \text{(IV-C-11)}$$

It is seen from Figure IV-C-9 that for the usual values (0.0001 to 0.001), κ does not have a large influence on the limiting values of ψ for weak shorts. The reason is that at such low values, the "environmental resistance" R_E cannot control the heat flow.

v_o is a geometrical parameter, which can be shown to have the following significance:

$$v_o = r_o / X_{Decay} \qquad \text{(IV-C-12)}$$

Since in practical cases X_{Decay} is the order of inches, and even several feet, v_o will usually be small for insulation attachments (pins, threads, etc.) and of the order of unity for pipes. For straight strips (e.g., edges of insulation panels), v_o becomes infinite and loses its influence (this is not indicated in Figure IV-C-9).

6. Design of Thermal Shorts When a Choice is Possible

We consider a given insulation: fixed number and type of foils, fixed insulation thickness B. Suppose that penetrations of a given material must be introduced to fulfill a certain function. The function may dictate the number of such penetrations, or their total cross-sectional area, or the radius of each, or the material. If a choice is left as to the radius and wall thickness, then it may be possible to choose a combination of these quantities so as to minimize the heat leak.

As an example, suppose that the total cross-sectional area of these penetrations is fixed. That is

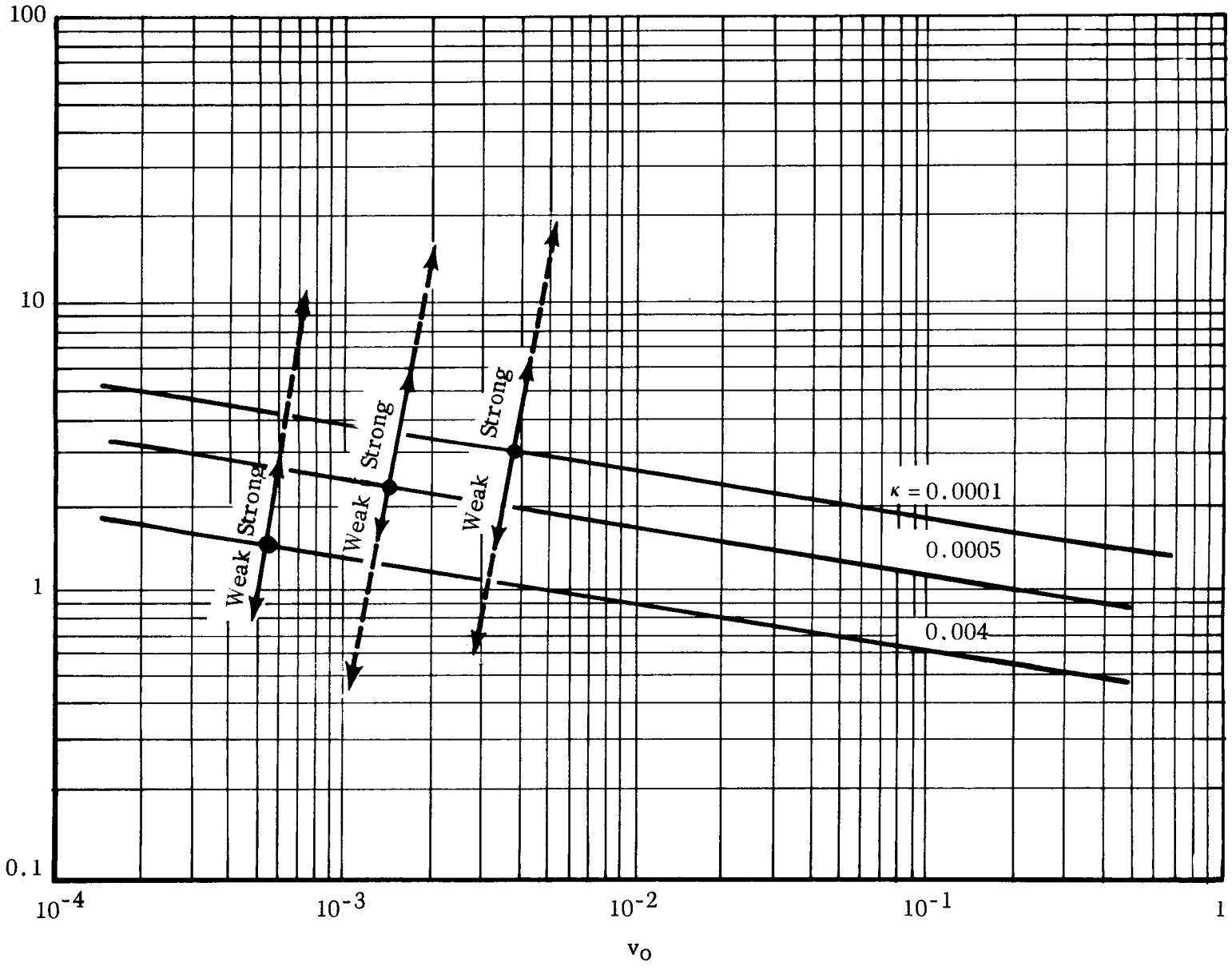

FIGURE IV-C-9 LIMITS BETWEEN WEAK AND STRONG THERMAL SHORTS SHOWN IN GENERALIZED PARAMETRIC FORM

$$n_p 2\pi r_o w \left(1 - \frac{w}{2r_o}\right) \approx n_p 2\pi r_o w_{eq} = A_{tot} \text{ a constant} \qquad \text{(IV-C-13)}$$

where n_p, w, r_o are the number, wall thickness, and radius of penetration, respectively, and A_{tot} is the total cross-section of all the penetrations. Such a condition might apply, for instance, to insulation attachments required to support the foils under launch acceleration. In this situation, the three variables are at the disposal of the designer, within a certain reasonable range. Since the thickness, B, of insulation and the thermal conductivity k_1 of the short are given, we can write

$$\frac{w_{eq} k_1}{B} = \frac{A_{Tot}\, k_1}{2\pi\, n_p\, r_o B}$$

$$= \frac{\text{constant}}{n_p\, r_o} \qquad \text{(IV-C-14)}$$

Corresponding to the insulation in question there will be one curve of the type shown in Figures IV-C-6 and 7, giving the maximum value of wk_1/B for weak shorts as a function of r_o. On the same graph, curves representing equation (IV-C-14) at fixed n_p can also be drawn; these will be straight lines at a negative slope of 45°, and will be higher on the graph the smaller the value of n_p.

Consider the highest of such lines, corresponding to the minimum practicable number of penetrations. If it has points above the curve of maximum wk_1/B, it is possible to design the penetrations as strong shorts. For these, $\Delta T_{max} = X\, T_a > 0.1\ T_a$, so that

$$(\Delta T)_{\text{penetrations}} = T_a - \Delta T_{max} - T_{liq}$$

$$= (1 - X)\, T_a - T_{liq}$$

$$< 0.9\, T_a - T_{liq} \qquad \text{(IV-C-15)}$$

or

$$(\Delta T)_{\substack{\text{penetrations} \\ \text{(strong short)}}} < (\Delta T)_{\text{weak short}} \qquad \text{(IV-C-16)}$$

The heat flow through all the penetrations will be

$$Q_{pen} = \frac{A_{ToT} k_i}{B} (\Delta T)_{penetrations}$$

$$= \text{constant } (\Delta T)_{penetrations}$$

$$< \text{constant } (\Delta T)_{weak\ shorts} \qquad \text{(IV-C-17)}$$

or

$$Q_{pen} < Q_{weak\ shorts} \qquad \text{(IV-C-18)}$$

The further the point is above the curve of maximum wk_i/B, the smaller will be Q_{pen}. Since we are considering points on the line of lowest practicable n_p, the furthest point will be attained by varying r_o. However, there will be practical limits to that variable also.

7. Decoupling of Thermal Shorts

When penetrations in thermal contact with the foil edges produce unacceptable heat leaks, it is necessary to interrupt that thermal contact. Mere separation of the penetration from the foil edges may not be satisfactory, for it introduces a gap that allows radiative heat leaks to the tank (see Chapter IV-C-3). Gaps around the perimeter of a penetration of modest radius may be tolerable (an example would be a small vent pipe [10]), provided there is adequate assurance that the gap will not widen or close unpredictably owing to distortions in the insulation blanket. Such distortions could be caused by thermal contraction during filling, by loading during launch acceleration, or by pressure differences within foils during ascent decompression.

There are cases where a gap is intolerable. Some examples are: (i) penetrations consisting of long straight strips, e.g., along a continuous support membrane, or along the edge of an insulation panel; (ii) circular penetrations of large radius, e.g., around a manhole or a transfer line; and (iii) perhaps a large number of small penetrations. In such cases it will be necessary to close the gap with some material of isotropic, low thermal conductivity. This procedure is illustrated schematically in Figure IV-C-10(a). Examples of insulator materials that appear promising are evacuated glass fiber and evacuated powder.

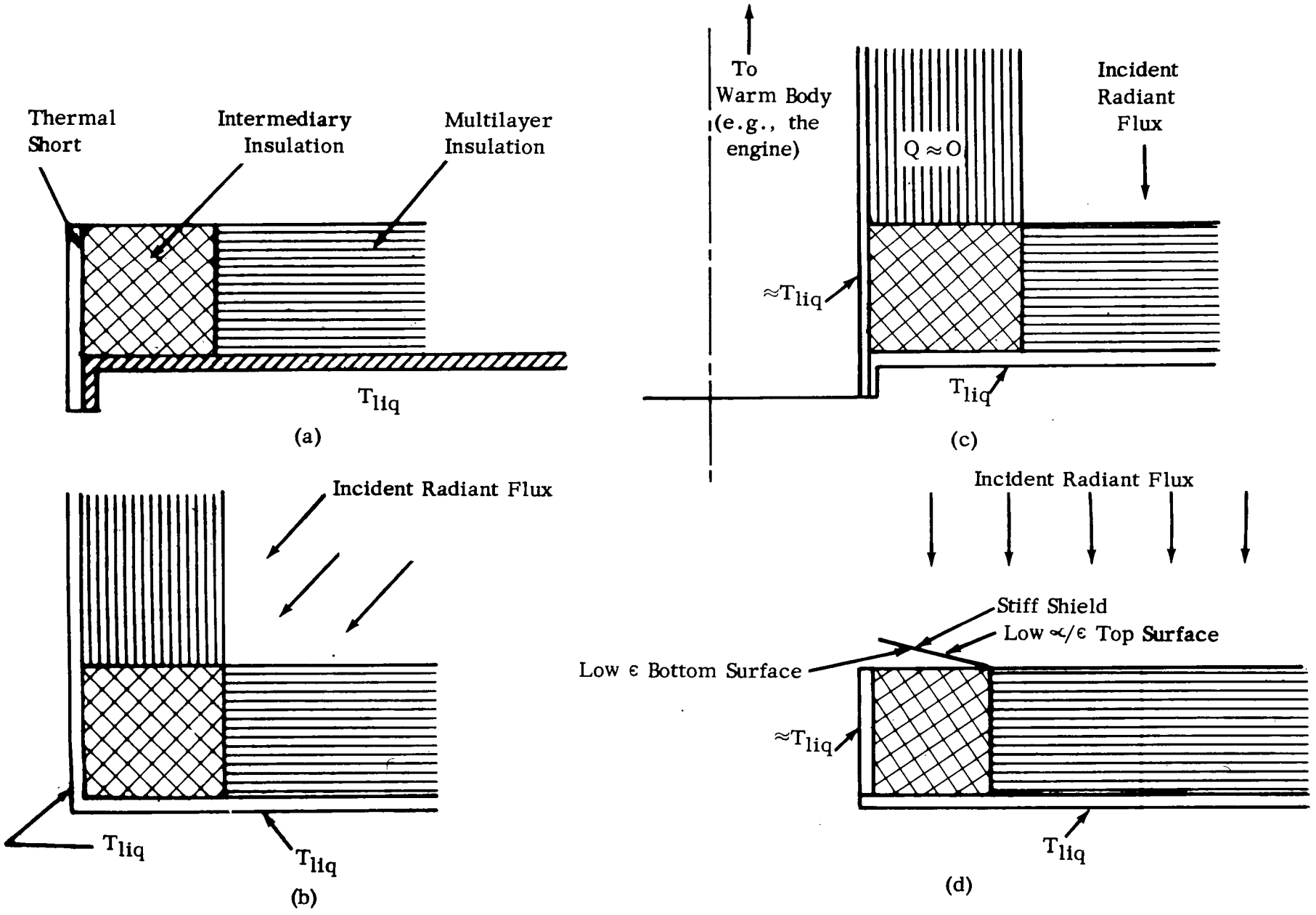

FIGURE IV-C-10 TECHNIQUES FOR DECOUPLING STRONG THERMAL SHORTS FROM FOIL EDGES

Figure IV-C-10(b) represents a square section of intermediary insulation at a corner, which protects the foils in one direction from being shorted by those in the other direction. The environmental radiation is incident on both outer surfaces of multilayer insulation. The radius of the short is large ($r_o >> X_{Decay}$). If k_2 is the thermal conductivity of the intermediary insulation, the heat leak per unit length normal to the drawing can be shown to be

$$Q_{corner} = k_2 (T_a - T_{liq}) \qquad \text{(IV-C-19)}$$

The dimensions of the square do not enter into the result. For $T_a = 280^oK$, $T_{liq} = 20^oK$ and $k_2 = 3.0 \times 10^{-3} \frac{\text{Btu-in}}{\text{ft}^2\text{-hr-}^oR}$ (evacuated powder), the heat leak for one foot of such insulation will be $0.112 \frac{\text{Btu}}{\text{hr}}$.

Figure IV-C-10(c) shows a square section of intermediary insulation, the upper side of which is adiabatic. This represents the joint between the tank wall and a large pipe or between the tank wall and support in the form of a sheet of metal, with negligible heat flow from the warm end to which these elements would presumably be connected. For this case, the heat leak per unit length can be shown to be

$$Q_{\substack{adiabatic \\ upper\ side}} = 0.74\, k_2 (T_a - T_{liq}) \qquad \text{(IV-C-20)}$$

The next case to be treated is a square section of intermediary insulation, the upper side of which receives the same solar flux as does the multilayer insulation. This represents a possible protection scheme for a seam on a side of the tank exposed to direct solar radiation. The surface absorbtivity-to-emissivity ratio on the exposed side of the intermediary insulation is assumed to be the same as for the outer surface of the insulation. This case is not shown, but would be that shown in Figure IV-C-10(d) without the stiff shield covering the intermediary insulation. The problem is non-linear and must be solved for each combination of k_2, α_o/ϵ_o and $(T_a - T_{liq})$. We have carried out the computation for one such combination:
$k_2 = 3.0 \times 10^{-3} \frac{\text{Btu-in}}{\text{ft}^2\text{-}^oR\text{-hr}}$, $\alpha_o/\epsilon_o = 0.2$, and $(T_a - T_{liq}) = 260^oK$. The result is:

$$Q_{\substack{exposed \\ upper\ side}} = 0.215 \text{ Btu/ft-hr} \qquad \text{(IV-C-21)}$$

In order to compare this result with the previous one, we write

$$Q_{\substack{\text{exposed} \\ \text{upper side}}} = \frac{2.08 \times 10^{-3} \, k_2 \, (T_a - T_{liq})}{4.3 \times 10^{-6} \times 260}$$

$$= 1.86 \, k_2 \, (T_a - T_{liq}) \qquad \text{(IV-C-22)}$$

The last equation is for comparison with Equation (IV-C-20) only, and cannot be applied as written except when the specific quantities k_2, etc., given above, are used. It indicates that for given values of the parameters, the heat flow can be more than doubled when the upper side of the intermediary insulation is left exposed. This is the reason for the stiff protective shield shown in Figure IV-C-10(d).

Figures IV-C-11 and IV-C-12 illustrate methods of using intermediary insulation for structural strips, seams and pipes. These figures are self-explanatory. The use of thin shaped strips as suggested in the lower sketch of Figure IV-C-11, also in Figure IV-C-12(b) can be highly valuable in solving the complex topological problems arising when combined thermal, structural and geometrical requirements are to be met. These shaped strips are equivalent to the stacked stainless steel washers discussed in Section IV-A; they are insulated from one another by a fine powder, and in vacuum they offer a high resistance to heat flow across adjacent strips.

The decouplers discussed so far have been square in cross-section. The question remains how, in this cross-section, the dimension parallel to the tank (shown as b in Figure IV-C-13) should be related to the thickness B of the insulation. In the case where the decoupling material has its exposed upper side shielded, as in Figure IV-C-10(d), the question can be settled by a linear analysis. Such an analysis has been performed, with the result shown in Figure IV-C-13, where the normalized added heat flow due to the penetration is plotted against the geometrical ratio b/B for various values of the parameter λ. The latter may be taken to represent the conductance of the penetration. It is seen from the figure that, no matter how high that conductance is, its effect is no longer felt when b/B = 1. Specifically, with a decoupler having a square cross-section, the heat flow per unit length (L) depends only on the thermal conductivity k_2 of the decoupler material and on the temperature difference $T_s - T_{liq}$. In fact, the horizontal asymptotic line in Figure IV-C-13 may be written

$$Q = 0.74 \, k_2 \, (T_s - T_{liq}) \qquad \text{(IV-C-23)}$$

which is exactly Equation IV-C-20 when $T_s = T_a$.

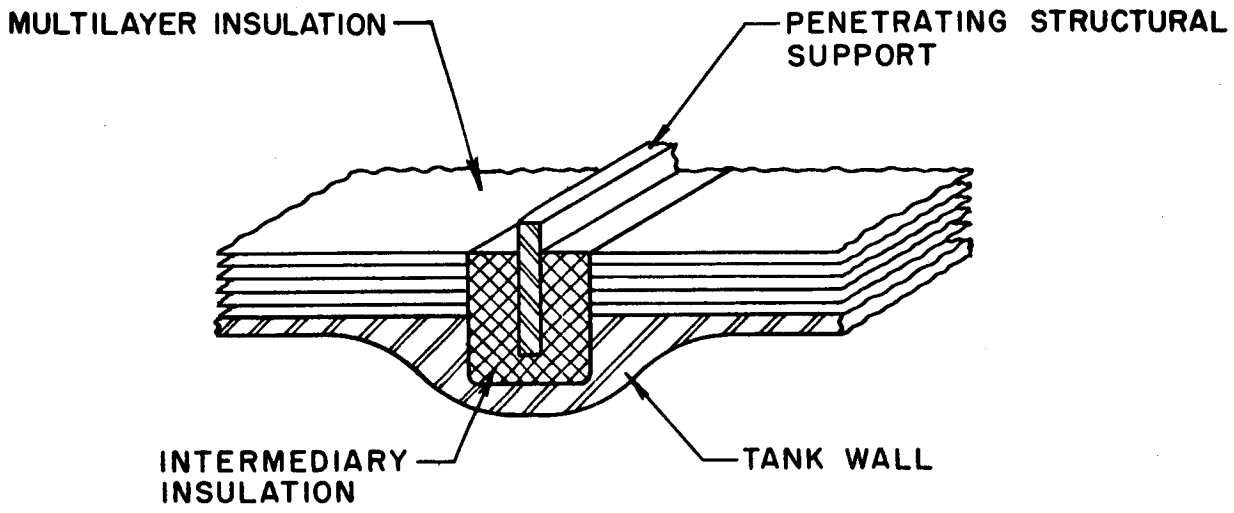

STRUCTURAL STRIP OR SEAM

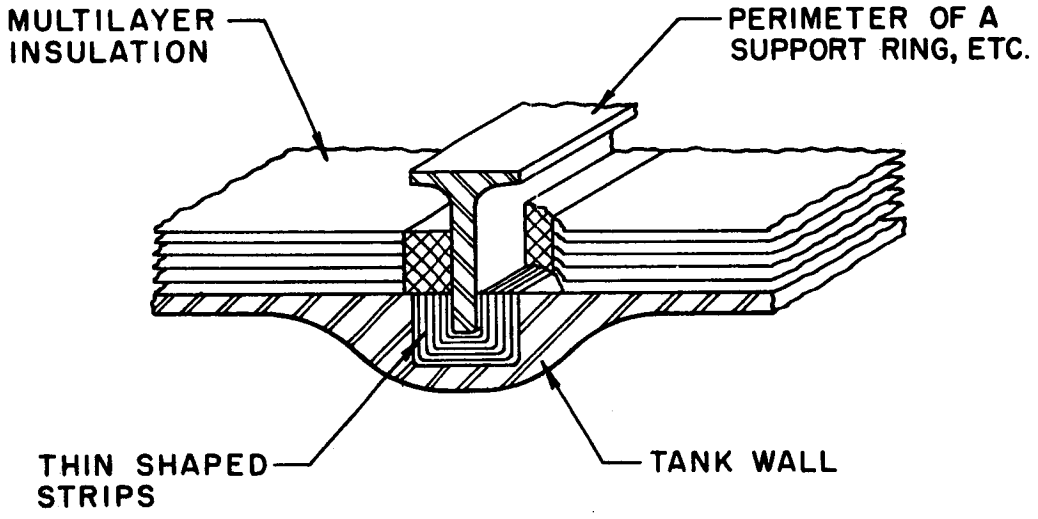

STRUCTURAL STRIP

FIGURE IV-C-11 EXAMPLES OF THE USE OF INTERMEDIARY INSULATION FOR STRUCTURAL STRIPS OR SEAMS

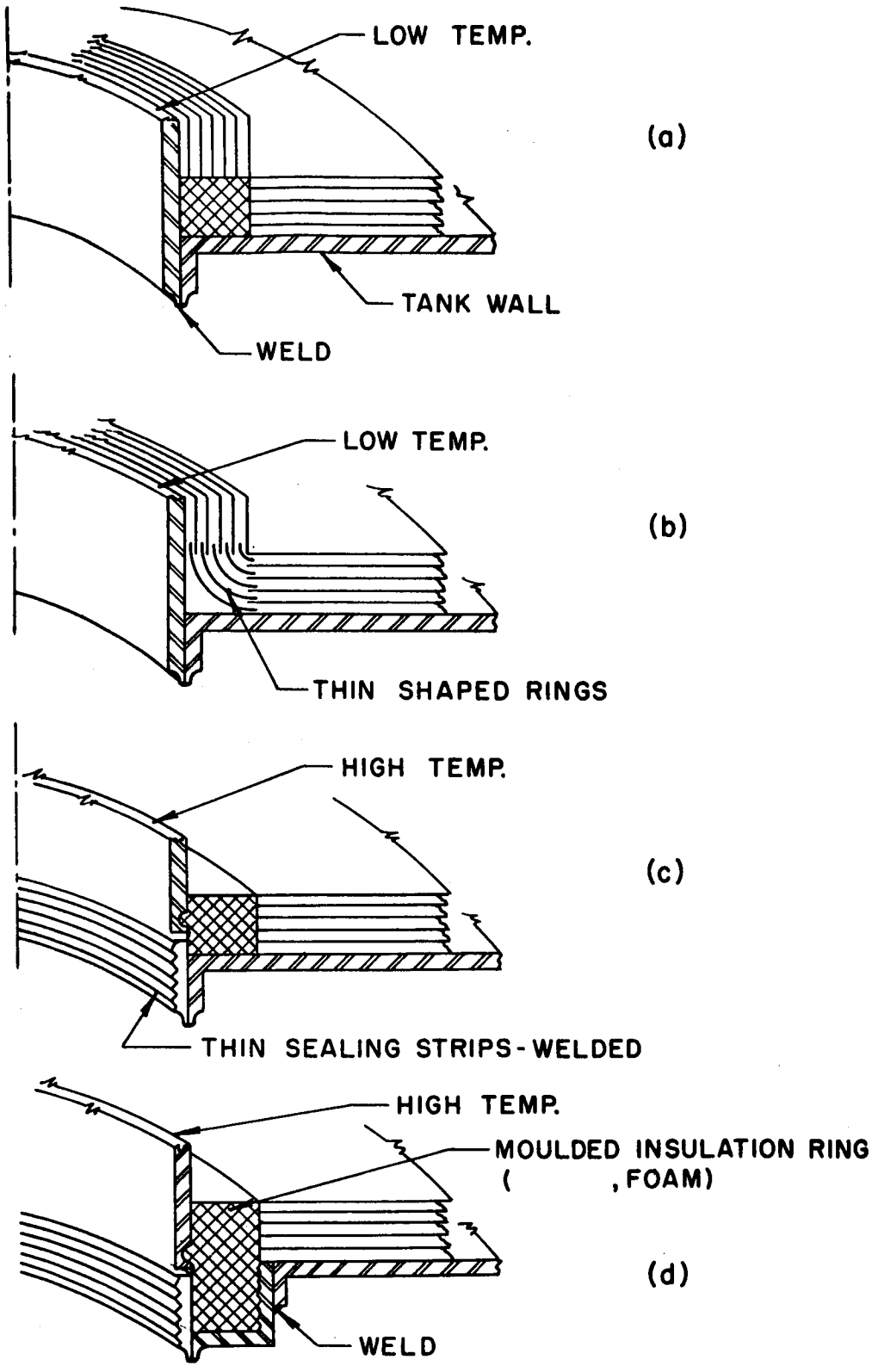

FIGURE IV-C-12 EXAMPLES OF THE USE OF INTERMEDIARY INSULATION FOR PIPING

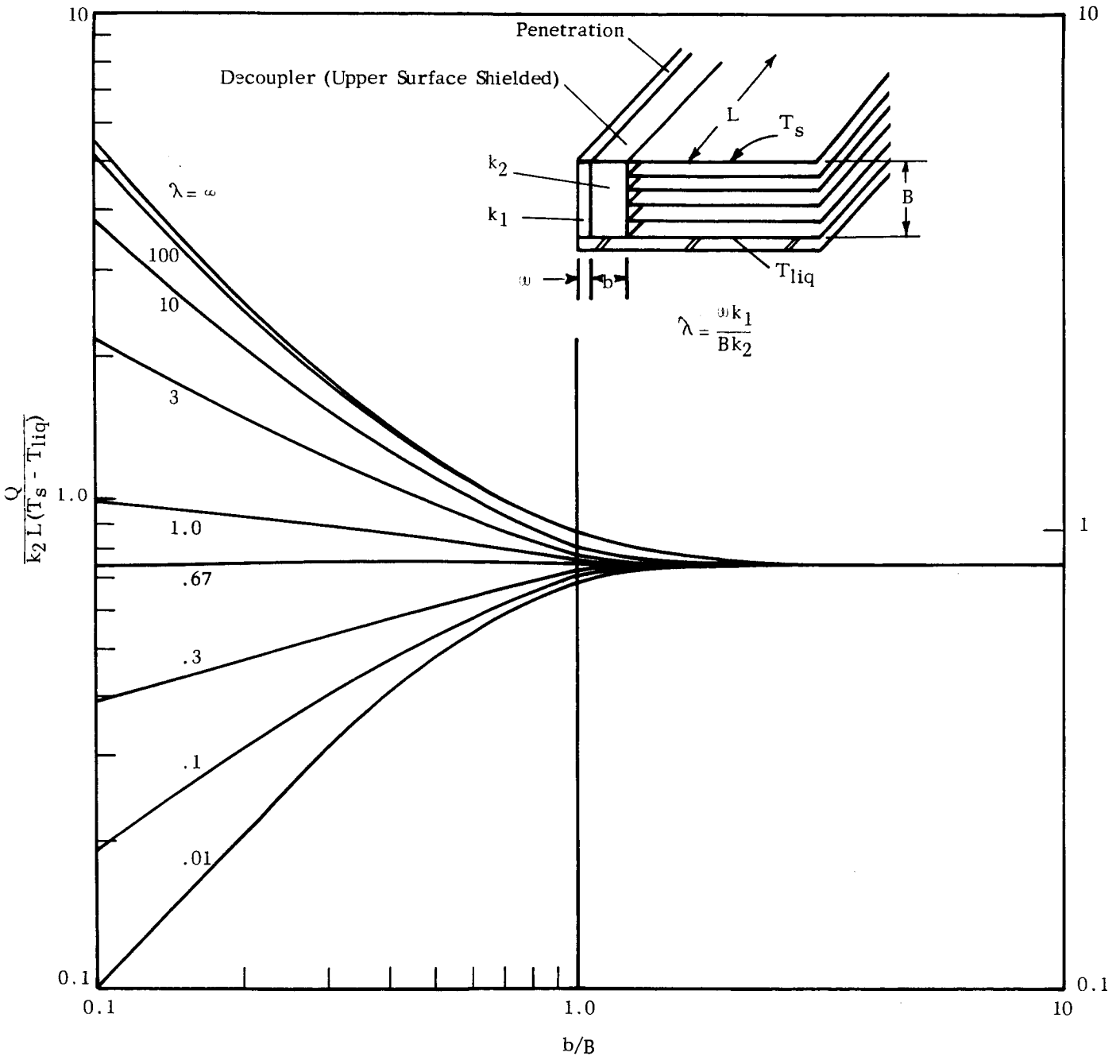

FIGURE IV-C-13 EFFECT OF DECOUPLER GEOMETRY ON HEAT FLOW-THROUGH

The curves of Figure IV-C-13 reveal one more thing: when $\lambda < 0.67$, the heat flow increases as b/B increases. Therefore, a decoupler is useless or worse, if its thermal conductivity k_2 is such that λ is less than 0.67. For a decoupler to be useful we must have

$$k_2 < \frac{w\, k_1}{0.67\, B} \qquad \text{(IV-C-24)}$$

8. Penetrations with Temperature-Dependent Thermal Conductivity

Over the temperature range from cryogenic to equilibrium under solar radiation (i.e., 20 - 400°K) the thermal conductivity of most materials changes markedly. The form of this temperature dependence is almost as varied as are the materials. Hence, a general analysis accounting for all possibilities is not possible. Moreover, there is the added diversity in foil type, number, and emissivity.

To show the effect of temperature-dependent conductivity, we have considered the case where each foil is isothermal, that is, where $B\sqrt{k_{\parallel}/k_{\perp}}/D \gg 1$, with a uniform intensity I of incident radiation over the outer insulation foil. Thus, the temperature is a function only of distance from the tank surface, and at a given point is the same for the penetration and for the foil situated there. Hence, this is a unidimensional problem.

We may write for the total heat flow across two adjacent foils, including that due to the penetration:

$$Q = \frac{A_o \sigma \Delta(T^4)}{(\frac{2}{\epsilon} - 1)} + A_1 k(T)\, \frac{\Delta T}{\Delta y} \qquad \text{(IV-C-25)}$$

where A_o and A_1 are areas shown in Figure IV-C-14. But $\Delta y = B/n$; also, $2/\epsilon \gg 1$; therefore,

$$Q\Delta y = \frac{A_o\, \sigma\, \epsilon B \Delta (T^4)}{2n} + A_1 k(T)\, \Delta\, T \qquad \text{(IV-C-26)}$$

When the number, n, of foils is large, the differences can be replaced by differentials

$$Q dy = \frac{A_o \sigma\, \epsilon B d(T^4)}{2n} + A_1 k(T)\, dT \qquad \text{(IV-C-27)}$$

At steady-state, the same heat Q flows across each pair of foils. Therefore, Equation (IV-C-27) can be integrated as follows, between the limits y = 0, B and T = T_{liq}, T_s:

$$Q = \frac{A_o \sigma \epsilon}{2n} \left(T_s^4 - T_{liq}\right) + \frac{A_1}{B} \int_{T_{liq}}^{T_s} k\,(T)\, dT \qquad \text{(IV-C-28)}$$

If k (T) is known, the last equation gives Q as a function of T_s. Another expression can be set down for Q, in terms of the incident radiation I and the outer foil surface properties α_o, ϵ_o:

$$Q = A_o \left(\alpha_o I - \sigma \epsilon_o T_s^4\right)$$

$$= A_o \sigma \epsilon_o \left(T_a^4 - T_s^4\right) \qquad \text{(IV-C-29)}$$

Here we have neglected A_1 as being small compared to A_o.

Equations (IV-C-28 and 29) are sufficient to determine Q, if k(T) is known. We have considered the following form:

$$k = k_a \left(T/T_a\right)^p \qquad \text{(IV-C-30)}$$

For such a form, it is found that a general relationship exists between a normalized Q and a parameter involving the quantities of interest:

$$\frac{Q}{A_o \alpha_o I} = \frac{K}{1+K} + f\,(G,p) \qquad \text{(IV-C-31)}$$

where

$$G \equiv \frac{A_1 k_a T_a}{A_o B \alpha_o I} \qquad \text{(IV-C-32)}$$

When G = 0 (no penetrations), f (G, p) = 0 and Equation (IV-C-31) becomes the usual one.

Figure IV-C-14 shows the relation for p = -1, 0 and +1, and for particular values of T_a and T_{liq}. When G is less than 0.1,

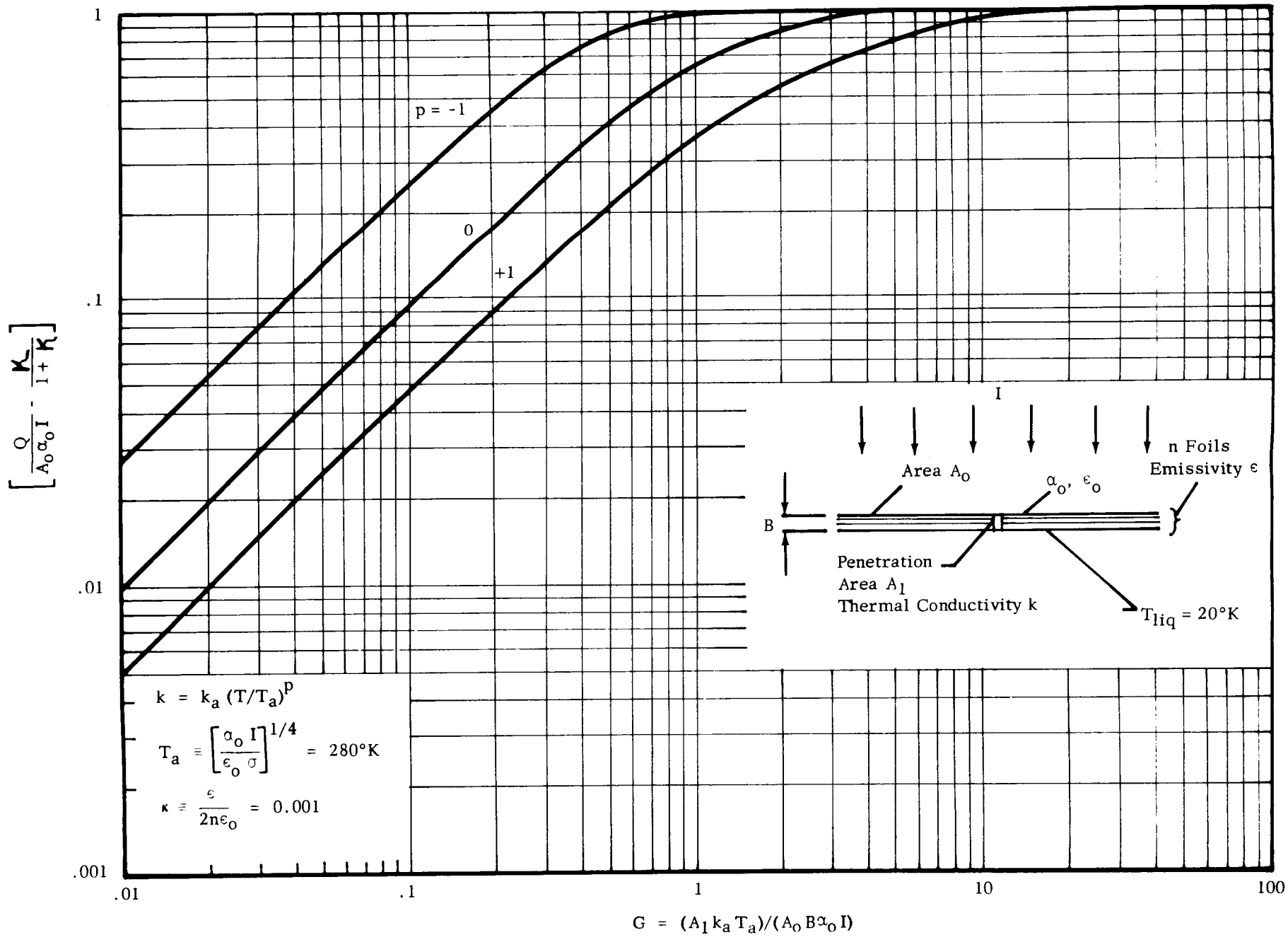

FIGURE IV-C-14 EFFECT OF A PENETRATION WITH TEMPERATURE DEPENDENT THERMAL CONDUCTIVITY

$$f = \frac{G}{p + 1}, \quad p \neq -1 \qquad \text{(IV-C-33)}$$

$$f = G \ln (T_a/T_{liq}), \quad p = -1 \qquad \text{(IV-C-34)}$$

When G is very large

$$f = \frac{1}{1 + K} \quad (G \to \infty) \qquad \text{(IV-C-35)}$$

so that $Q = A_o \kappa_o I$. This last result is of very little interest, but is shown in order to complete the picture in Figure IV-C-14.

IV-D. GENERAL SCALING RELATIONSHIPS

The heat leak through a penetration in multilayer insulation depends on the temperature distribution and external radiation flux in the locality of the penetration. Hence, there is a need to know that temperature distribution for an accurate assessment of the total heat leak to the tank. Fortunately, the penetrations themselves affect the temperature distribution in MLI either slightly or only locally. A strong short that has an extensive effect is by definition an intolerable one that must be decoupled from the MLI, in other words rendered weak. Thus, penetrations do not feed back strongly on the thermal state of the MLI, although their behavior depends on that thermal state.

It follows that the determination of the temperature distribution within the MLI, with or without penetrations, is desirable. The possibility of measuring the temperatures on a thermal model of a tank system and applying scaling laws to predict the distribution on a geometrically similar prototype is attractive in this context. We will now present the laws that must be obeyed in such a scaling process, in MLI blankets with or without penetrations. First, we will consider the MLI blanket alone.

1. Insulation Blanket

Following a development similar to that presented in Appendix F, a steady-state heat balance equation in three orthogonal coordinates can be written, governing the temperature within MLI, as follows:

$$\left(\frac{\sigma \epsilon T_{a,max}^3 D^2}{2 k t n^2} \right) \frac{\partial^2 \theta^4}{\partial u^2} + \frac{\partial^2 \theta}{\partial \xi^2} + \frac{\partial^2 \theta}{\partial \zeta^2} = 0 \qquad \text{(IV-D-1)}$$

where

$u = y/B$

y = perpendicular distance from the tank surface

B = thickness of insulation

$\xi, \zeta = x/D,\ z/D$

x, z = coordinates parallel to the tank surface (normal to y)

D = a representative tank dimension

$\theta = T/T_{a,max}$

$$T_{a,max}^4 = \frac{\alpha_o I_{max}}{\epsilon_o \sigma}$$

I_{max} = maximum external incident flux intensity

ϵ, ϵ_o, σ, k, t, n, as previously defined.

The coefficient of the first term can be written as:

$$\gamma^2 = \frac{\sigma \epsilon T_{a,max}^3 D^2}{2 n^2 kt} = \left(\frac{D}{x_{Decay}}\right)^2 \qquad \text{(IV-D-2)}$$

where x_{Decay} is as defined in Appendix D with $T_a = T_{a,max}$. The coefficient γ can also be expressed in terms of I_{max}

$$\gamma^2 = \sigma^{1/4} \left(\frac{\alpha_o}{\epsilon_o} I_{max}\right)^{3/4} \frac{\epsilon D^2}{ktn^2} \qquad \text{(IV-D-3)}$$

There are two boundary conditions for this problem, since the variables ξ and ζ gird the tank and hence have no boundaries. The two conditions are:

$$u = 0 : \theta = T_{liq}/T_{a,max} \qquad \text{(IV-D-4)}$$

$$u = 1 : K \frac{\partial \theta^4}{\partial u} + \theta_4 = \theta_a^4 (\xi, \zeta) \qquad \text{(IV-D-5)}$$

where K is as before and

$$\theta_a^4 (\xi, \zeta) = (T_a/T_{a,max})^4 = \frac{I(\xi, \zeta)}{I_{max}} \qquad \text{(IV-D-6)}$$

Solutions θ (u, ξ, ζ), for all geometrically similar tanks for which the normalized flux distribution I/I_{max} is similar, will depend on the parameters γ, K and $T_{liq}/T_{a,max}$. The solutions will be similar for any set of these parameters. If, as is usual, the last parameter, $T_{liq}/T_{a,max}$ is small compared with unity, the condition that it be kept constant is not a very stringent one; the other two parameters are usually the important ones.

The heat flow into the tank through the insulation blanket is, from Appendix E, (neglecting T_{liq}^4)

$$Q_B = \kappa \alpha_o \oint I dA \qquad \text{(IV-D-7)}$$

where the integral is performed over the entire tank area. Equation (IV-D-7) can be re-arranged:

$$Q_B = \kappa \alpha_o I_{max} D^2 \oint (I/I_{max}) \, d\xi \, d\zeta \qquad \text{(IV-D-8)}$$

For similar cases, I/I_{max} is the same function of ξ and ζ; hence, the integral in (IV-D-8) is a constant. Therefore, we have, for similar cases:

$$Q_B = (\text{constant}) \kappa (\alpha_o I_{max} D^2) \qquad \text{(IV-D-9)}$$

provided that ϵ has the same dependence on temperature for similar cases (which will be true if the same foil material is used in each case), or that ϵ is not a function of temperature (we have seen that little error is incurred in assuming that the latter is true). Since κ is presumed constant, we may rewrite Q_B as:

$$Q_B = (\text{constant}) \alpha_o I_{max} D^2 \qquad \text{(IV-D-10)}$$

The condition that the first two parameters, γ and κ be kept constant leaves some choice in the selection of the remaining variables. This choice will determine the scaling factor to be used in computing Q_B for a particular tank from the results (test or computer) on a similar tank of different size. In the following two examples, ϵ and kt are kept constant and the same foils are used.

a. <u>If n/D is kept constant</u>, then for similarity,

$$\alpha_o I_{max} \text{ must vary as } 1/D \qquad \text{(IV-D-11)}$$

and

$$\epsilon_o \text{ must vary as } 1/D \qquad \text{(IV-D-12)}$$

If these relationships are adhered to, Q_B will vary as D. Suppose that one were interested in determining the heat flow into a cylindrical cryogenic tank 20-ft. long, eight feet in diameter, axis at 45° to the

direction of the sun and insulated with 40 layers of a certain foil. The absorptivity, d_o, is 0.1 (i.e., 10 per cent of the solar radiation is absorbed) and the emissivity of the outer foil is 0.2. We have a test tank 4-ft. in diameter, 10 feet long.

For these similarity conditions are need to use 20 layers of foil (n/D the same in both cases), $\alpha_o = 0.2$ and $\epsilon = 0.4$ and I_{max} is identical as in the angle incident to the radiation. If Q_B measured is 8 watts, then we would predict Q_B for the large tank to be 16 watts.

b. <u>If n/D^2 is kept constant</u>, then for similarity,

$$\alpha_o I_{max} \text{ must vary as } D^{2/3} \qquad \text{(IV-D-13)}$$

and

$$\epsilon_o \text{ must vary as } 1/D^2 \qquad \text{(IV-D-14)}$$

If these relationships are adhered to, Q_B will vary as $D^{8/3}$. Suppose the 20-ft. tank referred to above were insulated with 80 layers of foil, we could still use the test tank (10-ft. diameter) with 20 layers since now n/D^2 is the same in both cases. For similarity of Q_o and ϵ_o,

$$\frac{\alpha_o \text{ (large tank)}}{\alpha_o \text{ (test tank)}} = \left(\frac{D \text{ (large tank)}}{D \text{ (test tank)}}\right)^{2/3} = 2^{2/3}$$

$$\alpha_o \text{ (test tank)} = 0.1/2^{2/3} = 0.063$$

and

$$\frac{\epsilon_o \text{ (large tank)}}{\epsilon_o \text{ (test tank)}} = \left(\frac{D \text{ (large tank)}}{D \text{ (test tank)}}\right)^{-2} = \frac{1}{2^2}$$

$$\epsilon_o \text{ (test tank)} = (0.2)(4) = 0.8$$

These are the values of α_o and ϵ_o which must be used on the test tank for similarity considerations. If experiments on the small tank showed that the heat leak $Q_B = 2$ watts, then we would predict for the large tank.

$$Q_B = 2\ (2)^{8/3} = 12 \text{ watts}$$

2. <u>Penetrations</u>

We have seen that for similarity in MLI, three parameters must be kept constant. In the case of penetrations, there are also some similarity parameters. In Appendix F, a set of these has been developed for cylindrical thermal shorts. Most shorts through MLI will be cylindrical, with their radius finite or infinite (straight strips). For non-cylindrical shorts, it is possible to transform Equation (F-17) into a new set of orthogonal coordinates, one of which is constant on the periphery of the thermal short. Such a transformation will not alter the significance of the parameters K, ψ, v_o and θ_{liq}, but will change the solution θ (u,--,--) and the value of the heat flow integral, which for cylindrical coordinates is given by (F-35). Therefore, for similarity it is still necessary and sufficient to keep the four parameters constant.

Since one of the boundary conditions for any short is $0^4 = f(u)$ at large distances, then $f(u)$ must be the same for similarity; hence, the blanket temperature distribution must also be similar. We may, therefore, list the requirements for similarity as follows:

	Parameter to be kept constant
Insulation Blanket:	γ, η, $T_{liq}/T_{a,max}$
Penetration	v_o, κ, T_{liq}/T_a, ψ

Suppose we have satisfied the similarity requirements for the MLI blanket, and we wish, in addition, to satisfy similarity for the penetrations. The requirement for κ is already satisfied. If we locate the penetration at the same geometrical location (i.e., same ξ and ζ), then since $T_a/T_{a,max}$ is the same function of ξ and ζ for similar blanket cases, and since $T_{liq}/T_{a,max}$ is the same, we will have, at the penetration, T_{liq}/T_a

$$T_{liq}/T_a = \frac{T_{liq}/T_{a,max}}{T_a/T_{a,max}} \qquad \text{(IV-D-15)}$$

$$= \text{(constant) } f(\xi, \zeta)$$

$$= \text{constant} \qquad \text{(IV-D-16)}$$

Comparing v_o (Appendix F) and γ, we see that their ratio is

$$\frac{v_o}{\gamma} = (r_o/D) \qquad \text{(IV-D-17)}$$

Therefore, since γ is constant for the blanket, keeping r_o/D constant is sufficient to ensure that v_o be constant. Fixing the ratio between r_o and D keeps the size of the penetration on the same scale as the tank. Finally, the parameter ψ, which is particular to the penetration and not to the blanket, must be kept constant. Incidentally, it is possible to keep ψ constant in a variety of ways. To recapitulate:

For similar MLI: γ, κ, θ_{liq} constant.

For similar shorts: same scale as tank, similar location on tank, ψ constant.

IV-E. METHODS OF TEMPERATURE FIELD AND HEAT FLOW COMPUTATIONS

Experimental results show that with care in design and application, multilayer insulation can be made to perform as intended, namely, as a stack of pure radiating foils. When this is so, many simplifications can be made in the determination of the heat flow through the insulation blanket. The presence of penetrations does not interfere seriously with this heat flow, because the disturbances in temperature that they cause is small. First, the average outer foil temperature is changed by a negligible amount. Second, disturbances within the MLI are either small (weak shorts) or localized.

On the other hand, as stated in IV-F, the heat leak through penetrations depends on local MLI temperatures, as well as on the local incident flux intensity. Except in special cases (e.g., uniform internal radiation environment), these local conditions cannot be determined with accuracy except by solving simultaneously for both the temperature distribution within the MLI and the incident radiosity distribution on the outer foil. While again it is valid in many cases to simplify the problem of calculating penetration heat leaks by some conservative averaging process (e.g., using $(\overline{T^4})^{1/4}$ for $\overline{T}$ as a mean outer foil temperature), strong shorts present a more pressing computational problem, that cannot be approached by linearization. Also, even without penetrations, the estimation of incident radiosity depends on conduction parallel to foils in cases where the radiation incident on the shroud is not fixed but depends on multiple reflections between the shroud and some other part of a vehicle, or between the shroud and another body such as the lunar surface.

Regardless of the usefulness, desirability or even apparent necessity of making a full-scale computation of the temperature field within MLI, the validity of such a computation must enter into the decision whether or not to carry it out. Now the validity hinges very critically on our knowledge of the detailed properties of the MLI in question.

In the case of pure radiating foils of known radiative properties, the detailed computation will have some significances, provided the heat flow across foils is taken to be radiative in the heat balance equations for difference elements, either by writing down the radiative heat transfer terms or by considering $k_\perp$ to vary with the third power of the local absolute temperature. The assumption that $k_\perp$ is uniform, at some mean value, is useful for screening purposes, and to clarify certain situations, but it is not valid in the prediction of heat flow into strong penetrations. Finally, to assume $k_\perp$ to be some arbitrary function of temperature, places the analysis on dangerous grounds. The conductive contribution to normal heat flow in MLI is due to the presence of a gas and/or mechanical contacts between foils or between foils and spacers.

The contact pressure, or the gas density, are extremely difficult to predict (the designer strives to avoid them altogether), and since the conductive component is a strong function of these causes, analysis will not give definitive answers.

Certain cases have been analyzed for screening purposes, and have been presented in a topical report [11]. The analysis of reference (11) is based on a constant value of $k_{\perp}$. The analytical method employed, and described to some extent therein, is called the method of zones. This method [13] permits the subdivision of a medium (the MLI blanket) into a smaller number of larger elements for a given accuracy.

An analysis for the more significant case of pure radiating foils ($k_{\perp} \sim T^3$) has been made for special cases (see Section IV-F). When the number of foils in the insulation is very small (e.g., less than 5), it may be desirable to abandon the concept of a continuous medium, and analyze each foil individually. Such a procedure was adopted in some of the calculations presented in Section IV-F.

IV-F. CORRELATION OF THEORY WITH EXPERIMENT

1. Geometrical Considerations

Figure IV-F-1 shows a cross-section through the axis of the tank used in the experimental program. It is seen that the section is symmetrical about the mid-plane except for the support neck (which also serves as the fill-and-vent duct). Three types of sections form the tank: a cylindrical section girding the tank; two toroidal sections, one above and one below the cylinder; and a spherical section at top and at bottom. The neck is guarded in such a way that the heat input to the tank by either conduction along the neck or radiation through the duct is made very small. The guard is essentially a station which is kept at the temperature of the liquid cryogen so that whatever conduction occurs is due to a difference in temperature of a degree Kelvin at most between the guard point and the point joining the neck and the tank. The radiation which arrives from the warm end of the neck is absorbed by a series of baffles which are at the guard temperature, so that the interior of the tank sees cold baffle surfaces. The radiation arriving at the baffles is conducted to the guard liquid.

a. Boundary Conditions

The tank has been constructed of copper of sufficient thickness to ensure that there be negligible gradients in temperature parallel to the tank wall from the bottom to the top, whatever the level of the liquid. Therefore, the tank-surface-side of any insulation may be considered to be at the liquid cryogen temperature. If the edge of the insulation adjacent to the neck surface is carefully protected, then at that edge the boundary condition may be imposed that the gradient in temperature parallel to the foils is zero. At the bottom of the tank, provision has been made for the insertion of various penetrations, that is, pipes, pins, etc., so that the boundary condition there would depend on what the penetration is. The remaining surface bounding the insulation is the outer foil and it is exposed to the radiation from sources consisting of baffles through which liquid is circulated.

Referring again to Figure IV-F-1, baffles 1 and 2 are kept at one controllable temperature while baffle 3 can be kept at a different controllable temperature. Of course, liquid at the same temperature may be circulated in all baffles at the same time in a given test. Nevertheless, it is possible to expose different parts of the tank to different environmental radiation fluxes. The two sources are separated by a lip (A in Figure IV-F-1). The closer the edge of the lip to the outer surface of the insulation the more closely the radiation environment may be considered to be changing abruptly. In practice, the separation will not be zero so that the insulation outer foil sees a gradually changing flux intensity. Note that this intensity distribution will in all cases be symmetrical about the axis of the tank.

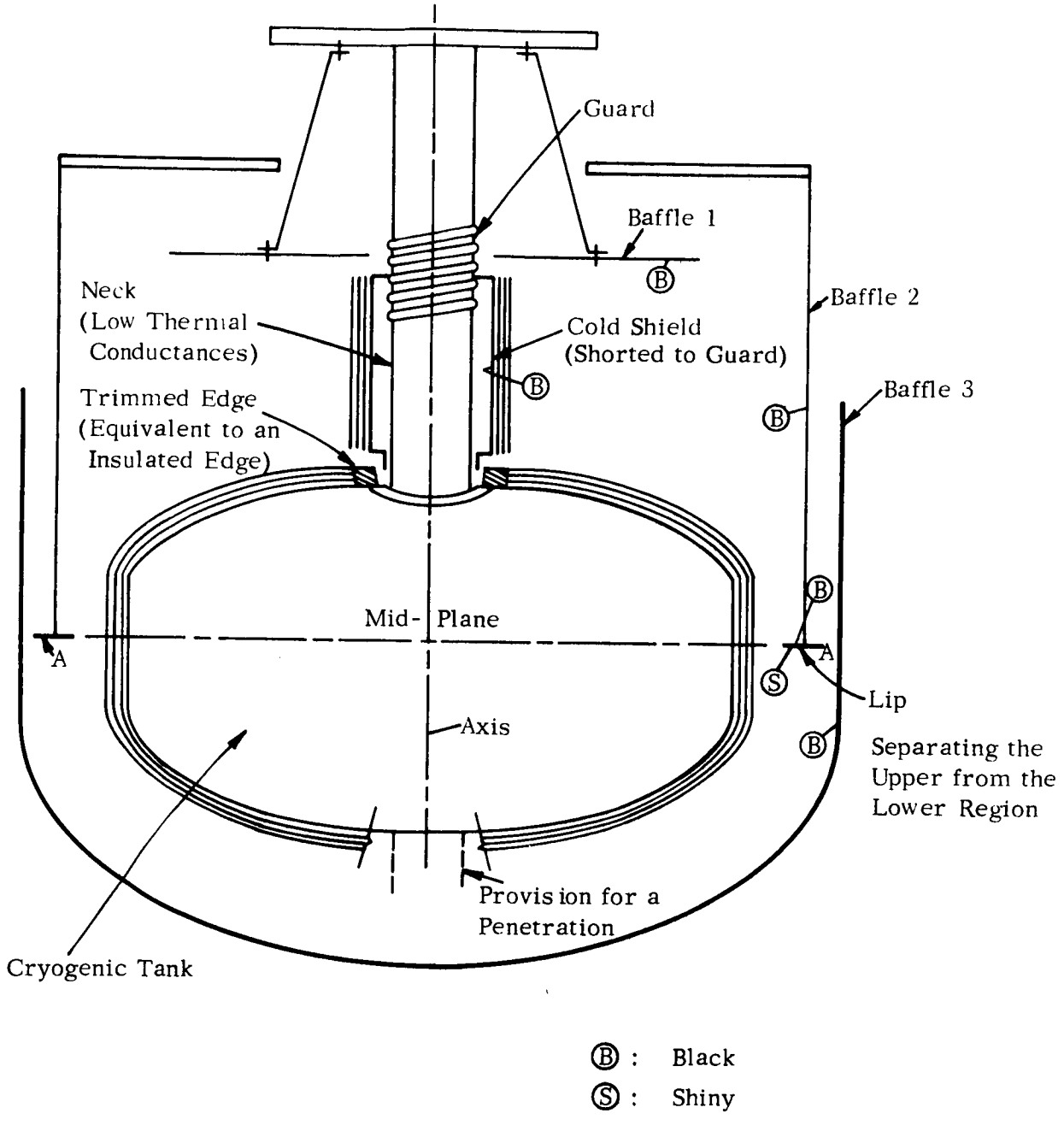

FIGURE IV-F-1 SCHEMATIC OF THE ENVIRONMENTAL TANK WITH INSULATION AND THERMAL ENVIRONMENT

b. Case of Axial Symmetry

If there is no penetration or if the penetration is circular in nature and concentric with the bottom central point of the tank, then the boundary conditions are completely symmetrical about that axis and the resulting temperature distribution will also be symmetrical.

Under the conditions of axial symmetry, the temperature and other thermal effects may be considered as varying along a gore of the insulation as shown in Figure IV-F-2, but to remain the same for each gore, so that only one need be considered. If the gore is developed and laid on a flat surface as suggested by Figure IV-F-2, the thermal problem then becomes one-dimensional, there being no gradients perpendicular to the main direction along the strip.

2. Interpretation of Tests on a Uniform Blanket of Multilayer Insulation in a Uniform Radiation Environment

An experiment was carried out with the tank insulated with five layers of multilayer insulation. Two types of foils were tested: 1) two-mil aluminum and 2) aluminized Mylar. There was no penetration on the bottom of the tank and the environmental flux was controlled and made uniform; that is, liquid at the same temperature was circulated in all baffles. Thermocouples were placed at various locations, and since these thermocouples indicated no temperature gradients parallel to the foils, even near the support neck (no heat flow to or from the neck via the insulation), the resulting total heat input as deduced from the boil-off rate could be divided by the entire tank surface to determine a relevant average normal flux through the insulation.

The flux calculated in this manner agrees reasonably well with that predicted by considering that only radiation heat transfer occurs normal to the foil, and using published values for the emissivity of the aluminum used for the tests. Most authors agree that the emissivity of aluminum in the infrared is in the range 0.02 to 0.04.

Reynolds et al [8] show a curve giving values of 0.02 at $77^{\circ}K$ and 0.028 at $300^{\circ}K$. Using the latter value one predicts a flux (in $Btu/hr\text{-}ft^2$) of 0.41 through five foils of aluminum on a liquid nitrogen tank in a $300^{\circ}K$ environment. The flux measured at Arthur D. Little, Inc., was 0.375 - 0.42. To predict the heat flux through aluminized Mylar, account must be taken of the fact that the uncoated side of the Mylar has an emissivity close to unity in the infrared. The predicted heat flux through five foils is double that for pure aluminum foils, namely, 0.82; the flux measured at Arthur D. Little, Inc., is 1.02.

In applying the foils, very great care had been taken to minimize mechanical contact pressure between adjacent layers and the spacer material. Also the chamber pressure was kept below 10^{-5} torr so that gaseous conduction across the foils could be neglected. A thermocouple

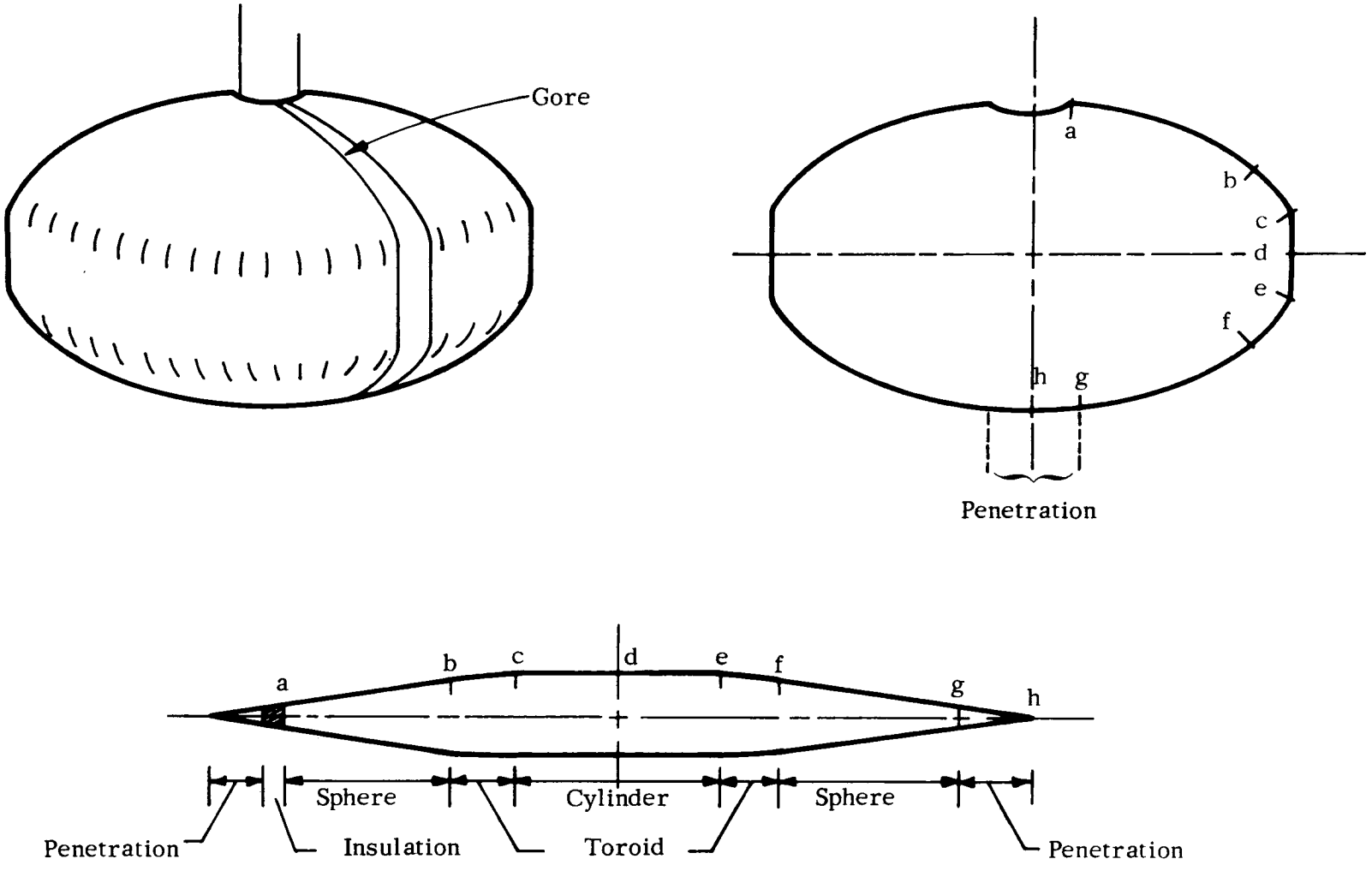

FIGURE IV-F-2 DEVELOPMENT OF A GORE STRIP FOR ANALYZING MULTILAYER INSULATION IN THE CASE OF AXIAL SYMMETRY

at each of the foils at a particular location on the surface of the tank indicated a linear variation in the fourth power of the absolute temperature at that location. This observation, together with the absence of gradients on the surface of the outer layer, and with the values of heat flux obtained, vindicates the contention that radiation was the sole mode of heat transfer normal to the insulation.

The results show that the theoretical performance of multilayer insulation can be achieved in practice. They also indicate that the concept of an average conductivity must be very carefully applied in detailed analyses of multilayer insulation. If the effects of shorts are to be screened using an average uniform thermal conductivity normal to the foils, the results will be of a qualitative nature and will represent facts in the large rather than in detail. Another important conclusion is that equations governing the thermal behavior of the foils can be written with confidence.

3. Variation in Incident Flux

Having established the radiative nature of heat transfer across the insulation, it is now possible to use this as a basis for predicting by calculations the behavior of multilayer insulation, in a given set of circumstances. A test, to be called the "hot-cold" test, was carried out with five layers of aluminized Mylar applied on the test tank, but with the upper baffles at room temperature and the lower baffles at liquid nitrogen temperature. In this case the radiation environment changes at the mid-plane of the test tank. As previously stated, the physical arrangement employed to produce a discontinuous surface distribution of flux intensity consists of a baffle in the form of a horizontal metal annulus (lip) that girds the tank at the mid-plane and prevents radiation from sources above this plane from reaching those portions of the outer foil surface situated below the plane, and vice versa. The closer the fit between the lip and the foils the more closely does the flux distribution approach a step function.

In actual practice the separation between the lip and the foils is not zero and the flux distribution changes over smoothly rather than abruptly. The actual distribution can be described by the formula:

$$Q(x) = \frac{\sigma}{2}\left[\begin{array}{l} T_h^4\left(1 + \dfrac{x/a}{\sqrt{1 + (x/a)^2}}\right) \\ +T_c^4\left(1 - \dfrac{x/a}{\sqrt{1 + (x/a)^2}}\right) \end{array}\right] \qquad \text{(IV-F-1)}$$

where

σ = the Stefan-Boltzmann constant,

T_h = the temperature of the warm baffle,

T_c = the temperature of the cold baffle,

x = the height above the mid-plane where the annulus lies, positive or negative, depending on whether the point considered is above or below that plane, respectively,

a = the spacing between the inner edge of the annulus and the outer foil surface.

This relationship is shown in Figure IV-F-3. For the case where the warm baffle is at temperature 300°K and the cold baffle is at 77°K the transition occurs over a range in x/a of about 4, that is, from x/a = -2 to x/a = +2. Beyond those points the outer surface of the insulation receives incident flux very nearly equal to that from the local baffle. The transition thus occurs over the distance 4a.

a. Calculations Based on Radiative Heat Transfer Normal to the Layers

Because it is important to confirm once more that the radiative properties alone dictate normal heat transfer, and also to determine the actual effect of parallel conduction, an analysis under the test conditions just described was carried out with an electronic computer. In the present case the equation which describes the behavior of each of the five layers is as follows:

$$k\,t\,\frac{d^2T_i}{dx^2} + \frac{\sigma\epsilon}{2}\left(T^4_{i-1} + T^4_{i+1} - 2T^4_i\right) = 0 \qquad \text{(IV-F-2)}$$

where

k = the thermal conductivity of the foil,

t = the thickness of the foil,

x = distance along the foil, (zero at the lip),

ϵ = emissivity of the foil,

T_i = the temperature of the ith foil,

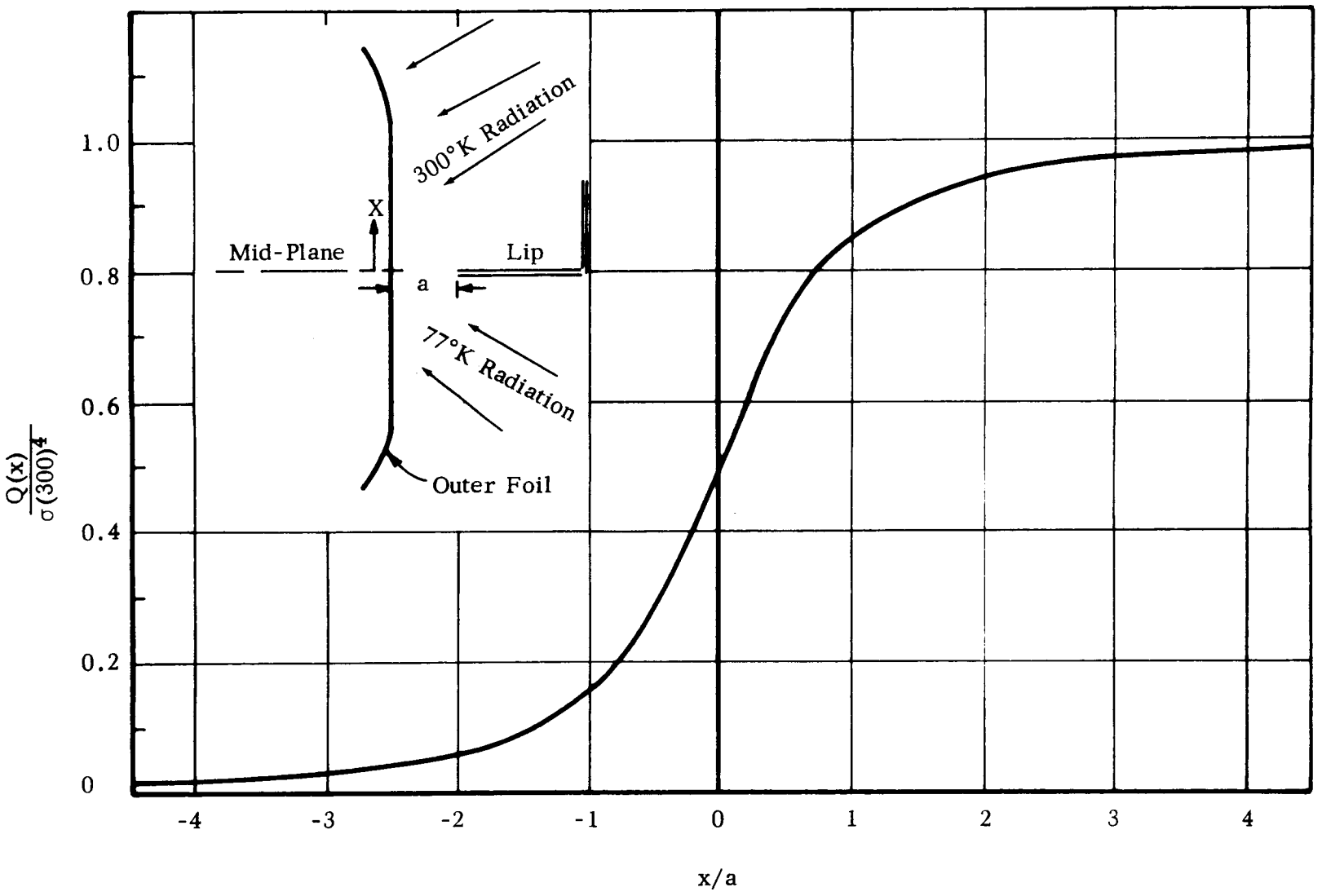

FIGURE IV-F-3 INCIDENT FLUX NEAR THE MID-PLANE OF THE TANK IN THE HOT-COLD TEST

T_{i-1} and T_{i+1} are the temperatures of adjacent foils opposite the same point on the tank wall.

Equation IV-F-2 applies to the intermediate foils, that is to foils that are surrounded by other foils. For the first and fifth foils, that is the outer foil and that which is adjacent to the tank wall, boundary conditions must be imposed. For the outer foil the following equation applies:

$$k\,t\,\frac{d^2T_1}{dx^2} + \frac{\sigma\epsilon}{2}\,(T^4_2 - T^4_1) + \alpha_o\,Q(x) - \sigma\epsilon_o\,T^4_1 = 0 \qquad \text{(IV-F-3)}$$

For the innermost foil the following equation applies:

$$k\,t\,\frac{d^2T_5}{dx^2} + \frac{\sigma\epsilon}{2}\,(T^4_4 - T^4_5) + \frac{\sigma(77^4 - T_5^4)}{\frac{1}{\epsilon_i} + \frac{1}{\epsilon_t} - 1} = 0 \qquad \text{(IV-F-4)}$$

The foils are numbered beginning from 1 at the outermost foil and ending at five at the innermost foil.

α_o = the absorptivity of the outermost foil for the incident radiation,

ϵ_o = the emissivity of the outer surface of the outermost foil,

$Q(x)$ = the function defined in Equation (IV-F-1),

ϵ_i = the emissivity of that side of the innermost foil facing the tank wall,

ϵ_t = the emissivity of the tank wall. In our case it is very close to unity.

In our case, ϵ_o is very nearly equal to α_o and is equal to the emissivity of the aluminum of the foils. The function Q (x) depends on the value of a. This was measured to be 1.25 inches.

It was anticipated that the effect of the change in environmental flux should not be felt at distances of more than a few inches from the mid-plane of the tank. (See Chapter IV-A-3b for an estimate of the decay distance in the case of aluminized Mylar.) Therefore, it

was decided to limit the region of interest along the gore strip of Figure IV-F-2 to region b c d e f, eighteen inches long, along which the width w(x) does not vary appreciably. Thus, only the plane problem need be dealt with. The validity of this procedure is, of course, subject to verification with the results.

At the toroidal sections, the tank surface curves away from the vertical and does not view the radiation arriving through the gap at the lip. Account was taken of this fact by truncating Q (x) at the beginning and end of the cylindrical sections (points c and e in Figure IV-F-2).

The distribution of the temperature of each of the five foils was calculated using equations of the types (IV-F-2, -3, -4). The result for the outer foil is shown in Figure IV-F-4. The temperature distribution of the outer foil was also measured with thermocouples and is also shown in Figure IV-F-4. The agreement between predicted and measured values is quite remarkable, but not so surprising as it might at first appear. The explanation is as follows.

Any point on the outer surface of the outermost foil receives thermal radiation at a flux intensity that is determined by the geometry, emissivity and temperature distribution of the bodies viewed by the point. But that incident radiation may be thought of as being emitted by a black body completely viewed by the point and held at some equivalent temperature T_e. Now in the present case, since the distribution of incident flux intensity is known (viz., Q (x), Figure IV-F-3), it is possible to determine a distribution of equivalent temperatures for radiation T_e (x).

$$\sigma T_e^4 (x) = Q (x) \qquad \text{(IV-F-5)}$$

For the baffle temperatures actually prevailing in the tests in question, Q (x) can be computed according to Equation (IV-F-1) and T_e (x) from Equation IV-F-5. This was done and is shown in Figure IV-F-4.

We see immediately the similarity between T_e (x) on the one hand and the theoretical and experimental results on the other hand. It is noted that the outer foil adopts a temperature distribution that follows T_e (x) closely (but not exactly since a net heat flow implies a temperature difference), and this is also predicted by calculation. Conduction parallel to the foils does not appear to have distorted the temperature distribution appreciably except at the edges of the transition, i.e., at some distance on both sides of the lip.

Thus, in this case (aluminized Mylar) the distance over which the change in flux occurs is greater than that necessary for the foils to adapt to the change. We saw previously that most of the change occurs

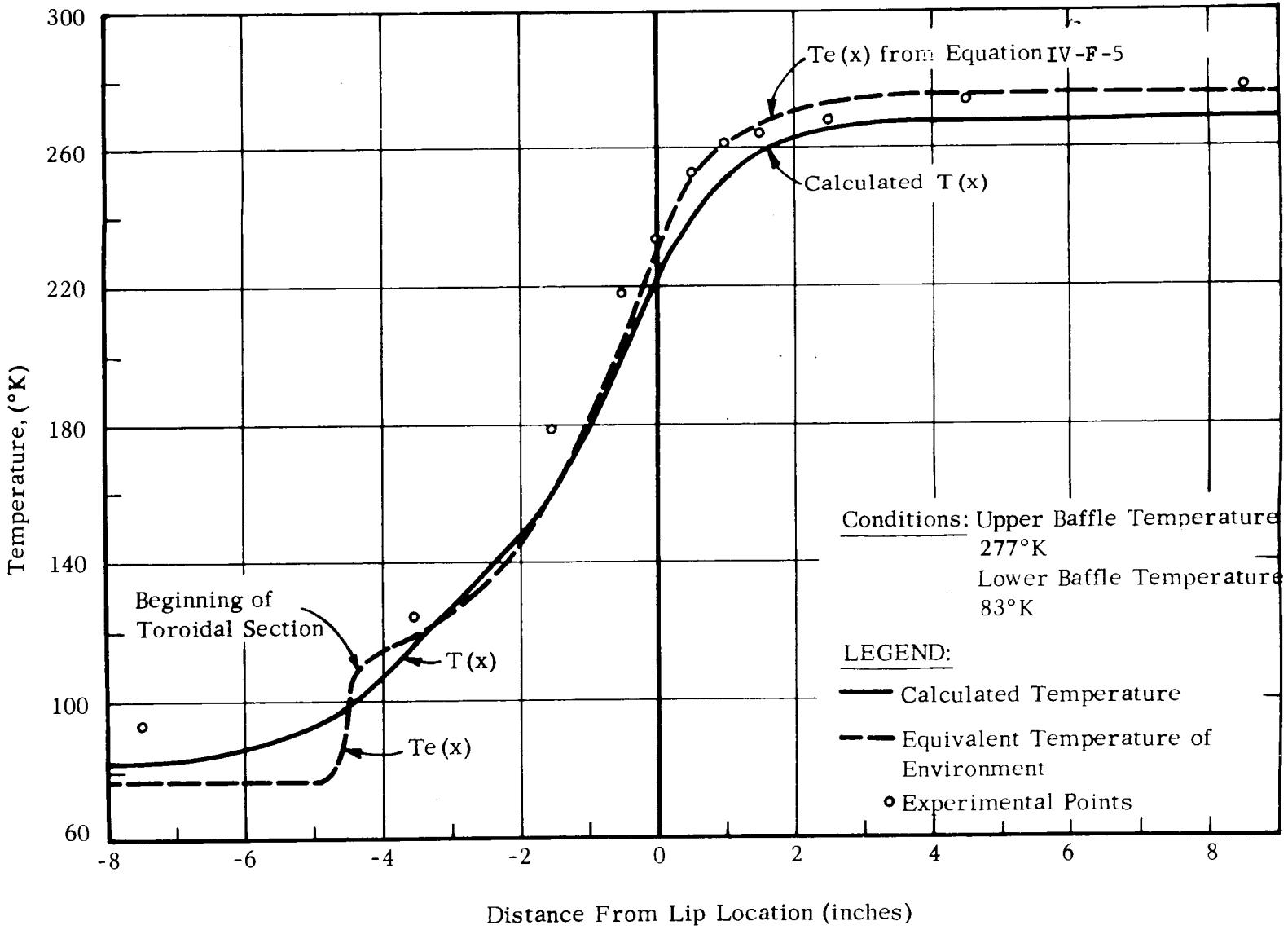

FIGURE IV-F-4 TEMPERATURE DISTRIBUTION IN THE TOP FOIL NEAR THE LIP SEPARATING UPPER AND LOWER BAFFLES

over a distance 4a, or five inches. The foils adapt to a change over a distance that is shorter than five inches. We have calculated this distance in the case of an abrupt change in flux (a = 0) over five foils; the distance of adaptation is an inch or so. The distribution in temperature associated with the latter calculation will not be shown because a more significant curve of the same type, presented hereafter (see IV-F-4 Copper Penetration) shows the same distance of adaptation.

b. Calculations Based on Average Values of the Conductivities

It is interesting to compare the decay distance found above with that formulated in a previous quarterly report on the basis of an average conductivity perpendicular and a conductivity parallel to the foils ($k_\perp$ and $k_\parallel$, respectively). We had that the decay distance could be expressed as follows:

$$x_{Decay} \doteq B\sqrt{k_\parallel / k_\perp} \qquad \text{(IV-F-6)}$$

where B is the thickness of the insulation. In the test on a uniform blanket of five layers of aluminized Mylar in a uniform radiation environment the average heat flux through the insulation was 0.0021 watts/in^2. This may be used to define a perpendicular conductivity as follows:

$$k_\perp = \frac{(Q/A)B}{T} = \frac{0.0021B}{300-77} = 9.5 \times 10^{-6}B \qquad \text{(IV-F-7)}$$

or, in terms of any value of n, the number of foils,

$$k_\perp n = n\,(9.5 \times 10^{-6})\,B = 5 \times 9.5 \times 10^{-6}B$$

$$k_\perp \frac{n}{B} = 4.75 \times 10^{-5}\ \frac{\text{watts}}{\text{in}^2\text{-}^\circ\text{K}} \qquad \text{(IV-F-8)}$$

The parallel conductivity can be defined as

$$k_{11} = kt\,\frac{n}{B} \qquad \text{(IV-F-9)}$$

In the case of aluminized Mylar the conductivity is that of aluminum (k = 6 watts/in - $^\circ$K approximately) since the Mylar base contributes a very small fraction of the conduction. The thickness t to be inserted in equation (IV-F-9) is 1 micro-inch. Therefore, k_{11} can be written as:

$$k_{11} \frac{B}{n} = 6 \times 10^{-6} \quad \frac{\text{watts}}{^{o}K} \qquad \text{(IV-F-10)}$$

Substituting Equations (IV-F-8) and (IV-F-10) into Equation (IV-F-6), we find

$$x_{Decay} \doteq 0.36\ n \text{ inches}$$

and since n is 5 in our case the decay distance is of the order of two inches. This decay distance, of course, applies on each side of the lip, totaling four inches. If we add the width of the transition, 4a or five inches, the total distance for the change-over in the temperature of the outer foil is about 9 inches. Of course, direct addition cannot be justified since some decay occurs simultaneously with the transition in flux, in a non-linear fashion. Nevertheless, it can be said that prediction based on an average conductivity gives realistic results even in the case where heat flow normal to the foils is almost purely radiative in nature.

c. Heat Flow

If the parallel conductivity of the Mylar insulation had been absolutely zero and the change in heat flux had been abrupt (a = o), the total heat flow into the tank in this test would have been exactly one-half that for the test in which all baffles are warm (the all-warm test). This is because the side exposed to $77^{o}K$ radiation would have received no net heat at all, the tank wall temperature on that side being also $77^{o}K$.

Now for non-zero values of a, the total radiation incident on the outer foil can be found by integrating, over all x, Q (x) as expressed in Equation (IV-F-1). If we make the assumption that the toroidal sections are outside the influence of the lip, we find that the total radiation incident on the outer foil is the same as if a were zero. For foils having zero parallel conductivity, the total heat flow into the tank would still be one-half that for the all-warm test. Furthermore, it can be shown that if heat flow normal to the foils is purely radiative, the total heat input to the tank is independent of k_{11}.

Hence, we can predict that the total heat flow to the tank under the experimental hot-cold conditions should be one-half that for the all-warm test. This is borne out by the experimental measurement of heat flow. Also, calculations based on the temperature distribution T(x) shown in Figure IV-F-4 predict an increase of 0.07 Btu/hr over the entire tank; this value can be accounted for by the possible error in the calculations of the temperature distribution.

4. Copper Penetration

As discussed in Section IV-C, the penetrations into multilayer insulation can be classified in one of three categories: weak, strong, and absolute thermal shorts. A test was carried out on the experimental tank with five layers of aluminized Mylar into which was inserted a disc of copper 3" in diameter. This constitutes an absolute thermal short. Great care was taken to ensure that full contact existed between each of the foils and the copper. This was done by using a number of copper discs which were squeezed together and sandwiched between them the five layers of aluminized Mylar.

The penetration was placed on the axis of the tank and on the bottom so that again axial symmetry was ensured. In this case, radial coordinates are used in the calculations. Also, the boundary condition at the edge where contact is made with the absolute short is that the temperature for each edge is $77^{\circ}K$. The flux over the entire tank was due to the baffles being uniformly warm, at a temperature of $279^{\circ}K$. (At the time of the analysis, however, it was assumed that the temperature was to be $300^{\circ}K$.)

Aside from cylindrical geometry and the inner boundary conditions just mentioned, the problem is similar to that discussed in the previous section. Equations are similar except for the fact that the radius enters as a factor in the terms. The solution to this problem was found by manual computation. The resulting temperature distribution for each of the foils when the baffles are at $300^{\circ}K$ is shown in Figure IV-F-5.

In order to compare the results of the computation with the experimental results, account had to be taken of the true temperature of the baffles, namely $279^{\circ}K$. With this new environmental temperature it is possible to calculate easily the equilibrium temperature of each of the foils at large distances from the penetration. A recomputation by hand of T (r) of each foil for the true baffle temperature was not deemed advisable at this time since it involves a considerable amount of effort, and since, as we shall discuss later, the general program which is being undertaken will permit easy computation of this case later on. Rather, temperature distribution curves were traced in from the known end temperatures, using the following reasoning.

Near the penetration each foil is at $77^{\circ}K$, and at very large distances each has its equilibrium value. The forms of the distributions between those extremes may be estimated from those computed for a $300^{\circ}K$ environment. In particular, the outer foil is at $272^{\circ}K$ at large distances from the penetration, under the new environment of $279^{\circ}K$. But in the $300^{\circ}K$ environment the second foil is at $274^{\circ}K$ at large distances. Hence, the equilibrium temperature of the outer foil in the true case is very close to that of the second foil in the $300^{\circ}K$ case. Therefore, the distribution computed for the second foil in the $300^{\circ}K$ case could

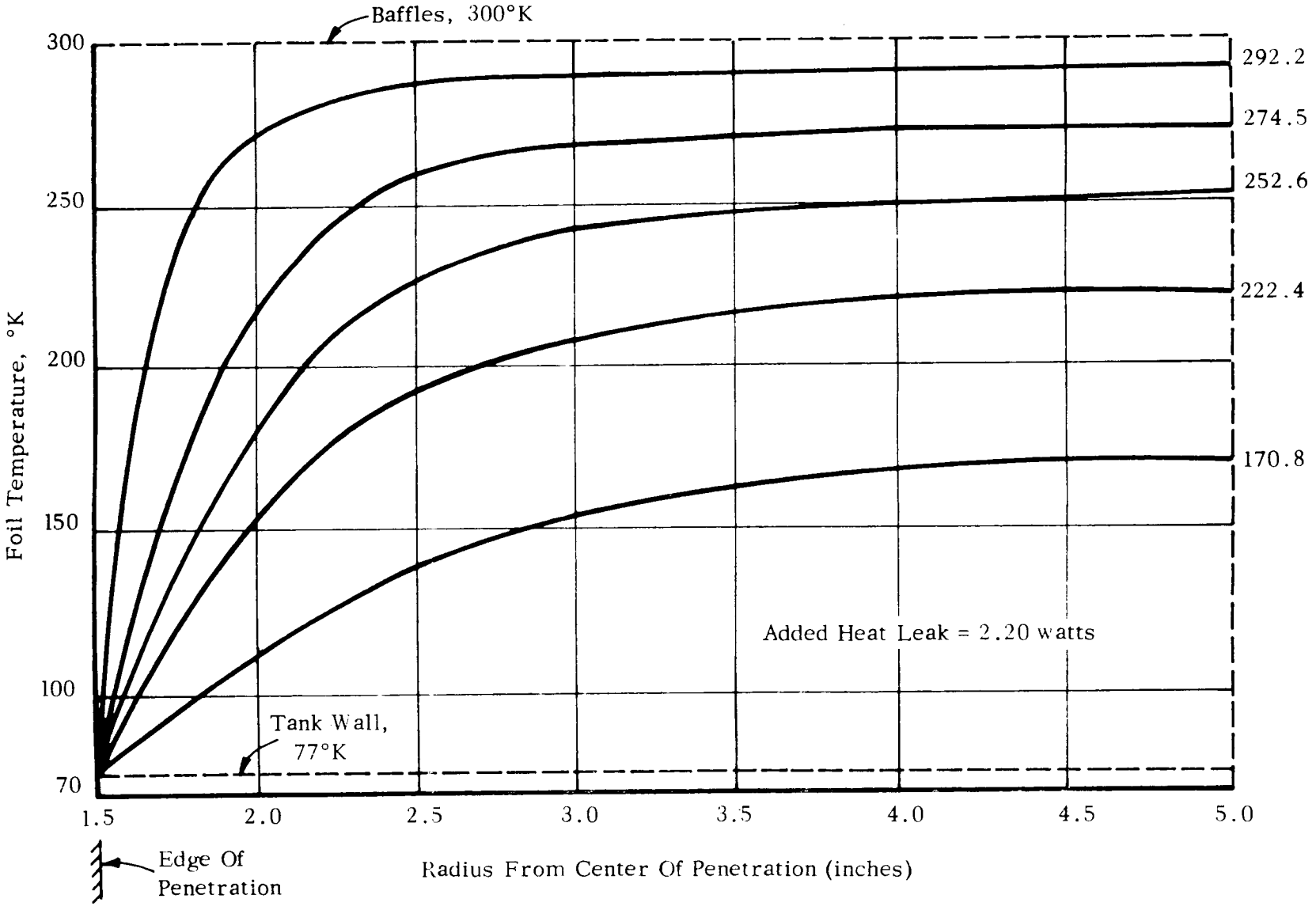

FIGURE IV-F-5 CALCULATED TEMPERATURE DISTRIBUTION IN FIVE LAYERS OF ALUMINIZED MYLAR AROUND A THREE-INCH DIAMETER COPPER PENETRATION (ABSOLUTE SHORT)

be used to trace approximately that for the top foil in the true case. However, in the true case the environment remains at 279°K throughout and right up to the penetration whereas in the previous (theoretical) case the second foil felt the environment of the outermost foil which, of course, did not retain its equilibrium temperature throughout, but had a temperature distribution which decreased to 77°K at the penetration. Thus, if one were to trace the curve for the top foil from the theoretical curve for the second foil, one would have to account for this stronger radiation environment near the penetration. This can be done by allowing the temperature of the first foil to rise rather more quickly near the penetration, giving a curve resembling that of the top foil in the 300°K case. The latter is, of course, an over-correction. The approximation cannot be too far off and is, of course, subject to verification when a result of an exact computation is obtained.

The estimated temperature distributions for the top foil and also for the third foil (based on similar reasoning) are shown in Figure IV-F-6. Also shown in that figure are temperature measurements for the top foil. First, the temperature was measured at large distances (of the order of 18 inches) from the center of the penetration. The value measured there was 274°K, whereas our computed equilibrium temperature was 271.8°K. The other two temperatures measured, namely at 2" from the center and about 2-1/2" from the center, lie between the under-corrected and the over-corrected curves. We again have a strong though qualitative confirmation of the hypothesis that radiation alone controls heat transfer normal to the foil. The experimental points are expected to lie between the under-corrected curve and the over-corrected curve, which they certainly do.

The total heat leak to the tank additional to that which would flow without a penetration has also been computed for the 300°K baffle case. The temperature distribution normal to the foils is shown both theoretically and experimentally to have reached the equilibrium distribution at a radius from the center of the penetration equal to 5.4". The heat flow over the area of a circle of 5.4" radius when there is no penetration and the environment is at 300°K, is 0.2 watt. Now with the penetration of diameter 3 inches with a blackened surface, the heat absorbed on the penetration itself is 2.1 watts, and the heat input through the disturbed insulation from the penetration out to 5.4" radius is 0.3 watts, giving a total of 2.4 watts. Subtracting from this 2.4 watts the heat flow through the undisturbed insulation over the area of a circle 5.4" radius, namely 0.2 watt, gives a net additional heat leak of 2.2 watts. Note that the heat leak due to the foils being lowered in temperature below their equilibrium value contributes only 10 percent of the additional heat leak in this case.

The experimental heat input to the tank for this test is much larger than could be accounted for by an error in estimating the additional heat leak. Hence, one must await a thorough review of the data and the experimental conditions before making comparisons between experimental and theoretical results for this test.

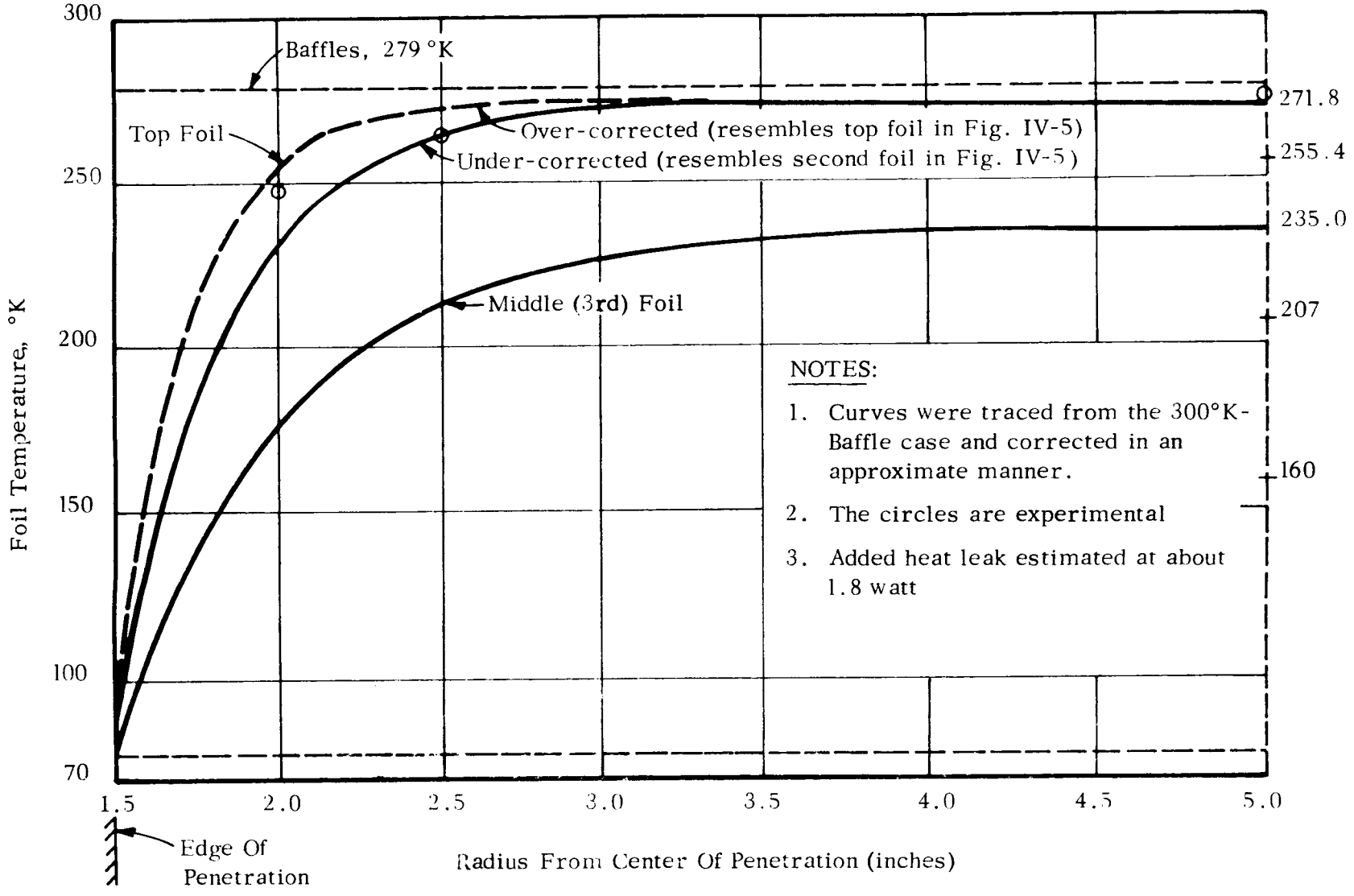

FIGURE IV-F-6 TEMPERATURE DISTRIBUTION IN FIVE-FOIL SYSTEM, ALUMINIZED MYLAR AROUND A THREE-INCH DIAMETER - COPPER PENETRATION

5. General Program

In the analysis of the hot-cold test for aluminized Mylar, the region of interest was limited to the cylindrical band around the tank plus the toroidal section. In the analysis of the copper penetration, the region of interest was limited to a circle a few inches in radius. There will be cases, particularly when aluminum foils are used, where the effect of a change in environment such as existed when the lip separated a hot from a cold region, or of a penetration as in the last case analyzed, will spread out to distances that are not small compared to the dimensions of the tank. In such a case the region of interest for analysis cannot be restricted but rather the entire insulation blanket must be considered and boundary conditions applied at the appropriate point. In other words, the entire gore strip of Figure IV-F-2 must be included in the analysis.

Since, moreover, various types of penetrations will be included in future tests as well as different types of insulation or combinations thereof, the institution of a general computer program for this particular tank will be warranted. In such a program, the environmental flux distribution can be left as an unknown function. Account will, of course, be taken of the spherical geometry of the insulation near the top and bottom of the tank; the number of foils and type can be varied; and penetrations of various types and sizes may be inserted theoretically on the bottom of the tank provided the resulting temperature distribution remains axially symmetric.

APPENDIX A

SHROUD RADIATION TO A TANK

It is the purpose of this appendix to determine the power radiating from a shroud inward. Once this is known, it becomes possible to determine, or at least to estimate with good accuracy, the power incident on the tank insulation. With that information, the heat flow into the tank itself can be determined using the results of Appendix E for pure radiating foils, or estimated for other types of foils.

Figure A-1 illustrates a tank, II, (more precisely, the outer foil of the MLI over a tank) and a shroud, I, that completely surrounds the tank. Both the shroud and tank (outer foil) surfaces have been subdivided into a large number of elements. The inner surfaces of the shroud elements are numbered 1 to n, and the outer surfaces of the tank outer foil elements are numbered n + 1 to m. Thus, there are m elements in all, that can exchange radiation with each other. Note that some shroud elements can be viewed from other shroud elements, and similarly for the tank.

The steady-state condition of each element may be characterized as follows: it radiates an amount of power R_i and has incident upon it an amount of power R_{Zi}. R_i may be called the radiosity of the i^{th} element, and R_{Zi} its "incident" radiosity.

The radiosity of an element is the sum of the power it emits and the power it reflects. For a gray body:

$$R_i = \sigma \epsilon_i T_i^4 A_i + (1 - \epsilon_i) R_{Zi} \qquad \text{(A-1)}$$

where ϵ_i is the emissivity of the i^{th} element, $(1 - \epsilon_i)$ its reflectivity, A_i its surface area and T_i its absolute temperature. The incident radiosity of the i^{th} element contributed by the j^{th} element is the fraction α_{ji} of the j^{th} radiosity that arrives at the i^{th} element. Therefore, R_{Zi} is the sum of all such fractions:

$$R_{Zi} = \sum_{j=1}^{m} \alpha_{ji} R_j \qquad \text{(A-2)}$$

We may, therefore, write R_i as

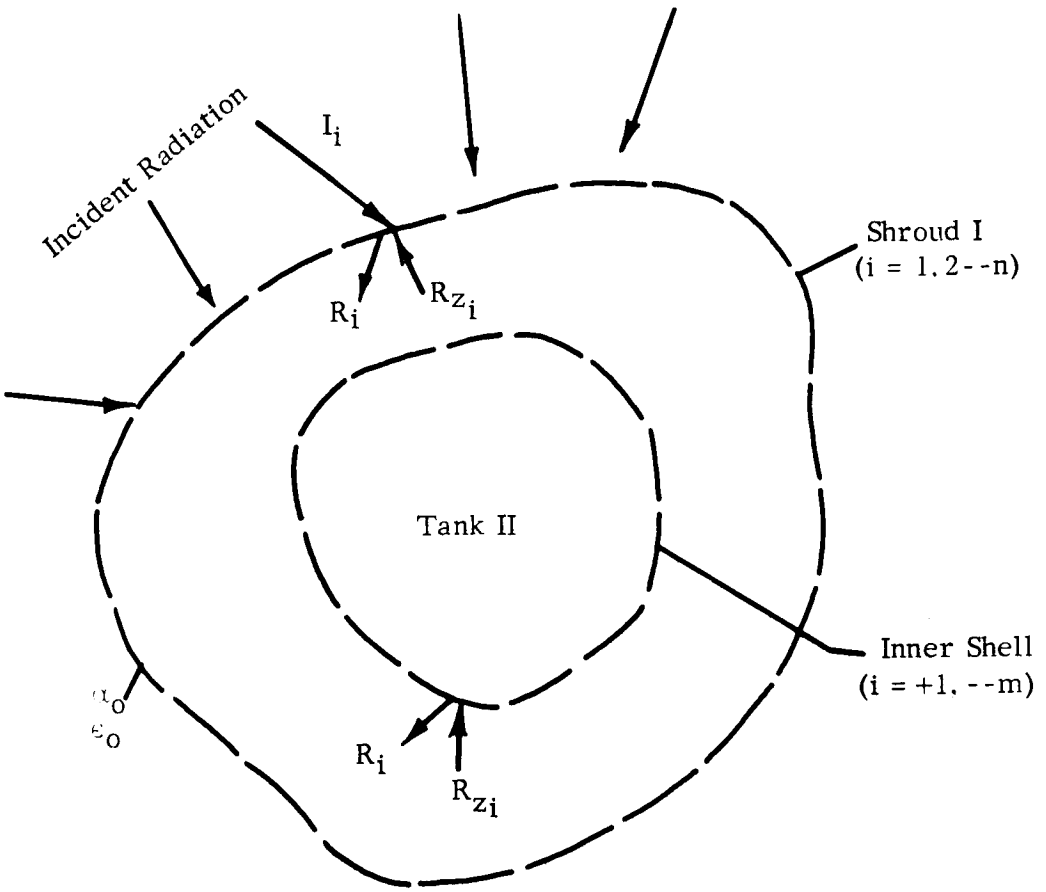

Note: Third Dimension Not Shown

FIGURE A-1 MODEL FOR SHROUD ANALYSIS

$$R_i = \epsilon_i T_i^4 A_i + (1 - \epsilon_i) \sum_{j=1}^{m} \alpha_{ji} R_j \qquad (A\text{-}3)$$

Now consider the shroud elements. Let the shroud emissivity be uniform and equal to ϵ_I.

$$R_i = \sigma \epsilon_I T_i^4 A_i + (1 - \epsilon_I) \sum_{j=1}^{m} \alpha_{ji} R_j \quad (i = 1, \ldots n) \qquad (A\text{-}4)$$

We can now add all shroud radiosities, from i = 1 to n, calling the sum R_I:

$$R_I \equiv \sum_{i=1}^{n} R_i \qquad (A\text{-}5)$$

$$= \epsilon_I \sum_{i=1}^{n} \sigma T_i^4 A_i + (1 - \epsilon_I) \sum_{i=1}^{n} \sum_{j=1}^{m} \alpha_{ji} R_j$$

(A-6)

In order to evaluate the double summation, we make use of the radiation balance between the two shells: shroud and tank outer foil. This balance is very nearly achieved because of the high shielding factor made possible with multilayer insulation (and without which cryogenics could not be stored for appreciable periods in space). We express this balance as follows:

$$\sum_{i=1}^{n} \sum_{j=n+1}^{m} \alpha_{ji} R_j = \sum_{i=n+1}^{m} \sum_{j=1}^{n} \alpha_{ji} R_j \qquad (A\text{-}7)$$

Equation (A-7) states that the sum of all radiosity fractions from the tank that reach the shroud equals the sum of all radiosity fractions from the shroud that reach the tank. In other words, all the power from the tank to the shroud equals all the power from the shroud to the tank. Note that Equation (A-7) does not include (nor should it include) direct radiation exchange between shroud elements or between tank elements. As suggested above, the difference between the two sides of Equation (A-6) is of the

order of the heat leak into the tank, which is small compared with either side of (A-7).

We now evaluate the double summation of Equation (A-6). We first break it up into two parts:

$$\sum_{i=1}^{n}\sum_{j=1}^{m} \alpha_{ji} R_j = \sum_{i=1}^{n}\sum_{j=n+1}^{m} \alpha_{ji} R_j + \sum_{i=1}^{n}\sum_{j=1}^{n} \alpha_{ji} R_j \qquad \text{(A-8)}$$

The first of the two double summations on the right side of (A-8) is replaced by its equivalent from (A-7), giving

$$\sum_{i=1}^{n}\sum_{j=1}^{m} \alpha_{ji} R_j = \sum_{i=n+1}^{m}\sum_{j=1}^{n} \alpha_{ji} R_j + \sum_{i=1}^{n}\sum_{j=1}^{n} \alpha_{ji} R_j$$

$$= \sum_{i=1}^{m}\sum_{j=1}^{n} \alpha_{ji} R_j \qquad \text{(A-9)}$$

We now reverse the order of summation:

$$\sum_{i=1}^{n}\sum_{j=1}^{m} \alpha_{ji} R_j + \sum_{j=1}^{n} \left(R_j \sum_{i=1}^{m} \alpha_{ji}\right) \qquad \text{(A-10)}$$

Now for any j, the summation inside brackets equals unity, since it is the sum of all view factors from a particular surface.

$$\sum_{i=1}^{m} \alpha_{ji} = 1 \text{ (any j)} \qquad \text{(A-11)}$$

Therefore,

$$\sum_{i=1}^{n} \sum_{j=1}^{m} \alpha_{ji} R_j = \sum_{j=1}^{n} R_j \qquad \text{(A-12)}$$

But, from the definition, (A-5), the right-hand side equals R_I. (This is true independently of the change in summation index.) We can now write Equation (A-6) as

$$R_I = \epsilon_I \sum_{i=1}^{n} \sigma T_i^4 A_i + (1 - \epsilon_I) R_I$$

or

$$R_I = \sum_{i=1}^{n} \sigma T_i^4 A_i \qquad \text{(A-13)}$$

This important result states that the total power emitted from the inner surface of the shroud (i.e., its total radiosity) equals the sum of the products area x fourth power of temperature x the Stefan-Boltzmann constant.

We can evaluate the right-hand side of (A-13) in terms of the space radiation environment. If we again neglect the heat flowing into the tank, we can state that all space radiation absorbed by the outer surface of the shroud must be re-emitted to space. Using the same shroud elements as before, and considering uniform absorbtivity α_o and emissivity ϵ_o for the outer shroud surface, we have:

$$\sum_{i=1}^{n} \alpha_o I_i A_i = \sum_{i=1}^{n} \sigma \epsilon_o A_i T_i^4$$

or

$$\sum_{i=1}^{n} \sigma T_i^4 A_i = \frac{\alpha_o}{\epsilon_o} \sum_{i=1}^{n} I_i A_i \qquad \text{(A-14)}$$

Substituting into (A-13):

$$R_I = \frac{\alpha_o}{\epsilon_o} \sum_{i=1}^{n} I_i A_i \qquad \text{(A-15)}$$

The result (A-15) is highly accurate when the shielding factor due to the multilayer insulation is greater than 50. Usually this factor ($\sim$50 x number of foils) is several thousands. The result is also independent of parallel conduction within the foils or along the shroud surface.

In order to make use of Equation (A-15) we must know what fraction of R_I directly reaches the tank outer foil. Usually this can be done within an error of 10 to 20 percent. There may be some extreme cases (not too likely in the usual tank system where space within the shroud is at a premium) in which care must be exercised since warmer shroud elements may view the tank differently from colder elements.

A simple illustrative example of such an extreme case is shown in Figure A-2. The shroud is an infinitely long box, square in cross-section; the "tank" is infinitely long, and very thin, represented by a flat plate (7, 8, in Figure A-2). The shroud is irradiated uniformly on its upper face by some external source (e.g., the sun). The "tank" location may be varied, by varying its height x above the bottom (6) of the shroud. We have analyzed this case, (i) assuming the sides 1 to 6 of the shroud to be thermally isolated from one another, but each to be isothermal and (ii) assuming the whole shroud to be isothermal. The "tank" is assumed isothermal. The emissivity ϵ of the inside surfaces of the shroud and of the two sides, 7 and 8, of the "tank" was assumed uniform and was varied. The resulting total incident radiation on the two "tank" surfaces is given in Table A-1.

TABLE A-1

TOTAL INCIDENT POWER ON THE "TANK" OF FIGURE A-2 ($\epsilon_o = 1$)

$$\left[R_{Z7} + R_{Z8}\right] / \alpha_o \quad I$$

		Isolated Shroud Elements			Isothermal Shroud
ϵ	x =	0	0.5	1.0	All x's
1		0.443	0.553	0.801	0.500
0.5		0.428	0.535	0.801	0.500
0.1		0.407	0.509	0.806	0.500

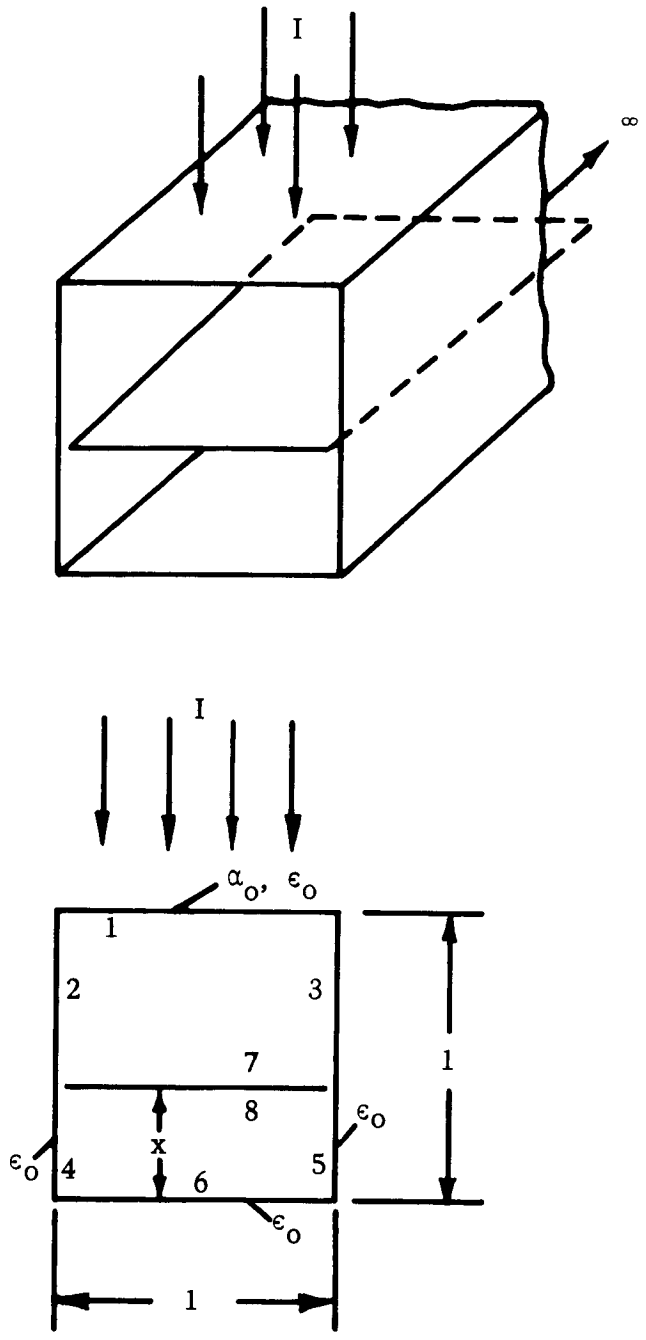

FIGURE A-2 A SIMPLIFIED ILLUSTRATION FOR SHROUD ANALYSIS

From Table A-1 will be seen the near-independence of the incident power on ϵ, and the effect of geometry. Regarding geometry, it will be remembered that this is an extreme case.

APPENDIX B

ANALYSIS OF INTERNAL PIPE RADIATION

1. ILLUSTRATION OF SOME FUNDAMENTALS

Consider a specific pipe, of diameter 10 inches and length 30 inches (L/D = 3), with a warm-end temperature of 300°K and a cold-end temperature of 20°K (liquid hydrogen at normal pressure).

a. Direct Radiation from the Warm End to the Cold End

Assuming the warm end (at 300°K) to be gray, and to emit diffusely with an emissivity ϵ_{end}, it will emit 23.3 ϵ_{end} watts. Of that radiation, 0.6 ϵ_{end} watts will reach the plane of the cold end directly, without first being reflected or re-radiated from the walls (see Figure B-1). The cold-end direct radiation heat leak, 0.6 ϵ_{end} watts, is not of serious importance, even when ϵ_{end} is unity. It can be made even smaller by decreasing the emissivity at the warm end, by increasing the length of the pipe, and by increasing the reflectivity (decreasing the emissivity) at the cold end.

The total amount emitted from the warm end (23.3 ϵ_{end} watts in the previous example) is not, itself, small in general. (It must be remembered that one watt will evaporate 175 lb. of hydrogen in 10,000 hours.) Hence, if an appreciable portion of the warm-end emission leaks into the cryogenic tank, the heat inleakage is indeed serious. From what was said in Section III, this heat leak does not arise to an important degree from direct emission to the cold end, but must occur primarily through reflection from, re-emission at, and conduction along the walls.

b. Effect of Wall Radiation Without Conduction

Consider the case in which the wall conductivity and/or thickness (i.e., the product kt) is very small, so that conductive flow can be neglected. Consider the walls to be insulated so that there is no radial heat flow. Then at steady-state any radiation incident at a point on the wall is completely re-radiated (by reflection and/or re-emission), regardless of the wall emissivity and reflectivity, since there is no other issue for the incident radiation. Let this re-radiation be diffuse.

The resulting pattern is illustrated in Figure B-2. Some of the radiation from the warm end at (a) for example arrives directly at the cold end. Some from (a) arrives on the wall at (b). Of the latter amount, some returns to the warm end at (c), some to other parts of the wall (which is again re-distributed), and some to the cold end. Similar

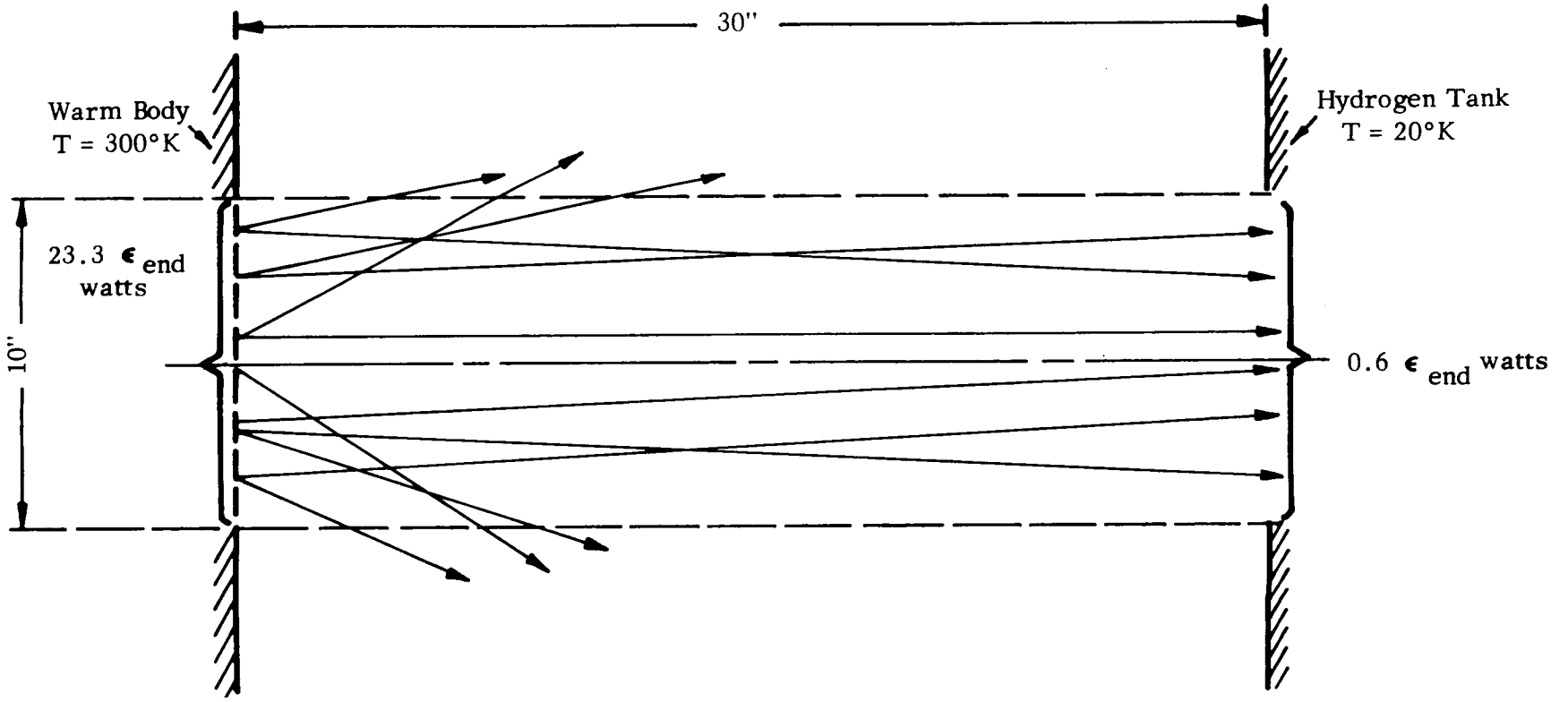

FIGURE B-1 RADIATION INSIDE A PIPE, CONSIDERING ONLY THE EMISSION FROM THE WARM END PROPAGATING DIRECTLY TO THE PLANE OF THE COLD END

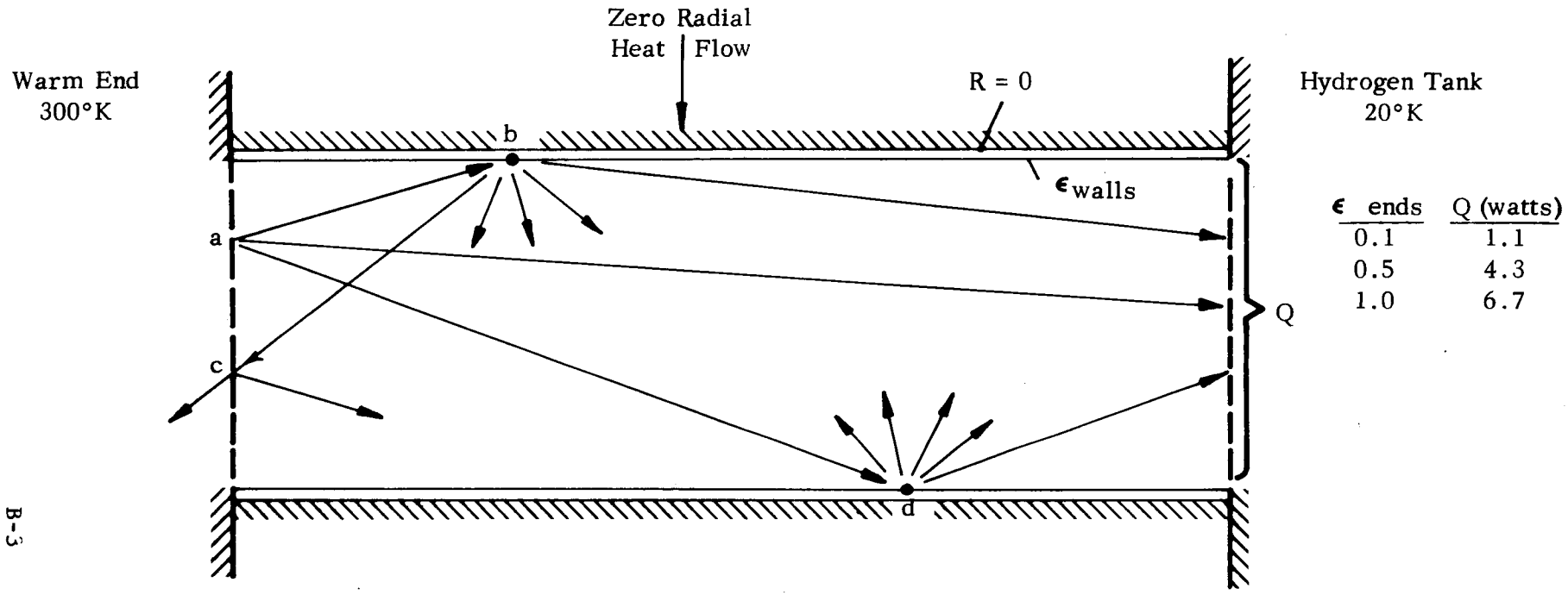

FIGURE B-2 RADIATIVE HEAT LEAK WHEN WALL CONDUCTIVITY IS NEGLIGIBLE, FUNCTION OF ϵ_{ends} BUT INDEPENDENT OF ϵ_{wall}

effects occur at other parts of the wall (e.g., at d). Of the radiation returning from the walls to the warm end, some may be reflected back, depending on the emissivity at that end. This pattern is independent of ϵ_{wall}, and depends only on ϵ_{ends}.

If the end emissivities are both equal to unity ($\epsilon_{ends} = 1.0$), the resulting net heat flow into the cold end is 6.7 watts; for $\epsilon_{ends} = 0.5$, it is 4.3 watts; and for $\epsilon_{ends} = 0.1$, it is 1.1 watt. These values are, as mentioned above, independent of the wall emissivity, ϵ_{wall}. Varying ϵ_{wall} will change the fraction of the incident energy that is re-emitted and the fraction reflected, but the sum of those two fractions is always unity. Incidentally, changing the fraction re-emitted will not change the wall temperature, but since in any event $k = 0$, the conductive contribution to heat inleakage always remains zero.

One final point in the discussion of this case: without the use of end baffles, it will be difficult to achieve effective emissivities at the ends very much less than 0.5.

c. Wall Radiation and Conduction Uncoupled ($\epsilon_{wall} = 0$)

In the case where $\epsilon_{wall} = 0$ (see Figure B-3), all radiation arriving at a point on the wall is reflected. If this reflection is diffuse, the same radiation pattern will exist within the pipe as for case b., just discussed. Hence, the radiative heat leak will have the same dependence on ϵ_{ends} as in that case. However, the conductive heat inleakage must be added. But, since $\epsilon_{wall} = 0$, no incident radiation is absorbed; hence, the temperature distribution along the wall is not affected by radiation. Therefore, the conductive heat leak is constant as we vary ϵ_{ends}. The conductive heat flow may be expressed as

$$Q_{cond} = \frac{\pi D t}{L} \int_{20^{\circ}K}^{300^{\circ}K} k dT \qquad \text{(B-1)}$$

$$= \pi D (k_m t) \frac{\Delta T}{L} \qquad \text{(B-2)}$$

where D is the pipe diameter, L its length, ΔT is the total temperature difference from end to end (= 280°K); k_m is the mean thermal conductivity of the pipe wall, and t its thickness.

The conductive heat leak must be added to the radiative heat leak (see case b) to obtain the total heat leak. For a stainless steel pipe,

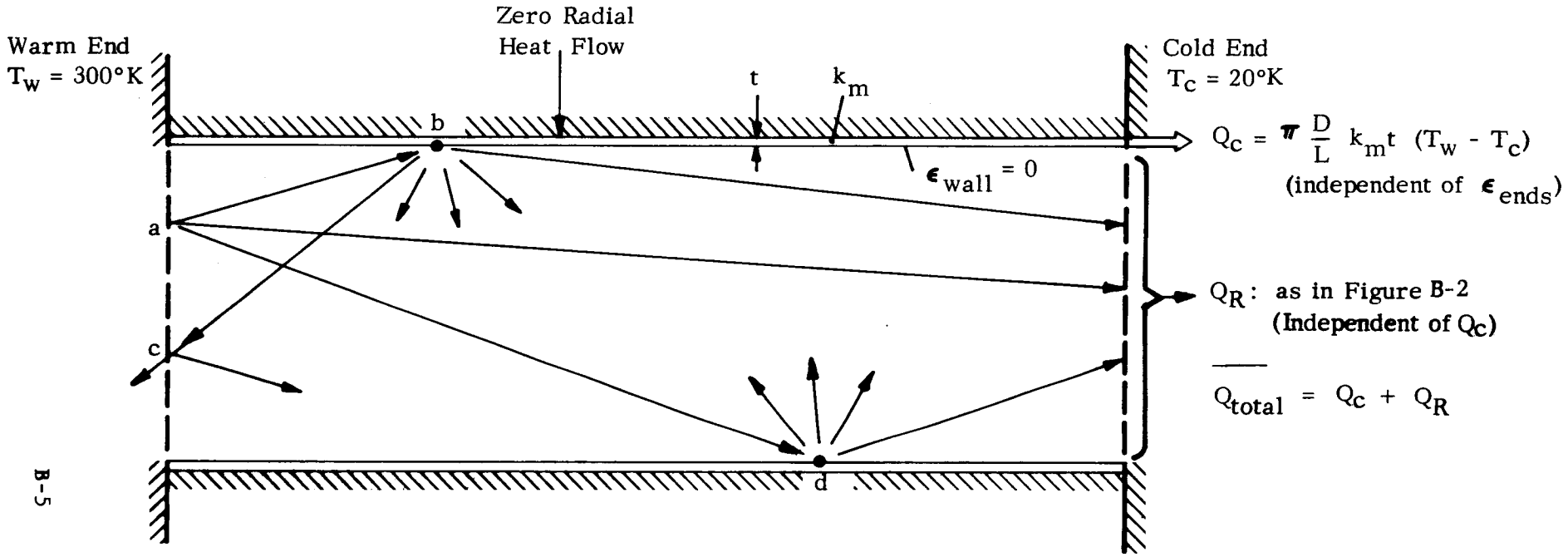

FIGURE B-3 RADIATION PATTERN FOR $\epsilon_{wall} = 0$, THE SAME AS FOR FIGURE B-2. CONDUCTIVE HEAT LEAK IS ADDED DIRECTLY TO THE RADIATIVE HEAT LEAK

0.030" thick, the conductive heat leak for the pipe considered is 1.8 watts. This value might perhaps be cut down by a factor of about 10, through the use of thinner walls, other pipe materials (e.g., asbestos fiber) and/or a longer pipe. Since ϵ_{wall}, although it can be made small, cannot be made zero, a discussion of the effects of varying (k_{mean} t) does not have the relevance at this point that it will in the subsequent discussion. Note, however, that conductive heat inleakages of about 2 watts, combined with a radiative leak of the same order (viz., case b) leads to a total leak that cannot be neglected.

2. ANALYSIS OF THE GENERAL CASE

In the general case, where neither ϵ_{wall} nor $k_m t$ is zero, the absorption of radiation at the pipe walls affects the wall temperature distribution and, hence, the conductive heat flow; on the other hand, conduction contributes in the determination of the temperature pattern and, hence, in the emission of radiation. It is, therefore, no longer possible to account for radiation and conduction separately; moreover, the interaction between these two effects is non-linear and each set of conditions must be treated individually. However, it is possible by the careful selection of cases, by attention to the laws of radiation, and by the observation of trends, to obtain a given amount of information with a surprisingly low number of computations.

a. Method of Treatment

First the pipe walls and ends are divided into a number of parts; then a heat balance is carried out for each part. This heat balance takes account of all inputs and outputs to the part, by radiation and conduction. At steady-state the total inputs must equal the total outputs.

Consider Figure B-4, showing a cylindrical ring element of axial length, dx. Axial symmetry in the temperature and radiation flux distributions is assumed. A heat balance has been carried out for the element, resulting in the equation

$$R - R_Z = (\pi D dx)\ (k_m t)\ \frac{d^2T}{dx^2} + Q_{ext} \qquad \text{(B-3)}$$

R is the sum total of all the radiation leaving the surface of the element, or the outward radiosity. R_Z is the inward radiosity. The factors πDdx have been grouped together, as their product is the surface area of the element; $k_m t$ is a parameter we wish to vary. Q_{ext} is the heat flowing into the element from sources external to the pipe.

Suppose now we had subdivided the pipe wall and ends into "n" elements of finite size. For each of these elements, Equation B-3 could be written

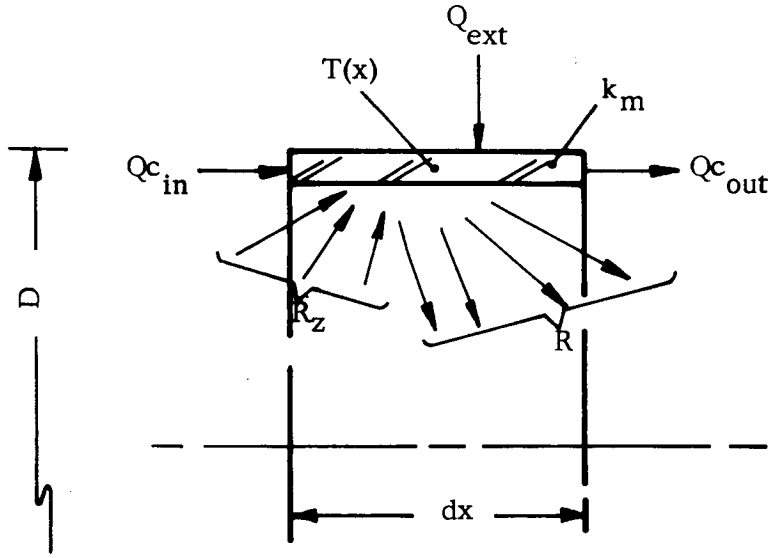

Heat Balance (Steady-State):

$$Q_{ext} + Qc_{in} + R_z = Qc_{out} + R$$

$$Qc_{in} = -k_m \, (\pi \, Dt) \, \frac{dt}{dx}$$

$$Qc_{out} = -k_m \, (\pi \, Dt) \, \frac{dt}{dx} + \frac{d}{dx} \left[-k_m \, (\pi \, Dt) \, \frac{dT}{dx} \right] dx$$

$$\therefore R - R_z = (\pi \, D \, dx) \, (k_m t) \, (\frac{d^2T}{dx^2}) + Q_{ext}$$

FIGURE B-4 HEAT BALANCE FOR A CYLINDRICAL ELEMENT OF PIPE

$$R_i - R_{Zi} = k_m t A_i \frac{d^2T}{dx^2} + Q_i \qquad \text{(B-4)}$$

where the subscript i indicates that the i^{th} element is being considered. More concisely,

$$R_i - R_{Zi} = C_i + Q_i \qquad \text{(B-5)}$$

where Q_i is the external heat input to element i. C_i represents the net heat input into the i^{th} element through conduction. It can be applied to plane annular elements at the pipe ends also, by using radial instead of axial temperature derivatives, if applicable. Since the elements are finite in size, the usual finite-difference approximations can be used to express derivatives.

The inward radiosity R_{Zi} is the result of all the elements radiating toward the i^{th} element. The contribution of the j^{th} element to R_{Zi} is the outward radiosity of the j^{th} (R_j) times the fraction (α_{ji}) of R_j arriving at element i:

$$R_{Zi} = \sum_j \alpha_{ji} R_j \qquad \text{(B-6)}$$

Note that a cylindrical ring can radiate to itself, so that α_{ii} is not zero in general.

The outward radiosity R_i is composed of two parts: the emitted radiation, and that part of the inward radiosity that is reflected.

$$R_i = A_i \epsilon_i \sigma T_i^4 + (1 - \epsilon_i) R_{Zi} \qquad \text{(B-7)}$$

A corrective factor can be applied to the emission term to account for variations in T^4 over the element.

Finally, the nature of the problem imposes boundary conditions of the type

$$\begin{aligned} Q_i &= \text{a given quantity} \\ &\text{or} \\ T_i &= \text{a specific temperature} \\ &\text{or} \\ Q_i &= f(T_i, \text{---}) \end{aligned} \qquad \text{(B-8)}$$

For the problem we are treating at present, all Q_i are zero for wall elements (insulated walls), but the temperatures are unknown quantities; all T_i are specified for end elements, but the external heat inputs are unknown.

Equations B-5 to B-8 are 4n equations in the 4n unknowns: R_i, R_{zi}, C_i and Q_i. With the use of matrix algebra they can be manipulated into the most useful form for a given problem.

In particular, equations B-5, -6, -7 can be combined to give a set of n equations:

$$(I - [A])(I - [C])^{-1}\vec{k} = \frac{\mu\vec{c}}{(n-m)} + \vec{q} \qquad \text{(B-9)}$$

where $\vec{k}$, $\vec{c}$ and $\vec{q}$ are vectors:

$$k_i = \frac{A_i}{\pi R^2}\,\epsilon_i\,\theta_i^4$$

$$\theta_i = T_i/T_1$$

$$c_i = \begin{cases} (d^2\theta/d\xi^2) & \text{for pipe wall elements} \\ 0 & \text{for pipe end elements, in this case} \end{cases}$$

$$q_i = Q_i/(\pi R^2 \sigma T_1^4)$$

$$\mu = \frac{2k_m t}{LR\sigma T_1^3}$$

$$\xi = X/L$$

n = total number of elements

m = number of end elements (both ends)

$$[A] = [a_{ij}] = [\alpha_{ji}]$$

$$[C] = [c_{ij}] = [(1 - \epsilon_i)\ \alpha_{ji}]$$

The solution of Equation B-9 with terms as defined depends only on the parameters L/D, ϵ_{wall}, ϵ_{ends}, and μ. It also depends on n and m, but for large values of these, the solution converges and their effect disappears. The solution gives the n-m unknown pipe wall element temperatures (in terms of θ_i) and the m unknown external heat flows into the pipe end elements (in terms of q_i). These non-dimensional quantities can thus be plotted as functions of L/D, ϵ_{wall}, ϵ_{ends} and μ. In particular, the sum of q_i at the cold end annular elements represents the radiative heat flow into the tank. If we add to this the conductive heat flow from the last cylindrical pipe element (cold end), we obtain q, the total heat leakage into the tank.

3. RESULTS OF COMPUTATIONS FOR L/D = 3

Figure B-5(a) shows curves of total pipe heat flow (radiation plus conduction) into a cryogenic tank, as a function of gray wall emissivity, for three values of μ, with the emissivities of both ends kept constant at a value of 0.1. The basic curve for $\mu = 0$ is a horizontal line, as was explained in the section on fundamentals. The rise in total heat flow at $\epsilon_{wall} = 0$ for non-zero values of μ (the jump from one curve to another) is due solely to conduction,

$$Q_{cond} = \frac{\pi D k_m t \Delta T}{L} \doteq \mu \pi R^2 \sigma T_1^4$$

or (B-10)

$$q_{cond} = Q_{cond}/\pi R^2 \sigma T_1^4 = \mu$$

since in that case there is no radiation absorption at the walls. The increase in this rise as ϵ_{wall} increases is to be noted: the rise can no longer be accounted for by μ alone. The gradient at the cold end is larger than before, since the walls have absorbed heat (ϵ_{wall} not zero); also, the temperature now generally being higher near the cold end, the intensity of the radiation there is higher. The curves flatten out for

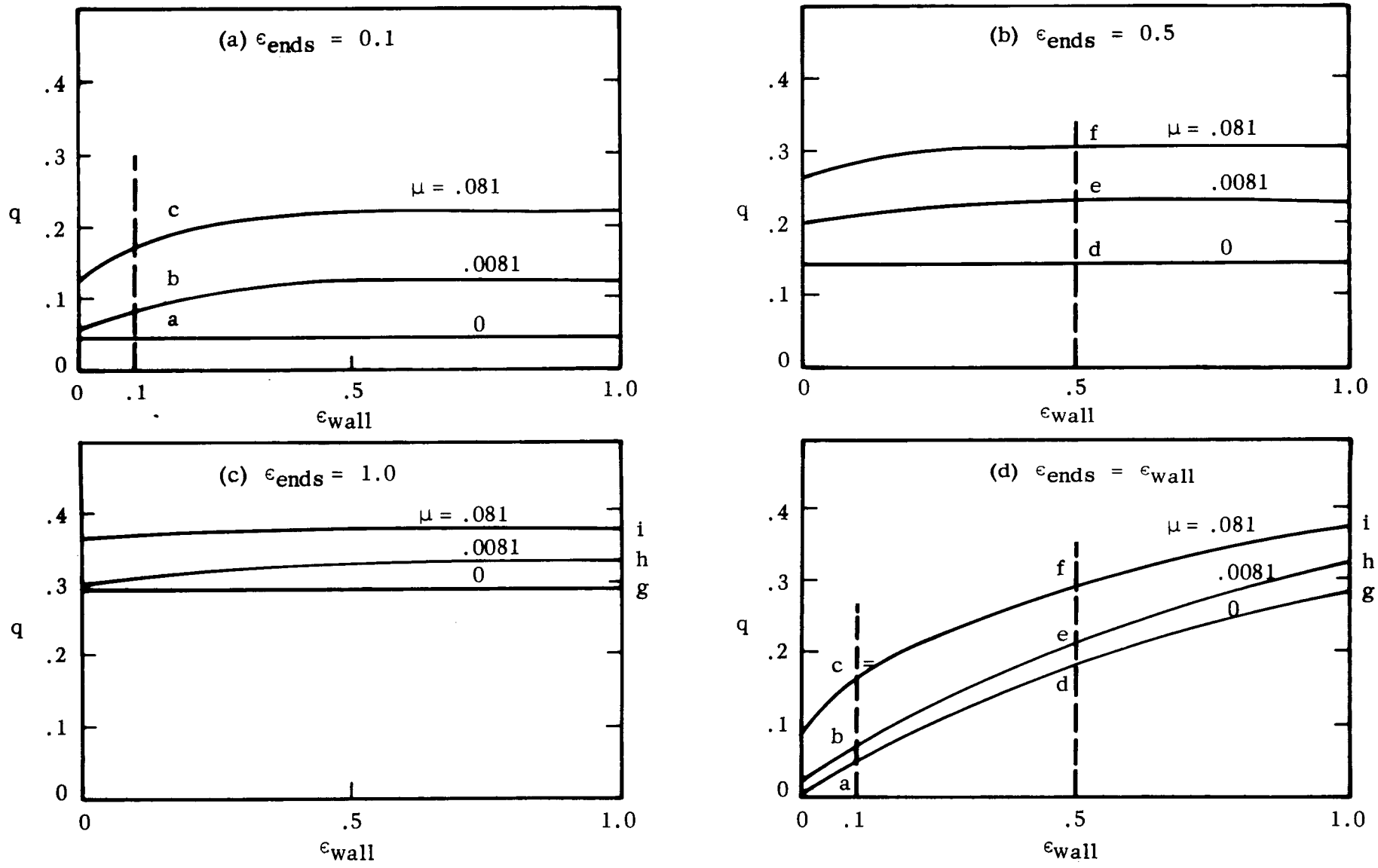

Definitions: $q \equiv \frac{Q_{total}}{\pi R^2 \sigma T_1^4}$; $\mu \equiv \frac{2 k_m t}{LR \sigma T_1^3}$

FIGURE B-5 TOTAL HEAT LEAK (DIMENSIONLESS) TO A TANK VIA A STRAIGHT PIPE, VERSUS ϵ_{wall}, FOR VARIOUS ϵ_{end} AND μ; L/D = 3

larger values of ϵ_{wall}, indicating the predominance of radiation. The conductive component acts as if it became saturated; along most of the pipe length, any additional radiation absorbed by the walls due to increased ϵ_{wall} is re-radiated with only slight changes in temperature along with the reflected part of the incident energy, producing a pattern almost independent of ϵ_{wall}. The radiation from this pattern, seen near the cold end, must be absorbed either at the cold end or at the walls near the cold end. The latter part is conducted to the cold end.

Figures B-5(b) and B-5(c) show curves for end emissivities of 0.5 and 1.0, respectively. Again, at $\epsilon_{wall} = 0$, the effect of $\mathcal{M}$ is to add a heat leak of $\mathcal{M}(\pi R^2 \sigma T_1^4$ watts to that for $\mathcal{M} = 0$. The flatness of the curves over a wide range of ϵ_{wall} indicates the predominance of radiation, now contributed to by the high ϵ_{ends} as well as ϵ_{wall}.

Figure B-5(d) shows curves for the same three values of $\mathcal{M}$, but now all emissivities, including those of the ends, vary simultaneously. These curves can be constructed from those of the other three figures: points a, b, c, in Figure B-5(a) correspond to points a, b, c in Figure B-5(d); similarly, points d, e, f in B-5(b) and points g, h, i in B-5(c) correspond, respectively, to d, e, f and g, h, i in B-5(d).

Figure B-6(a) shows the temperature distribution as affected by ϵ_{wall}, for $\mathcal{M} = 0.0081$ and $\epsilon_{ends} = 0.5$. Note the closeness of the curves over a large portion of the pipe length, indicating a "saturation" of the radiative effect.

Figure B-6(b) shows the effect of $\mathcal{M}$ on the temperature distribution, for $\epsilon_{wall} = \epsilon_{ends} = 0.1$. Figure B-6(c) shows this effect for $\epsilon_{wall} = \epsilon_{ends} = 1.0$, and includes a curve for $\mathcal{M} = 0$. The latter curve shows the extreme "floating" or adiabatic temperature distribution. The gradients at the cold end are quite high, but there is no conductive heat leak since $\mathcal{M}$ is zero for this case.

4. A RESULT FOR L/D = 9

A single case for a pipe with a L/D ratio equal to nine was also treated. For $\epsilon_{ends} = 1.0$ and zero wall emissivity and/or conductance (ϵ_{wall} and/or $\mathcal{M} = 0$) the radiative heat leak q into the tank is 0.115. For a 10-inch diameter pipe, 90 inches long, warm end at 300°K, the number above represents 2.7 watts.

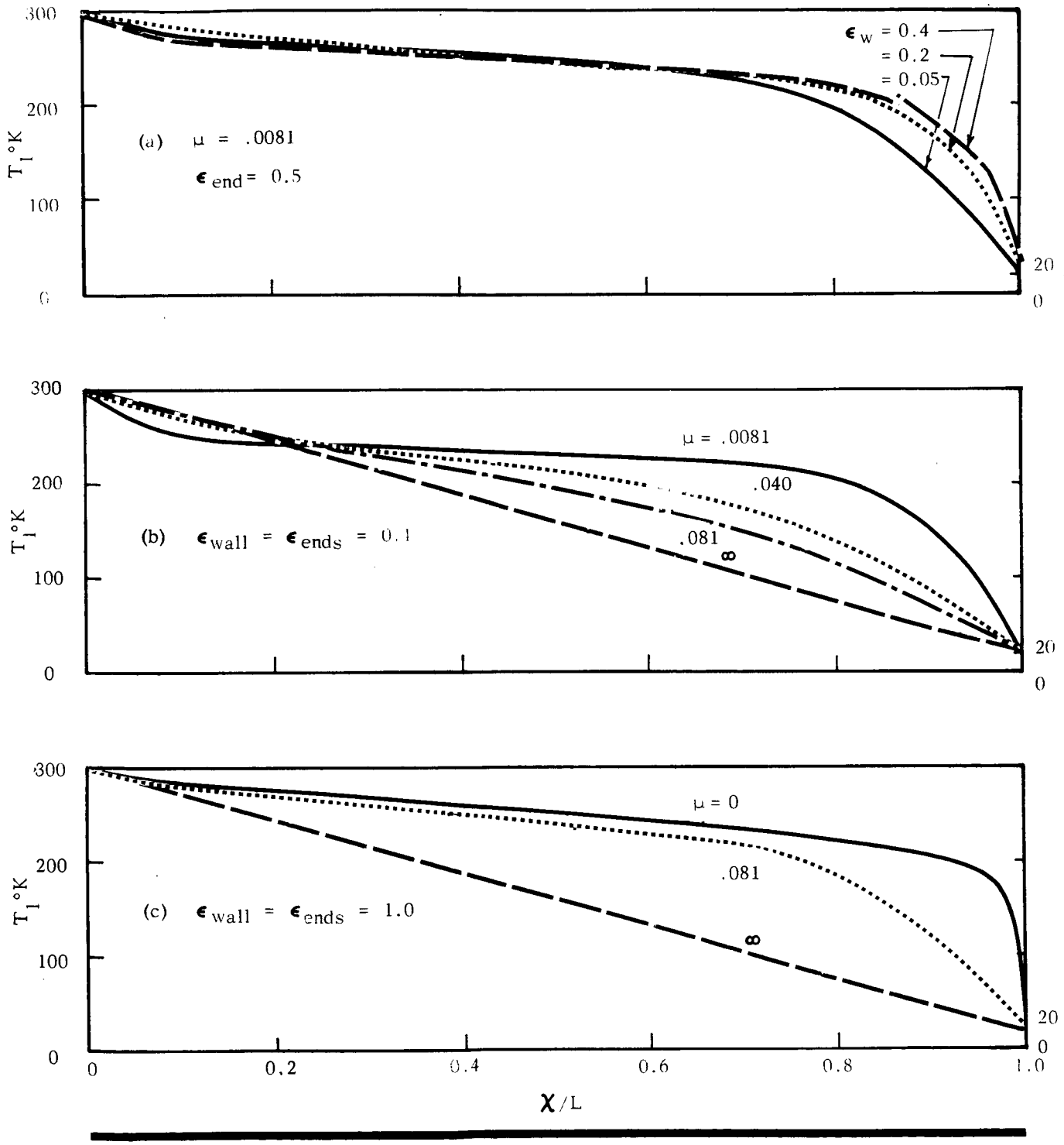

FIGURE B-6 AXIAL TEMPERATURE DISTRIBUTION OF PIPE WALLS UNDER VARIOUS CONDITIONS

APPENDIX C

VENTING OF MULTIFOIL INSULATION DURING ASCENT

I. ANALYSIS

Consider the multifoil insulation system as a porous solid made up of individual elements having an identical porous structure arranged in layers. Assume that the perfect gas equation of state holds and that the continuum flow is isothermal. Further, assume that the resistance to the flow of gas through this porous structure is controlled by viscous effects; that is, the flow is characterized by low Reynolds numbers. For convenience of analysis we fix our attention on the flow process within a single characteristic element of the structure. Under these circumstances the pressure drop per layer becomes

$$\Delta P_n = \frac{32\, K \mu L\, \dot{w}}{\rho\, b\, \delta^3} \qquad \text{(C-1)}$$

where

ΔP_n = pressure drop per layer

μ = viscosity of interstitial gas

ρ = density of interstitial gas

L = characteristic length of flow path

b = characteristic width of flow path

δ = characteristic height of flow path

K = constant to account for fine structure geometry

$\dot{w}$ = mass flow through single characteristic element

Figure C-1 on page C-5 may serve as a typical model to clarify some physical aspects of the problem posed. Letting n be the number of layers per unit depth of insulation, we get

$$\frac{\partial P}{\partial x} = \frac{-32\, n\, K \mu L\, \dot{w}}{\rho\, b\, \delta^3} \qquad \text{(C-1a)}$$

$$\frac{\partial P}{\partial \theta} = \frac{1}{32\, k\, n^4 \mu L^2} \cdot P \frac{\partial^2 P}{\partial x^2} \qquad \text{(C-4a)}$$

Equation (C-4a) is a non-linear, partial differential equation. In order to obtain an approximate solution, we linearize. In other words, we assume that the pressure differences within the insulation are small in respect to some average value, or

$$P = \bar{P} + p$$

$$\text{with } p \ll \bar{P}$$

Letting $32K\, n^4 \mu L^2 = \alpha$, Equation (C-4a) becomes

$$\frac{\partial}{\partial \theta} (\bar{P} + p) = \frac{1}{\alpha} (\bar{P} + p) \frac{\partial^2}{\partial x^2} (\bar{P} + p) \qquad \text{(C-4b)}$$

and reduces to

$$\frac{\alpha \partial \bar{P}}{\bar{P} \partial \theta} = \frac{\partial^2 p}{\partial x^2} \qquad \text{(C-4c)}$$

In line with the assumption for linearization, the term $\frac{\partial \bar{P}}{\bar{P} \partial \theta}$ can be identified with the pressure events taking place outside the insulation during ascent. The pressure changes taking place outside the launch vehicle may be used to compute this term in most cases (this is the conservative approach); in the case of a relatively tight shroud, one may take advantage of the modification of the pressure history in the atmosphere surrounding the insulation. In any event the solution to Equation (C-4c) is

$$P = P_o - \frac{\alpha \beta}{2} (t^2 - x^2) \qquad \text{(C-5)}$$

where $\beta = \frac{\partial \bar{P}}{\bar{P} \partial \theta}$, t is the total thickness of the insulating layers, P_o is the outside pressure. The maximum gradient occurs at x = t, and is equal to

$$\left. \frac{\partial P}{\partial x} \right|_{max} = \alpha \beta t$$

The maximum pressure difference across any single layer occurs across the outside layer, and is equal to

$$\Delta P_n \Big|_{max} = \frac{dP}{dx}\Big|_{max} \cdot \frac{1}{n} = \frac{\alpha \beta t}{n} \qquad \text{(C-6)}$$

The total pressure difference across the layered system is

$$\Delta P_{max} = -\frac{\alpha \beta}{2} t^2 \qquad \text{(C-7)}$$

The maximum rate of outflow of gas occurs at the outermost foil and is equal to

$$\dot{w} = -\frac{b L t}{RT} \frac{\partial \bar{P}}{\partial \theta} \qquad \text{(C-8)}$$

The characteristic Reynolds Number (where the major resistance to flow is due to the lateral motion of the gas between foils as it seeks escape through gaps between the foils or through perforations in the foils) is

$$Rey = \frac{\dot{w}}{b\delta} \times \frac{\delta}{\mu}$$

$$= -\frac{L t \partial \bar{P}/\partial \theta}{\mu RT} \qquad \text{(C-9)}$$

Example 1 - Consider the problem of venting a multilayered insulation system having the general construction features identified in the accompanying figure. This system may be characteristic of a multifoil insulation laid up in gore strips or in a bandage wrap. Selecting (only order of magnitude estimates are warranted):

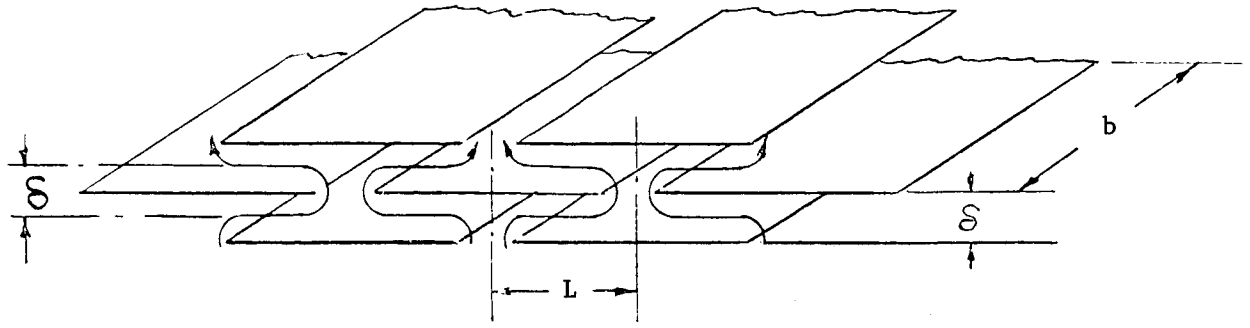

Figure C-1

$k = 1.0$

$L = 0.5$ ft.

$t = 1.2$ in. $= 0.10$ ft.

$n = 50/\text{in.} = 600\ \text{ft}^{-1}$

$\beta|_{max} = 0.3\ \text{sec}^{-1}$

$\frac{\partial \bar{P}}{\partial \theta} = -70\ \text{lbf/ft}^2 - \text{sec}$

} typical of rapid boost-out.

$T = 540^{\circ}\text{R}$

$\mu = 4.1 \times 10^{-7}\ \text{lbf - sec/ft}^2$

$R = 386\ \frac{\text{ft - lbf}}{\text{lbm - }^{\circ}\text{R}}$

} helium gas

we calculate:

$\alpha = 4.25 \times 10^5\ \text{lbf - sec/ft}^4$

$\alpha\beta = 1.28 \times 10^5\ \text{lbf/ft}^4$

and finally,

$$\Delta P_n\Big|_{max} = 21.2 \text{ lbf/ft}^2$$

$$\Delta P\Big|_{max} = 637 \text{ lbf/ft}^2$$

$$Rey_{max} = 1.27$$

Example 2 - As another example consider the venting of a perforated multifoil insulation arranged as shown in Figure C-2. This figure depicts a plan view of two foils. The venting gases enter the holes in one foil (shown in solid line) and drain through the holes in the next foil (shown in dotted line). Assuming the conditions of the previous example with the exception that we take L equal to one inch and estimate that K equals 2, we find:

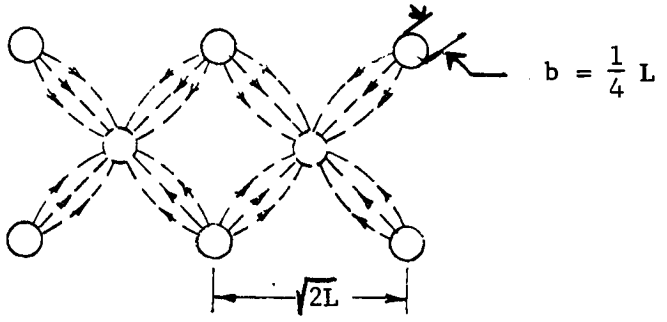

Figure C-2

$$\Delta P_n\Big|_{max} = 2.36 \text{ lbf/ft}^2$$

$$\Delta P \Big|_{max} = 70.8 \text{ lfb/ft}^2$$

$$\text{Rey}_{max} = 0.211$$

Also, if the hole area is one percent of the foil area (one percent perforation), the Reynolds Number based on hole diameter is approximately unity for this case.

II. SUMMARY AND CONCLUSIONS

The foregoing analysis and example calculations are based on order of magnitude considerations only. Of all the limitations in the mathematical analysis made obvious by the simplifying assumptions inherent to it, the physical model of the insulation system as a well-ordered porous structure is prominent. Although such a structure is ideally suited to reduce the problem of venting, problems of application and considerations of minimum heat inleakage may well produce systems which deviate from this ideal. Moreover, during the venting operation, should some layer under the action of the induced pressure gradients tend to compress more than others, the result would be an increase in these gradients and a greater tendency to rupture.

Irrespective of these limitations, the analysis and example calculations provide a guide to the venting problem of super-insulations. It seems clear that containment and support for decompression forces during boost-out must be provided. The amount of support necessary is proportional to the fourth power of the number of layers per unit depth of insulation and the square of path length of the venting gases. Although not specifically illustrated by example, the use of a spacer material between foils increases the resistance to flow (the effect of a spacer can be included in the value, K) and, hence, the support requirements.

Of course, it is desirable to minimize the support requirements for the decompression process. One promising way to accomplish this is to perforate the radiation shields in a regular pattern of circular holes. As previously shown (section IV-A-1), these perforations lead to an increase in heat inleakage but a hole fraction of one percent may be considered acceptable. Within this limitation, the venting problem is reduced by using small holes close together. The perforation of the foils also serve another purpose during space operation; that is, the tolerance to degradation of the insulation due to interstitial gas buildup from outgassing or leakage is increased.

APPENDIX D

TEMPERATURE PERTURBATIONS IN MULTILAYER INSULATION

In order to analyze perturbations and their extent in MLI, we use as a model the bi-dimensional situation illustrated in Figure D-1. An infinitely long, straight penetration (strip) of width w and thermal conductivity k_1 is in thermal contact with the edges of the foils in multilayer insulation of thickness B and thermal conductivities $k_\perp$ and $k_\parallel$ in the y- and x- directions, respectively, both conductivities being assumed uniform. The upper foil is irradiated by a flux of uniform intensity I.

At very large distances x from the penetration, where the effect of the penetration is not felt, the temperature in the insulation is a function of y only, and since heat therefore flows in that direction only, the temperature gradient is independent of x or y. From the boundary condition (given in Figure D-1) and the above discussion we have, for large x:

$$k_1 \frac{\partial T}{\partial y} = k_\perp \frac{(T_\infty - T_{liq})}{B} = \beta (T_a - T_\infty) \qquad \text{(D-1)}$$

or

$$T_\infty - T_{liq} = \frac{T_a - T_{liq}}{1 + \frac{k_\perp}{\beta B}} \qquad \text{(D-2)}$$

where T_∞ is the outer foil temperature at large x. Because of the uniform gradient we can write the temperature distribution

$$T(y) - T_{liq} = \frac{T_a - T_{liq}}{1 + \frac{k_\perp}{\beta B}} \cdot \frac{y}{B} \qquad \text{(D-3)}$$

Where x is not large, x-gradients in temperature cannot be neglected, and the differential equation in the two variables must be used. At steady-state, this is

$$k_\parallel \frac{\partial^2 T}{\partial x^2} + k_\perp \frac{\partial^2 T}{\partial y^2} = 0 \qquad \text{(D-4)}$$

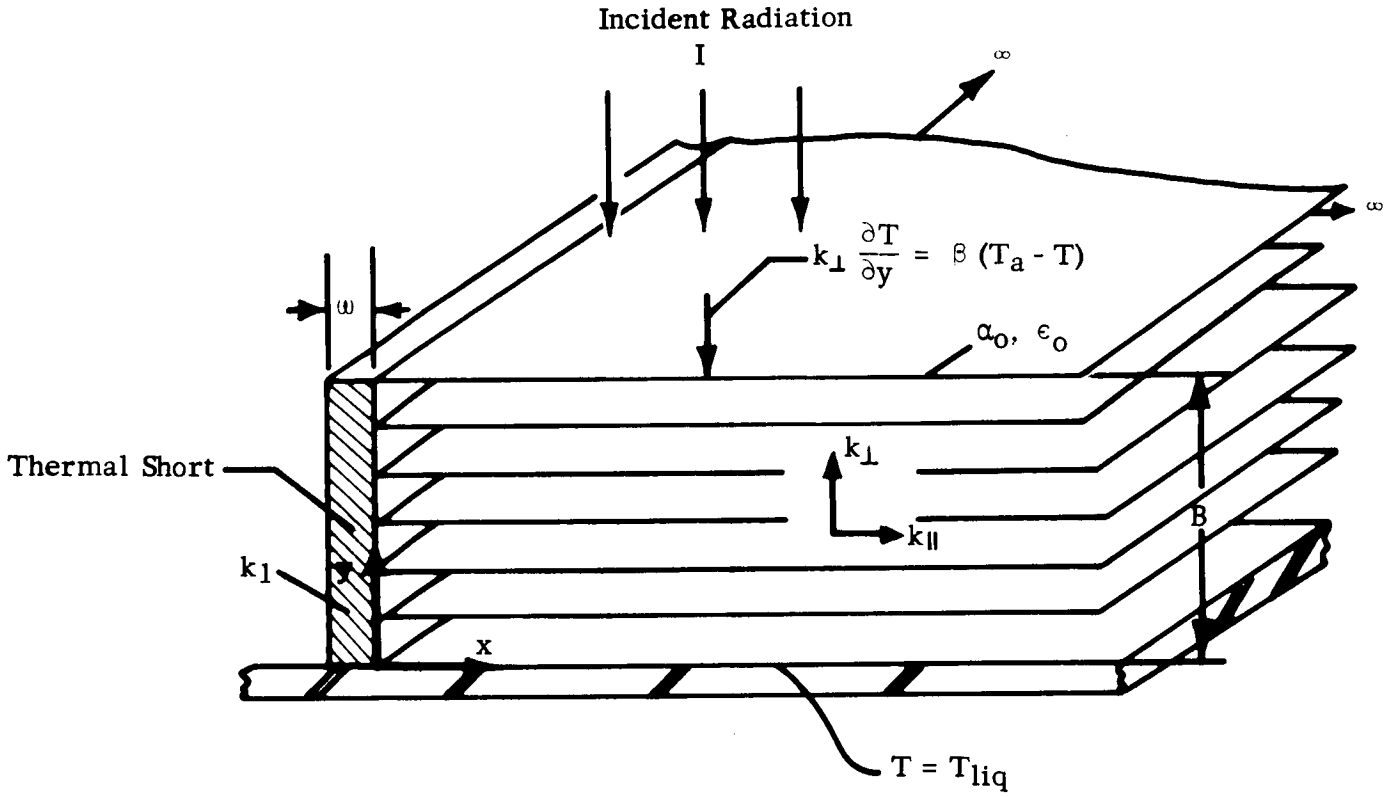

$$\beta = 4 \sigma \epsilon_o T_a^3$$

$$T_a^4 = \frac{\alpha_o I}{\sigma \epsilon_o}$$

FIGURE D-1 MODEL FOR ANALYZING THE TEMPERATURE FIELD NEAR A WEAK THERMAL SHORT (k_1 ASSUMED CONSTANT)

The solution of (D-4), finite and satisfying (D-3) at large x, is

$$T(x\ y) = T_{liq} + \frac{T_a - T_{liq}}{1 + \frac{k_\perp}{\beta B}} \cdot \frac{y}{B} + \sum_{n=1}^{\infty} C_n e^{-\alpha_n \sqrt{\frac{k_\perp}{k_{\parallel}}}\, x} \operatorname{Sin} \alpha_n Y \qquad \text{(D-5)}$$

where α_n are constants, functions of n only, to be evaluated with the remaining boundary conditions. The condition that $T = T_{liq}$ at $y = 0$ is already satisfied. The remaining conditions are that at $y = B$, given in Figure D-1, and that at $x = 0$. From the condition at $y = B$, one finds

$$\tan \alpha_n B + \left(\frac{k_\perp}{\beta B}\right) \alpha_n B = 0 \qquad \text{(D-6)}$$

If usual values are substituted for $k_\perp$, β and B, the parameter $(k_\perp/\beta B)$ is found to be quite small (less than 0.001); it is in fact $K/4$ where K is the reciprocal view factor discussed in chapter IV-A. For such values, $\alpha_n B$ is very nearly equal to $n\pi$

$$\alpha_n = n\pi/B \quad (n = 1, 2, \text{---}) \qquad \text{(D-7)}$$

and now equation (D-5) can be written

$$T(x,y) = T_{liq} + \frac{T_a - T_{liq}}{1 + \frac{k_\perp}{\beta B}} \cdot \frac{y}{B} + \sum_{n=1}^{\infty} C_n e^{-\frac{n\pi x}{B}\sqrt{\frac{k_\perp}{k_{\parallel}}}} \sin \frac{n\pi y}{B} \qquad \text{(D-8)}$$

The boundary condition at $x = 0$ can now be applied to evaluate the C_n, and thus obtain the temperature distribution throughout the insulation. This condition is

$$\frac{k_{\parallel}}{k_\perp w} \frac{\partial T}{\partial x} + \frac{\partial^2 T}{\partial y^2} = 0 \qquad \text{(D-9)}$$

When substituted into (D-6) this gives, after much manipulation, the solution

$$T(x,y) = T_{liq} + \frac{T_a - T_{liq}}{1+q} \cdot \frac{y}{B}$$

$$+ \frac{T_a - T_{liq}}{1+q} \; \frac{2q \sum_{n=1}^{\infty} \frac{e^{-\frac{n\pi x}{B}\sqrt{\frac{k_\perp}{k_{//}}}} \; \mathrm{Sin}\,(\mu_n\, y/B)}{\cos \mu_n \,(1 + q + q^2 n^2 \pi^2)\,(n\pi + H)}}{\left[1 - 2q \sum_{n=1}^{\infty} \frac{n\,\pi}{(1 + q + q^2 n^2 \pi^2)(n\pi + \psi)}\right]} \qquad \text{(D-10)}$$

where $q \equiv k_\perp / \beta B$ (D-11)

$$H \equiv \frac{\sqrt{k_{//} k_\perp}}{w k_\perp / B} \qquad \text{(D-12)}$$

$$\mu_n = \alpha_n B \qquad \text{(D-13)}$$

Equation (D-10) permits evaluating the temperature distribution as a function of q and H . Incidentally, H is the ratio $R_p/R_{//}$ used in the resistance concept of Chapter IV-C-1.

If we consider the right-hand side of (D-10) to consist of three terms, then the first two are the distribution at large x and the third is the perturbation. Because of the negative exponential in x, the perturbation will have a maximum value at x = 0 and will decay with increasing x. When H is small, the largest term of the summation in the numerator of the perturbation will be the first term. When H is large, the largest term will not be the first; the terms will increase slowly as n increases, reach a maximum then decrease. Consider the value of x such that

$$\frac{\pi x}{B}\sqrt{\frac{k_\perp}{k_{//}}} = \pi \qquad \text{(D-14)}$$

Then the exponential factor in the first term of the numerator will be $e^{-\pi} = 0.043$. In the second term it will be $e^{-2\pi} = 0.0018$, and so on. Thus, at such a value of x, all the terms following the first will be decreased by factors each $e^{-\pi}$ larger than the preceding one, so that in spite of the fact that the first term may not be the largest, it will predominate at the value of x given by (D-14). Moreover, at that value of x, the first term will have about 4 percent of the value it

had at x = 0. Therefore, the summation will have much less than 4 percent of its value at x = 0. We may, therefore, say that the perturbation will have decayed to very small values when x satisfies (D-14). We call this value x_{Decay}:

$$x_{Decay} \equiv B\sqrt{\frac{k_{\parallel}}{k_{\perp}}} \qquad \text{(D-15)}$$

APPENDIX E

HEAT FLOW THROUGH A BLANKET OF PURE RADIATION FOILS

We consider a cryogenic tank completely enclosed in a continuous blanket of multilayer insulation consisting of foils that exchange heat with each other by radiation only. However, heat may flow parallel to the planes of the foils.

The total radiosity R_1 of the inner surface of the first foil equals the sum of its emitted and reflected powers. For a gray body, with emissivity ϵ, we have

$$R_1 = \oiint \sigma \epsilon \, T_1^4 dA + (1 - \epsilon) \, R_2 \qquad \text{(E-1)}$$

where the integral is performed over the entire area of the foil--in this case of the tank also. R_2 is the radiosity of the outer surface of the second foil, i.e., the surface facing that of radiosity R_1. Equation (E-1) assumes that the foils are close enough together so that their mutual view factors are unity.

Likewise, the total radiosity R_2 of the second surface just discussed may be expressed as

$$R_2 = \oiint \sigma \epsilon T_2^4 \, dA + (1 - \epsilon) \, R_1 \qquad \text{(E-2)}$$

Since heat is exchanged between foils only by radiation, the net heat flowing from the first foil to the second must be the difference between R_1 and R_2

$$Q_{12} = R_1 - R_2 \qquad \text{(E-3)}$$

The difference $R_1 - R_2$ can be found from equations (E-1) and (E-2). Solving, we obtain

$$Q_{12} = \frac{\sigma}{\frac{2}{\epsilon} - 1} \left[\oiint T_1^4 \, dA - \oiint T_2^4 \, dA \right] \qquad \text{(E-4)}$$

We may write similar expressions for the heat flowing between any two adjacent foils

$$Q_{i,i+1} = \frac{\sigma}{\frac{2}{\epsilon} - 1} \left[\iint T_i^4 \, dA - \iint T_{i+1}^4 \, dA \right] \qquad \text{(E-5)}$$

At steady-state, all such $Q_{i,i+1}$ must be equal to each other. We may, therefore, write a set of n equations

$$\begin{aligned} \left(\frac{2}{\epsilon} - 1\right)\frac{Q}{\sigma} &= \iint T_1^4 \, dA - \iint T_2^4 \, dA \\ &= \iint T_2^4 \, dA - \iint T_3^4 \, dA \\ &\vdots \\ &= \iint T_{n-1}^4 dA - \iint T_n^4 dA \\ &= \iint T_n^4 dA - \iint T_{liq}^4 dA \end{aligned} \qquad \text{(E-6)}$$

If all the equations are added, we obtain

$$\left(\frac{2}{\epsilon} - 1\right) \frac{nQ}{\sigma} = \iint T_1^4 dA - \iint T_{liq}^4 dA$$

or

$$Q = \frac{\sigma}{\left(\frac{2}{\epsilon} - 1\right) n} \left[\iint T_1^4 dA - \iint T_{liq}^4 dA \right] \qquad \text{(E-7)}$$

Equation (E-7) relates the unknown total heat flowing into the tank with the unknown temperature integral of the outer foil. Another relation exists between these two unknowns, in terms of the known incident flux and radiative properties of that outer foil:

$$Q = \oiint (\alpha_o \; I - \sigma \epsilon_o \; T_1^{\,4}) \; dA$$

$$= \alpha_o \oiint I \; dA - \sigma \epsilon_o \oiint T_1^{\,4} \; dA \qquad \text{(E-8)}$$

We can combine (E-7) and (E-8) to solve for Q in terms of known quantities. The result is

$$Q = \frac{\alpha_o \oiint I dA - \sigma \epsilon_o \oiint T_{liq}^{\,4} \; dA}{1 + \left(\frac{2}{\epsilon} - 1\right) \; n \; \epsilon_o} \qquad \text{(E-9)}$$

This result is valid for a continuous blanket of pure radiation foils. It holds independently of any thermal conduction parallel to the foils, since (i) the derivation leading to equation (E-5) is based on arbitrary temperature distributions in the foils; (ii) the equalities (E-6) and their consequence (E-7), are true at steady-state regardless of parallel conduction; and (iii) the outer foil surface radiation heat balance (E-8) is obviously independent of parallel conduction.

The denominator of (E-9) can be simplified in practical cases. First, since $2n/\epsilon \simeq 50\ n$, we may neglect the first term, unity. We may also neglect unity in brackets compared with $2/\epsilon \simeq 50$. Therefore, the denominator can be re-written within about 2 percent as $2n\epsilon_o/\epsilon \equiv 1/K$, where K is the shielding factor frequently used in this report. Equation (E-9) may then be written with good approximation as

$$Q = K \left[\alpha_o \oiint I \; d \; A - \sigma \epsilon_o \oiint T_{liq}^{\,4} \; dA \right] \qquad \text{(E-10)}$$

or, in terms of the adiabatic wall temperature distribution:

$$Q = K \; \sigma \epsilon_o \left[\oiint (T_a^{\,4} - T_{liq}^{\,4}) \; dA \right] \qquad \text{(E-11)}$$

In many cases the integral involving the liquid temperature raised to the fourth power can be neglected. However, the use of shadow-shields and radiators can lower the values of $T_a^{\,4}$ to the same order.

APPENDIX F

EQUATIONS FOR THE GENERAL CYLINDRICAL THERMAL SHORT IN PURE RADIATION FOILS

The steady-state heat conduction equation in cylindrical coordinates, in a medium of continuous (though not uniform or isotropic) thermal conductivities as represented in Figure F-1, is

$$\frac{\partial}{\partial y}\left(k_{\perp}\frac{\partial T}{\partial y}\right) + \frac{1}{r}\frac{\partial}{\partial r}\left(r\,k_{\parallel}\frac{\partial T}{\partial r}\right) = 0 \qquad \text{(F-1)}$$

The basic assumption not exactly represented by fact is that of continuity. However, when the number of foils is large, such that the spacing between two adjacent foils can be considered as a differential of distance, the equation retains its validity, so long as the solution is not interpreted on a scale smaller than such spacings. With that understanding, both $k_{\perp}$ and $k_{\parallel}$ can be expressed in terms of foil properties and spacing:

$$k_{\perp} \equiv \frac{2\sigma\epsilon\, B\, T^3}{n} \qquad \text{(F-2)}$$

$$k_{\parallel} \equiv \left(k_f\, t_f + k_s\, t_s\right)\frac{n}{B} \qquad \text{(F-3)}$$

In these equations, the spacing, B/n is assumed uniform. In (F-3), the subscripts f and s refer to foils and spacers, respectively. For convenience the products k t (thermal conductivity times thickness) will be grouped together as a single term

$$k_{\parallel} = \frac{k\, t\, n}{B} \qquad \text{(F-4)}$$

with the understanding that k t represents all contributions: that of spacers as well as foils. Some foils consist of metal vacuum-deposited on a plastic. The product includes the contribution of the plastic as well. Even in such cases the contribution of the metal predominates.

The expressions (F-2) and (F-4) can be substituted into (F-1), which, after some simplification, becomes

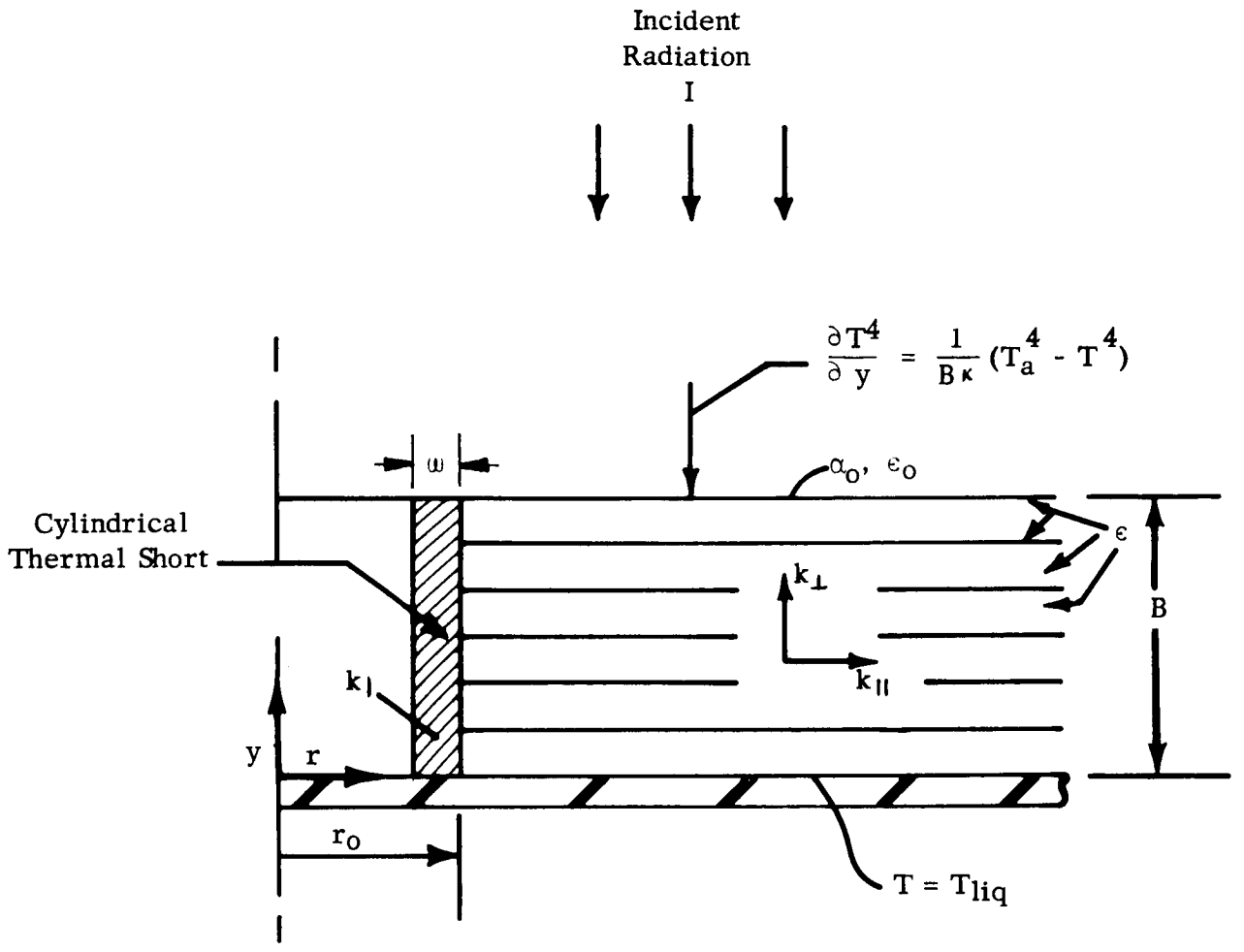

$$\kappa = \epsilon/2n\epsilon_o$$

$$T_a^4 = \frac{\alpha_o I}{\epsilon_o \sigma}$$

FIGURE F-1 MODEL FOR ANALYZING THE GENERAL CYLINDRICAL THERMAL SHORT

$$\left(\frac{\sigma \epsilon B^2}{2n^2 kt}\right) \frac{\partial^2 T^4}{\partial y^2} + \frac{1}{r} \frac{\partial}{\partial r}\left(r \frac{\partial T}{\partial r}\right) = 0 \qquad \text{(F-5)}$$

The boundary conditions are as follows:

$$y = 0 : T = T_\ell \qquad \text{(F-6)}$$

$$y = B : \alpha_o I = \sigma \epsilon_o T^4 + k_\perp \frac{\partial T}{\partial y}$$

or

$$\frac{2 \sigma \epsilon B T^3}{n} \frac{\partial T}{\partial y} = \sigma \epsilon_o (T_a^4 - T^4)$$

or

$$\frac{\partial T^4}{\partial y} = \frac{1}{\kappa_B} (T_a^4 - T^4) \qquad \text{(F-7)}$$

where $\kappa \equiv e/2n\epsilon_o$ (as usual)

$$r \to \infty : T = f(y) \text{ (given)} \qquad \text{(F-8)}$$

$$r = r_o : w \frac{\partial}{\partial y}\left(k_\perp \frac{\partial T}{\partial y}\right) + k_{\parallel} \frac{\partial T}{\partial r} = 0$$

or

$$\left(\frac{w k_\perp}{B}\right)\left(\frac{B^2}{nkt}\right) \frac{\partial^2 T}{\partial y^2} + \frac{\partial T}{\partial r} = 0 \qquad \text{(F-9)}$$

Equations (F-5) to (F-9) can be put into dimensionless form. Let

$$T_a^4 \equiv \frac{\alpha_o I}{\epsilon_o \sigma} \qquad \text{(F-10)}$$

$$\theta \equiv T/T_a \text{ (dependent variable)} \qquad \text{(F-11)}$$

$$u \equiv y/B \text{ (independent variable)} \qquad \text{(F-12)}$$

$$v \equiv r \frac{\sigma \epsilon T_a^3}{2n^2 kt} \quad \text{(independent variable)} \qquad \text{(F-13)}$$

$$v_o \equiv r_o \sqrt{\frac{\sigma \epsilon T_a^3}{2 n^2 k t}} \quad \text{(parameter)} \qquad \text{(F-14)}$$

$$\chi \equiv \frac{w k_i / B}{\frac{\sigma \epsilon T_a^3 kt}{2}} \quad \text{(parameter)} \qquad \text{(F-15)}$$

$$\theta_{liq} \equiv T_{liq}/T_a \quad \text{(parameter)} \qquad \text{(F-16)}$$

In terms of the quantities just defined, the differential equation (F-5) can be expressed as

$$\frac{\partial^2 \theta^4}{\partial u^2} + \frac{\partial^2 \theta}{\partial v^2} + \frac{1}{v} \frac{\partial \theta}{\partial v} = 0 \qquad \text{(F-17)}$$

and the boundary conditions become:

$$u = 0 : \theta = \theta_{liq} \qquad \text{(F-18)}$$

$$u = 1 : \frac{\partial \theta^4}{\partial u} = \frac{1}{\eta} (1 - \theta^4) \qquad \text{(F-19)}$$

$$v = v_o : \chi \frac{\partial^2 \theta}{\partial u^2} + \frac{\partial \theta}{\partial v} = 0 \qquad \text{(F-20)}$$

$$v \to \infty : \theta^4 = f(u) \qquad \text{(F-21)}$$

For the special case where the outer foil surface is irradiated uniformly out to distances very far from the region of influence of the thermal short,

$$f(u) = \theta_{liq}^4 + \frac{1 - \theta_{liq}^4}{1 + K} u \qquad \text{(F-22)}$$

For the usual cryogens and the usual values of T_a, the parameter θ_{liq} is not an influential one; it might be neglected.

The solution of (F-17) with a given set of parameters (v_o, λ, ψ, θ_{liq}) gives the function θ (u, v) for that set. From θ (u, v) the added heat leak due to the short can be calculated. (We assume that the top surface of the annular short is shielded from incident radiation, and that the hollow region is filled with good insulation or otherwise baffled to prevent internal radiation.) Before discussing this calculation, the significance of the variable v must be explained. In undisturbed insulation the heat that would flow through unit area of the insulation is

$$\frac{Q}{A} = \frac{\sigma (T_a^4 - T_{liq}^4)}{\left(\frac{2}{\epsilon} - 1\right) n (1 + \kappa)} \qquad \text{(F-23)}$$

$$\simeq \frac{\sigma \epsilon T_a^4}{2n} \qquad \text{(F-24)}$$

This heat flow can also be expressed in terms of an overall transverse thermal conductivity $k_{\perp m}$

$$\frac{Q}{A} \equiv k_{\perp m} (T_a - T_{liq})/B$$

$$\simeq k_{\perp m} T_a/B \qquad \text{(F-25)}$$

Comparing (F-24) and (F-25) allows a definition of $k_{\perp m}$ for pure radiation foils:

$$k_{\perp m} \equiv \frac{\sigma \epsilon T_a^3 B}{2n} \qquad \text{(F-26)}$$

In terms of $k_{\perp m}$, and of $k_{\parallel}$ as defined in (F-3), the variable v can be expressed as

$$v \equiv \frac{r}{B} \sqrt{\frac{k_{\perp m}}{k_{\parallel}}} \qquad \text{(F-27)}$$

In terms of x_{Decay} as defined in Appendix D, v can also be expressed as

$$v \equiv \frac{r}{x_{Decay}} \qquad \text{(F-28)}$$

Similarly, for the parameter v_o

$$v_o \equiv \frac{r_o}{x_{Decay}} \qquad \text{(F-29)}$$

Now, the radius of the region of influence will not be more than one or two decay distances from the outer surface of the thermal short:

$$v \rightarrow v_o + 2 : \theta^4 = f(u) \qquad \text{(F-30)}$$

Therefore, to evaluate the added heat flow one need not consider values of v beyond $v_o + 2$.

The net radiative flow into the insulation is given by

$$\frac{Q}{A} = \sigma \epsilon_o (T_a^4 - T_s^4) \qquad \text{(F-31)}$$

At $v = v_o + 2$,

$$T_s^4 = \frac{T_a^4}{1 + K} \qquad \text{(F-32)}$$

At smaller v,

$$T_s^4 = T_a^4 \theta^4 (u = 1, v)$$

$$\equiv T_a^4 \theta_1^4 (v) \qquad \text{(F-33)}$$

where $\theta_1(v)$ denotes the value of θ at $u = 1$, function of v. From (F-32) and (F-33) we can form

$$\frac{Q}{A}_{\text{added}} = \sigma \epsilon_o T_a^4 \left[(1 - \theta_1^4(v)) - \left(1 - \frac{1}{1+\eta}\right) \right]$$

$$= \sigma \epsilon_o T_a^4 \left[\frac{1}{1+\eta} - \theta_1^4(v) \right] \qquad \text{(F-34)}$$

Therefore,

$$Q = \sigma \epsilon_o T_a^4 \int_{r_o}^{\infty} \left(\frac{1}{1+\eta} - \theta_1^4(v) \right) dA$$

$$= \sigma \epsilon_o T_a^4 \int_{r_o}^{\infty} \left(\frac{1}{1+\eta} - \theta_1^4(v) \right) 2\pi r dr$$

$$= 2\pi \frac{nktT_a}{K} \int_{v_o}^{v_o + 2} \left[\frac{1}{1+\eta} - \theta_1^4(v) \right] v \, dv \qquad \text{(F-35)}$$

The added heat can be made to take other forms, in which the integral will take different meanings.

APPENDIX G

BIBLIOGRAPHY

1. Bonneville, J.M.,
"Techniques for Computing the Thermal Radiation Incident on Vehicles in Space."
Arthur D. Little, Inc. Report No. 63270-04-05,
June 1962.

2. Swalley, F.,
"Thermal Radiation Incident on Non-Spinning Earth Satellites",
George C. Marshall Space Flight Center, Huntsville, Ala.,
June 15, 1961.

3. Ballinger, J.C., J.C. Elizade and E.H. Christensen,
"Thermal Environment of Interplanetary Space",
SAE National Aeronautics Meeting, New York, N.Y., 1961.

4. Altshuler, T.L.,
"A Method for Calculating the Thermal Irradiance Upon a Space Vehicle and Determining its Temperature",
General Electric Company, MSVD, T.I.S. Report
R60SD386, Aug.60 (ASTIA AD 240768).

5. Stevenson, J.A. and J.C. Grafton,
"Radiation Heat Transfer Analysis for Space Vehicles",
Space and Information Systems Division, North American Aviation, S.I.D. 61-91, Dec. 61, ASD TR 61-119.

6. Ballinger, J.C., and E.H. Christensen,
"Environmental Control Study of Space Vehicles, Part II, Thermal Environment of Space. Supplement A-Graphical Presentation of Solar, Planetary Thermal and Planetary Albedo Radiation Incident to Space Vehicles",
General Dynamics Astronautics Report
No. GDA ERR-AN-016, Jan. 10, 1961.

7. Bennett, H.E., Jean M. Bennett and E.J. Ashley
"Infrared Reflectance of Evaporated Aluminum Films",
J. Opt. Soc. Am. 52, 11, 1245-50 (Nov. 62).

8. Reynolds, M.M., et al
"A Preliminary Report on the Infrared Absorption of Metals At Low Temperature" NBS, TM. No. 16.

9. Bonneville, J.M., and A.A. Fowle,
"Space Transport Capabilities of Chemically-Fueled Propulsion Systems Using Storable and Cryogenic Propellants",
Arthur D. Little, Inc., Summary Report to NASA, Office of Space Sciences and Applications, June 1964. Contract No. NASw-876.

10. Emslie, A.G.,
"Radiative Heat Leaks Through Seams and Penetrations in Panels of Multilayer Metal-Foil Insulation",
Arthur D. Little Report No. 63270-04-04, April, 1962.

11. Bonneville, Jacques, and Frank Gabron
"A Guide to the Computation of Heat Flow in Insulated Cryogenic Storage Vessels in the Space Environment",
Arthur D. Little, Inc., Topical Report No. 63270-13-01, September, 1962, to NASA.

12. Ehrenfeld, John, and Peter Strong,
"Analysis of Thermal Protection Systems for Propellant Storage During Space Missions",
Arthur D. Little, Inc. Topical Report No. 63270-04-03, December 1961, to NASA.

13. Strong, Peter F., and Alfred G. Emslie,
"The Method of Zones for the Calculation of Temperature Distribution",
Arthur D. Little, Inc., July 1963.

14. Fowle, Arthur A.,
"Estimation of Weight Penalties Associated with Alternate Methods for Storing Cryogenic Propellants in Space".
Arthur D. Little, Inc., Topical Report No. 63270-11-01, to NASA, May 1962.

15. Moore, Raymond W., Jr.,
"Conceptual Design Study of Space-Borne Liquid Hydrogen Recondensers For 10 and 100 Watts Capacity",
Arthur D. Little, Inc., Topical Report 63270-11-02 to NASA, May 1962.

16. Emslie, A.G.
"Gas Conduction Problem with Multilayered Radiation Shields",
Arthur D. Little, Inc., Topical Report No. 63270-04-01, to NASA, April 1961.

17. Emslie, A.G.,
"Radiation Transfer by Closely Spaced Shields",
Arthur D. Little, Inc., Topical Report No.
63270-04-02, to NASA, May 1961.

GT-3 INFORMATION MISSION ORGANIZATION

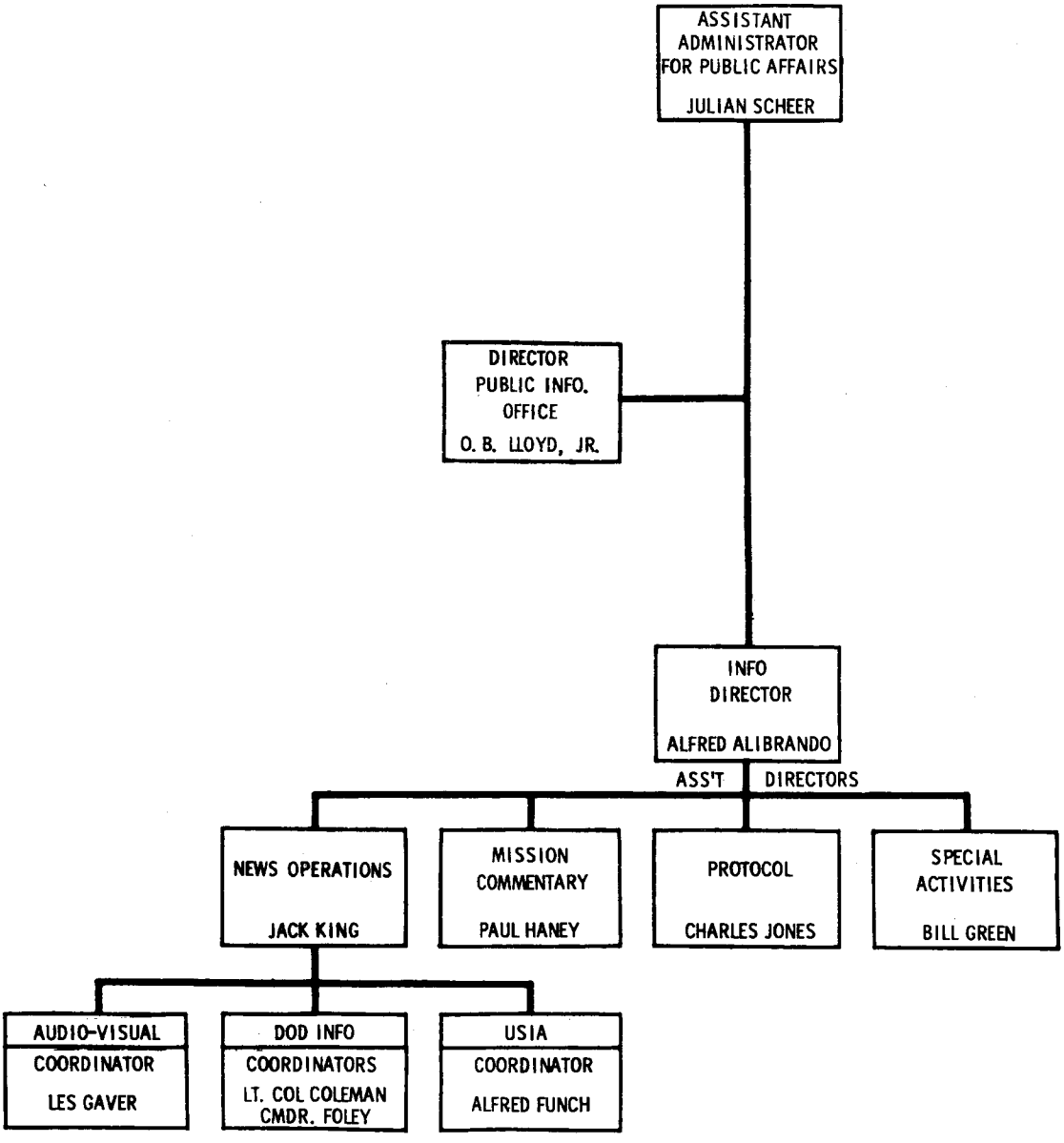

PROJECT OFFICIALS

George E. Mueller	Associate Administrator, Office of Manned Space Flight, NASA Headquarters. Acting Director, Project Gemini.
William C. Schneider	Deputy Director, Project Gemini, Office of Manned Space Flight, NASA Headquarters.
E. E. Christensen	Director, Missions Operations, NASA Headquarters
Charles W. Mathews	Gemini Program Manager, Manned Spacecraft Center, Houston, Tex.
Christopher C. Kraft	Mission Director, Manned Spacecraft Center, Houston, Tex.
Lt. Gen. Leighton I. Davis	USAF, National Range Division Commander and DOD Manager of Manned Space Flight Support Operations.
Maj. Gen. V. G. Huston	USAF, Deputy DOD Manager
Col. Richard C. Dineen	Director, Directorate Gemini Launch Vehicles, Space Systems Division, Air Force Systems Command.
Lt. Col. John G. Albert	Chief, Gemini Launch Division, 6555th Aerospace Test Wing, Air Force Missile Test Center, Cape Kennedy, Fla.
R. Admiral B. W. Sarver	USN, Commader Task Force 140.

- end -

REPORT DISTRIBUTION LIST FOR
CONTRACT NO. NAS3-4181

National Aeronautics and Space Administration (1)
Washington, District of Columbia 20546
Attention: Mel Rosche, Code RV-2

National Aeronautics and Space Administration (6)
Washington, District of Columbia 20546
Attention: Code MLPL

National Aeronautics and Space Administration (1)
Washington, District of Columbia 20546
Attention: J. Salmanson, Code SV

NASA Ames Research Center (1)
Moffett Field, California 94035
Attention: Library

NASA Flight Research Center (1)
P. O. Box 273
Edwards, California 93523
Attention: Library

NASA Goddard Space Flight Center (1)
Greenbelt, Maryland 20771
Attention: Code 204

NASA Goddard Space Flight Center (1)
Greenbelt, Maryland 20771
Attention: Code 240

NASA Goddard Space Flight Center (1)
Greenbelt, Maryland 20771
Attention: Code 243

NASA Goddard Space Flight Center (1)
Greenbelt, Maryland 20771
Attention: Code 250

NASA Goddard Space Flight Center (1)
Greenbelt, Maryland 20771
Attention: Library

NASA Langley Research Center (1)
Langley Station
Hampton, Virginia 23365
Attention: Library

NASA Langley Research Center (1)
Langley Station
Hampton, Virginia 23365
Attention: D. Davis

NASA Langley Research Center (1)
Langley Station
Hampton, Virginia 23365
Attention: Richard Heldenfels

NASA Lewis Research Center (2)
21000 Brookpark Road
Cleveland, Ohio 44135
Attention: Library

NASA Lewis Research Center (4)
21000 Brookpark Road
Cleveland, Ohio 44135
Attention: James R. Barber, M.S. 500-209

NASA Lewis Research Center (1)
21000 Brookpark Road
Cleveland, Ohio 44135
Attention: J. A. Durica, M.S. 500-210

NASA Lewis Research Center (1)
21000 Brookpark Road
Cleveland, Ohio 44135
Attention: Jack Esgar, M.S. 49-1

NASA Lewis Research Center (1)
21000 Brookpark Road
Cleveland, Ohio 44135
Attention: Henry Hunczak, M.S. 21-5

NASA Lewis Research Center (1)
21000 Brookpark Road
Cleveland, Ohio 44135
Attention: R. Knoll, M.S. 4-7

NASA Lewis Research Center (1)
21000 Brookpark Road
Cleveland, Ohio 44135
Attention: Norman T. Musial,
M.S. 77-1

NASA Lewis Research Center (1)
21000 Brookpark Road
Cleveland, Ohio 44135
Attention: Report Control Office, M.S. 5-5

NASA Lewis Research Center (1)
21000 Brookpark Road
Cleveland, Ohio 44135
Attention: Office of R & QA, M.S. 500-203

NASA Manned Spacecraft Center (1)
Houston, Texas 77001
Attention: Technical Library

NASA Manned Spacecraft Center (1)
Houston, Texas 77001
Attention: Merlyn Lausten (EP2)

NASA George C. Marshall Space Flight Center (1)
Huntsville, Alabama 35812
Attention: Library

NASA George C. Marshall Space Flight Center (1)
Huntsville, Alabama 35812
Attention: Research Projects Division (M-RP-R)

NASA George C. Marshall Space Flight Center (1)
Huntsville, Alabama 35812
Attention: James B. Bramlet (M-SAT)

NASA George C. Marshall Space Flight Center (1)
Huntsville, Alabama 35812
Attention: James W. Carter (MFPO)

NASA George C. Marshall Space Flight Center (1)
Huntsville, Alabama 35812
Attention: Chester O. Gray, M-S & M-M

NASA George C. Marshall Space Flight Center (1)
Huntsville, Alabama 35812
Attention: Clyde Nevins

NASA George C. Marshall Space Flight Center (1)
Huntsville, Alabama 35812
Attention: R. Wegrich

NASA George C. Marshall Space Flight Center (1)
Huntsville, Alabama 35812
Attention: Charles C. Wood (P-VE)

NASA Western Operations Office (1)
150 Pico Boulevard
Santa Monica, California 90406
Attention: Library

Chief of Staff (1)
U. S. Air Force
The Pentagon
Washington, District of Columbia 20525
Attention: DCS/D, AFDRD-AN

Materials Engineering Branch (1)
Application Laboratory-Materials Control
Aeronautical Systems Division
Air Force Systems Command
Wright-Patterson Air Force Base, Ohio
Attention: W. P. Conrardy, Chief

Commander (2)
Air Research and Development Command
Andrews Air Force Base
Washington, District of Columbia 20525

Headquarters, ARDC (1)
Wright Air Development Division
Wright-Patterson Air Force Base, Ohio
Attention: Materials Central (WWRCEP-1)

Headquarters, ARDC (1)
Wright Air Development Division
Wright-Patterson Air Force Base, Ohio
Attention: Charles R. Martel (WWRMFS-a)

Commander (1)
Air Technical Intelligence Center
Wright-Patterson Air Force Base, Ohio
Attention: AFOIN-4B1a

Army Reactors (1)
Division of Reactor Development
Atomic Energy Commission
Germantown, Maryland
Attention: Capt. J. H. Higman

Jet Propulsion Laboratory (2)
4800 Oak Drive
Pasadena, California 91103
Attention: Earl E. Newham, Reports Group

Jet Propulsion Laboratory (1)
4800 Oak Drive
Pasadena, California 91103
Attention: V. Jaffe

Jet Propulsion Laboratory (1)
4800 Oak Drive
Pasadena, California 91103
Attention: Thomas O. Thostesen

Jet Propulsion Laboratory (1)
4800 Oak Drive
Pasadena, California 91103
Attention: Library

Liquid Propellant Information Agency (3)
Johns Hopkins University
Applied Physics Laboratory
8621 Georgia Avenue
Silver Spring, Maryland

National Bureau of Standards (1)
Cryogenic Engineering Division
Boulder, Colorado
Attention: Richard H. Kropschot

Naval Research Laboratory (1)
Washington, District of Columbia 20525
Attention: J. K. Kallander, Code 6464

Rocket Propulsion Laboratory (1)
DGRPP
Edwards, California
Attention: Second Lieutenant D. W. Ryter

Scientific and Technical Information
Facility (6)
P. O. Box 5700
Bethesda, Maryland
Attention: NASA Representative

Aerojet-General Corporation (1)
Azusa, California
Attention: A. Weinstein

Aerojet-General Corporation (1)
Azusa, California
Attention: Myra T. Grenier, Library

Air Products and Chemicals, Inc. (1)
Allentown, Pennsylvania
Attention: Abraham Lopin

Air Products and Chemicals, Inc. (1)
West Broad Street
Emmaus, Pennsylvania
Attention: Andrew Hospider

Bell Aerosystems, Inc. (1)
P. O. Box No. 1
Buffalo, New York
Attention: Kurt Berman

Boeing Company (1)
Seattle, Washington
Attention: Charles Tiffany, Box 15-56

Boeing Company (1)
Seattle, Washington
Attention: Library

University of California (1)
Los Alamos Scientific Laboratory
P. O. Box 1663
Los Alamos, New Mexico

Chrysler Corporation (1)
P. O. Box 26018
New Orleans, Louisiana
Attention: Miss Elayne M. Bower

Cryonetics Corporation (1)
Northwest Industrial Park
Burlington, Massachusetts
Attention: James F. Howlett

Curtiss-Wright Corporation (1)
Wright Aeronautical Division
Wood Ridge, New Jersey
Attention: Henry Ryffel, Dept. 8332

Douglas Aircraft Company (1)
3000 Ocean Park Boulevard
Santa Monica, California 90406
Attention: H. Dixon

The Garrett Corporation (1)
1625 Eye Street, North West
Washington, District of Columbia
Attention: G. R. Shepard

General Dynamic Corporation (1)
Convair Astronautics Division
P. O. Box 1128
San Diego, California
Attention: Karl Leonhard

General Dynamics Corporation (1)
Convair Astronautics Division
P. O. Box 1128
San Diego, California
Attention: Library and Information
Services (128-00)

General Electric Company (1)
Valley Forge Space Technology Center
P. O. Box 8555
Philadelphia, Pennsylvania 19101
Attention: Michael W. Mitchell

General Electric Company (1)
Valley Forge Space Technology Center
P. O. Box 8555
Philadelphia, Pennsylvania 19101
Attention: A. D. Cohen

Goodyear Aerospace Corporation (1)
1210 Massillon Road
Akron, Ohio
Attention: Clem Shriver, Dept. 481

Grumman Aircraft Engineering
Corporation (1)
Bethpage, Long Island, New York
Attention: John Tlasmati, Library

Linde Company (1)
Tonawanda, New York
Attention: L. Smith

Linde Company (1)
Tonawanda, New York
Attention: R. Lindquist

Ling-Temco-Vought (1)
Box 5907
Dallas, Texas
Attention: Library

Lockheed Aircraft Corporation (1)
Marietta, Georgia
Attention: Library

Lockheed Missiles and Space Company (1)
3251 Hanover Street
Palo Alto, California
Attention: A. Gilcrest

Lockheed Missiles and Space Company (1)
Sunnyvale, California
Attention: W. Sterbentz, Bldg. 537

Lockheed Missiles and Space Company (1)
Sunnyvale , California
Attention: C. Merlet, Bldg. 537

Lockheed Missiles and Space Company (1)
Sunnyvale, California
Attention: Library

The Martin Company (1)
Baltimore, Maryland
Attention: Science-Technology Library

The Martin Company (1)
Baltimore, Maryland
Attention: R. Crawford

National Research Corporation (1)
70 Memorial Drive
Cambridge, Massachusetts

New York University (1)
University Heights
New York, New York
Attention: Paul F. Winternitz

North American Aviation (1)
12214 Lakewood Boulevard
Downey, California
Attention: Donald Jellinek

North American Aviation (1)
12214 Lakewood Boulevard
Downey, California
Attention: Mr. Boogard

North American Aviation (1)
Rocketdyne Division
6633 Canoga Boulevard
Canoga Park, California
Attention: R. V. Burry

Pratt and Whitney Aircraft (1)
Florida R. & D. Center
West Palm Beach, Florida

Space General Corporation (1)
333 West First Street, Room 436
Dayton, Ohio
Attention: Charles Hodges

Space General Corporation (1)
9200 East Flair Drive
El Monte, California
Attention: John Kortenhoeven,
Dept. 5131

Space Technology Laboratories (1)
5500 West El Segundo Boulevard
Los Angeles, California
Attention: Joseph M. Denney

Space Technology Laboratories (1)
5500 West El Segundo Boulevard
Los Angeles, California
Attention: Physical Research and
Analysis Section

Stanford Research Institute (1)
Menlo Park, California
Attention: P. R. Gillette

Radio Corporation of America (1)
Defense Electronics Products
Astro-Electronics Division
Princeton, New Jersey
Attention: Library